Chemical-Scale Investigations of Cys-Loop Neurotransmitter Gated Ion Channels

Thesis by

Ariele Patrice Hanek

In Partial Fulfillment of the Requirements

for the Degree of

Doctor of Philosophy

Division of Chemistry and Chemical Engineering

California Institute of Technology
Pasadena, CA

2009

(Defended May 26, 2009)

Acknowledgements

The most exciting phrase to hear in science,
the one that heralds the most discoveries, is
not "Eureka," but "That's funny…"
-Isaac Asimov

The past six years were not what I expected them to be when I came to Caltech six years ago. It is no secret that I struggled at the beginning and that I've had my ups and downs along the way. My eventual success would not be possible without the support and aid of many people along the way.

First and foremost, I would like to thank my advisor, Dennis Dougherty. I came to Caltech unsure of what type of research I wanted to do. The elegance of Dennis's experiments appealed to me from the start and I have never regretted joining the lab. Dennis has an uncanny ability to give his students leeway while keeping us focused on the end goal. His patience, encouragement, and scientific insight have been invaluable to me. I couldn't have asked for a better advisor.

The research described in the following pages would have been more limited in scope if not for Henry Lester and the members of his lab. Through countless "unnatural club" meetings, Henry provided a fresh perspective for puzzling results and was a never-ending source of new experiments.

My work on the anionic Cys-loop receptors would not have been possible without my very capable collaborators. I want to thank Stephen Pless and Claire Padgett for proposing to study these receptors and travelling to Caltech to do so. Both were enormously patient with my lack of knowledge of their systems. I wish them both the best of luck with their post-doc research. Sarah Lummis has been a constant source of aid to me during the second half of my graduate career. Her guidance on my $GABA_AR$

projects was invaluable and I cannot thank her enough for providing me with $GABA_AR$ DNA that actually worked and offering to corroborate my results on her own time.

I would like to thank the other members of my thesis committee, Peter Dervan, Bill Goddard, and David Tirrell, for the feedback and words of encouragement during my graduate career.

My day-to-day life in graduate school would have dull indeed, if not for the amazing group of friends and lab mates I've been fortunate to have along the way. I was privileged to meet and benefit from meeting Darren Beene, James Petersson, Tingwei Mu, Steven Spronk, Lori Lee, and Amanda Cashin, all of whom helped me get started in the lab and have now moved on to pursue their various career paths during my first few years.

Joanne Xiu, Amy Eastwood, Mike Torrice, Erik Rodriguez, Kiowa Bower, and Kristin Gleitsman have been my compatriots through the years. Joanne is an amazing scientist and mentor, guiding me through my first projects in the lab. She was a wonderful person to work with and I'm sure she'll do wonderful things in the future. Although I was often struggling to breathe, the conversations I had with Amy during our runs were always helpful and insightful and I only hope that she enjoyed them as much as I did. Erik could always be counted on to give you the worst-case scenario for new experiments – often saving me from pursuing avenues to nowhere. Mike was a wonderful Opus co-captain and his willingness to deal with the bureaucratic mess that is molecular devices was a huge help. I wish him the best of luck with science writing. I have always enjoyed my conversations with Kiowa, both scientific and otherwise, and will always remember him trying to show me slides while we were driving to San

Francisco. Kristin has been invaluable comfort to me especially during the last year. She has exhibited remarkable patience in listening to my complaints and been endlessly kind in helping me with my research. I wouldn't have been able to finish my final project without her help.

Although I have not known Angela Blum or Jai Shanata for as long as some of the other lab members, I owe them special thanks for helping me edit my thesis and proposals. Their feedback and quick turn-around time has been invaluable. I also need to acknowledge Nyssa Puskar, who also helped with my thesis and proposals, but more importantly has been an amazing friend to me. She has dragged me to the pool on countless occasions probably saving me from running myself into the ground. I hope she doesn't regret taking over my responsibilities as Opus captain. I wish the newer members of the Dougherty Lab, Sean Kedrowski, Kay Limapichat, Shawna Frazier, Darren Nakamura, Noah Duffy, Maggie Thompson, Kristina McCleary, Ximena Da Silva Tavares Bongoll, and Ethan van Arnam, the best of luck. You'll know it's time to graduate when you stop aiming for "great" and set your sights on "good enough."

While I am fortunate to call my lab mates friends, I was also extremely lucky to meet a great group of fellow graduate students shortly after coming to Caltech. I can't imagine what my experience here would have been like without the support and friendship of Heidi Privett, Michelle Robbins, Heather Wiencko, Katie Brenner, Mike Adams, Greg ver Steeg, Jeff Krimmel, Paul Cook, and Roger Donaldson. Bert Lai gets a special mention for being my running partner and willingly getting up with me at 6 am to go for a 12-mile run even when I barely spoke two words the entire time. I don't know who I will train with now.

I have always been able to count on the support of my oldest friend, Shaelah Reidy. As a fellow graduate student she has understood the trials and tribulations of my graduate career better than most. My friends from home and from Bowdoin have been a wonderful luxury throughout my time on the west coast and I want to especially mention Karen Finnegan, Cory Lown, and Caitlin Jamali, who have always found time for me in their busy schedules.

Last, but certainly not least, I want to thank my entire family for their love and support even when I haven't deserved it. I hope I have made you proud. My parents have logged countless frequent flyer miles flying between the two coasts coming to see me when I couldn't get away from the lab, and always brought a touch of home with them. Although she is my younger sister, Bailey has provided me with sage advice on more than one occasion during graduate school. I am lucky to have her as a sister and am so proud of her. I only hope I can return the favor to her and the rest of my family.

Abstract

Cys-loop ligand gated ion channels mediate rapid synaptic transmission in the mammalian central and peripheral nervous system. Proper functioning of this superfamily of receptors is critical to brain function and as such the proteins are implicated in a number of neuropathies and are a target for many pharmaceuticals. A central concern is how these receptors recognize and bind their neurotransmitter agonists as well as how these binding events lead to a conformational change spanning a distance of at least 50 Å. Using the nonsense suppression methodology, we are able to incorporate unnatural amino acids into these proteins and identify the precise molecular interactions involved in neurotransmitter binding and the conformational changes that take place during channel activation.

In chapters two through four we investigate the role of the nicotinic acetylcholine receptor (nAChR) α_1 loop 2 residues in channel activation. Using conventional mutagenesis, we have identified several residues that are part of a global electrostatic network. This is the first study to present an element of activation that is universal to the entire Cys-loop superfamily. Using unnatural amino acids, we identify the pro-S methyl group of αVal46 as a critical element in the activation pathway of the muscle type nicotinic acetylcholine receptor, thereby validating a proposed the pin-into-socket mechanism for this residue.

We switch our focus from the excitatory nAChR to the inhibitory glycine (Gly) and γ-aminobutyric acid type A ($GABA_A$) receptors in chapter 5. By incorporating successively fluorinated phenylalanine analogs into the binding site of both the GlyR and $GABA_AR$ we were able to identify a cation-π interaction at α_1Phe159 of the GlyR and

β_2Tyr97 of the $GABA_AR$, providing further evidence that the cation-π interaction is conserved across the superfamily.

Finally we investigate the mechanisms of GABA activation and flurazepam (FLZM) potentiation in the $GABA_AR$. Incorporation of a photo-activated backbone cleaving unnatural amino acid reveals that an unstructured linker connecting loops A and E of the $GABA_AR$ α_1 subunit is critical to GABA but not pentobarbital activation. We further investigate this region of the receptor and its role in GABA activation and flurazepam potentiation using conventional mutagenesis and incorporation of α-hydroxy acids. The data indicate that GABA activation and FLZM potentiation are differentially affected by side chain mutations in this region, but not by backbone mutations. Loss-of-function due to incorporation of α-hydroxy acids strongly suggests the unstructured linker becomes more structured during channel activation.

Table of Contents

List of Figures

List of Tables

Chapter 1

Introduction

1.1 A Chemical Understanding of the Brain

The brain is the most complex organ in the human body. On average, the adult human brain contains 10^{11} neurons, each of which makes 10^3 to 10^4 interactions with other neurons through junctions called synapses. Communication from one neuron to another takes place through synaptic transmission. Each synapse involves the communication of two neurons (Figure 1.1), the one producing the signal, called the pre-synaptic neuron, and the one receiving it, called the post-synaptic neuron. The pre-synaptic neuron receives information from other neurons through its dendrites. After processing this information, the neuron fires an electrical impulse, the action potential, which travels down the axon of the pre-synaptic neuron. Upon reaching the axon terminus, the electrical impulse causes vesicles containing neurotransmitter to fuse to the cell membrane, thereby releasing neurotransmitter into the synaptic cleft, the small space between neurons. This effectively turns the electrical signal, the action potential, into a chemical signal, the neurotransmitter. Receptors within the cell membrane of the post-synaptic neuron recognize and bind the neurotransmitters. Activation of the neuroreceptors directly or indirectly leads to the flow of ions across the membrane of the post-synaptic cell, thereby converting the chemical signal back to an electrical one.

Brain function is much more complex than simply understanding synaptic transmission. Neuroreceptors are located in both the pre-synaptic and post-synaptic densities and recognize a variety of ligands. Their activation leads to a myriad of down-

stream effects resulting from the flow of ions across the membrane. Neurotransmitters are most often small organic molecules

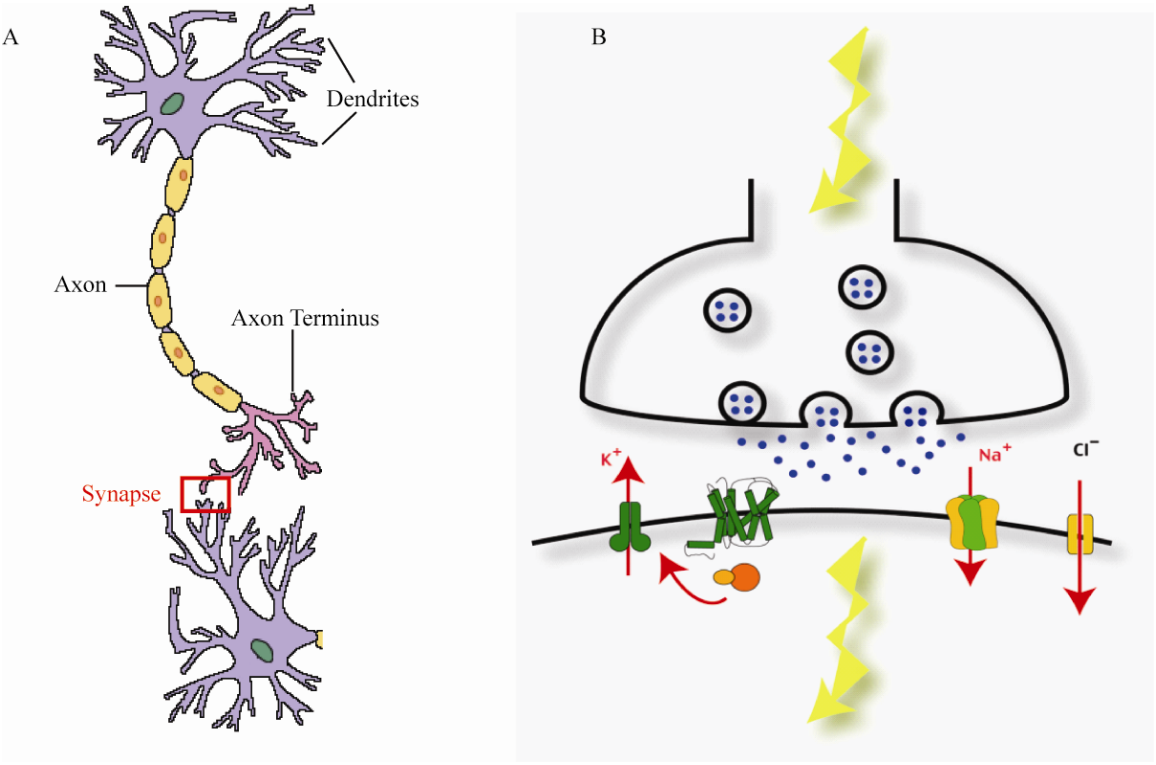

Figure 1.1 Synaptic Transmission. **A**, The interaction of two neurons takes place between the axon terminus (pink) of the pre-synaptic cell and the dendrites (purple) of the post-synaptic cell. The synapse is highlighted (red box). **B**, A cartoon of synaptic transmission. Neurotransmitter is depicted as blue dots.

but can also be peptides or fatty acids. The electrical signals that result from neuroreceptor activation can be either inhibitory or excitatory. A given neuron receives multiple signals at different synapses, further complicating matters. The interplay of various inputs at specific regions of the brain give rise to higher brain function, including learning and memory, addiction, and sensory input. Given the complexity of the brain, how can we hope to use chemical-scale studies to elucidate brain function?

We focus our efforts on developing an in-depth understanding of a specific type of neuroreceptor – the Cys-loop ligand gated ion channels. Neurotransmitter binding and

activation of the receptor are chemical-scale events that can be studied by site-specific incorporation of unnatural amino acids.

1.2 Cys-loop ligand gated ion channels

The Cys-loop ligand gated ion channels constitute a superfamily of receptors that mediate rapid synaptic transmission in the mammalian central and peripheral nervous systems through the binding of a neurotransmitter agonist. At rest, the receptor is in an unliganded, closed, non conducting state. Upon binding of agonist, the receptor undergoes a conformational change to an open ion-conducting state, thereby allowing ions to cross the cell membrane. The conformational change removes a hydrophobic barrier that prevents ion permeation, analogous to a gate swinging open; therefore the change from the closed state to the open state is often referred to as channel gating.

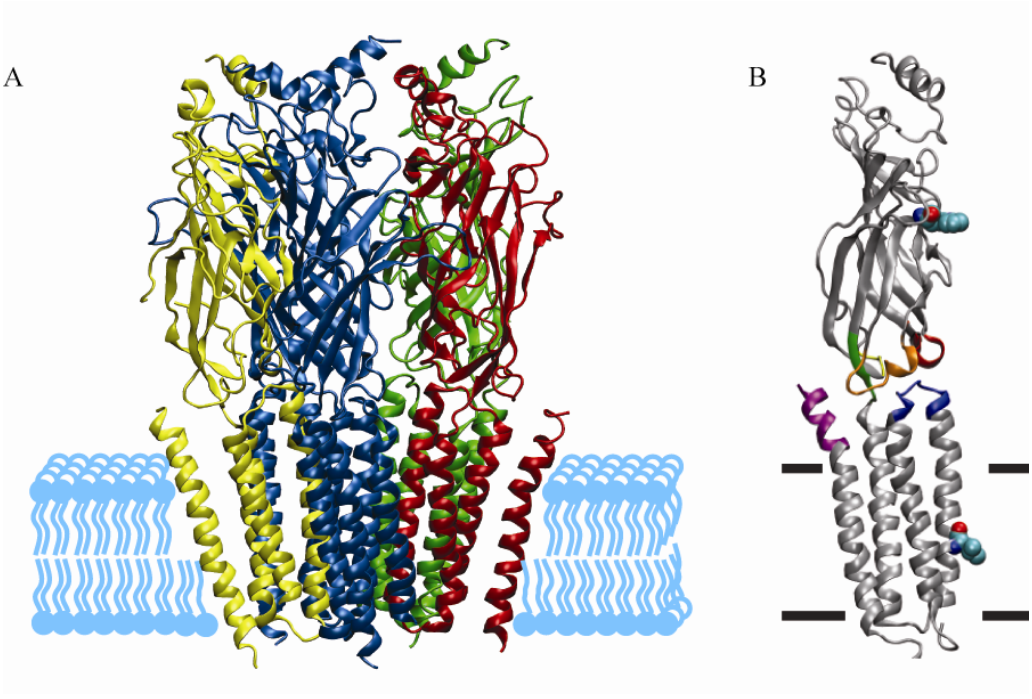

Figure 1.2 General topology of Cys-loop receptors. **A**, The nAChR, a prototypical Cys-loop receptor, has two α_1 (blue), one β_1 (green), one δ (red), and one γ or ε (yellow) subunit. **B**, Each subunit has a predominantly beta sheet, N-terminal extracellular domain and four membrane-spanning helices. The ligand binding site and channel gate are highlighted as VDW residues.

The superfamily includes the excitatory, cation conducting, nicotinic acetylcholine receptors (nAChR) and serotonin type 3A receptors ($5HT_{3A}R$), as well as the inhibitory, anion conducting, γ-aminobutyric acid (GABA) type A and type C receptors ($GABA_AR$ and $GABA_CR$, respectively) and the glycine receptors (GlyR). Each receptor is comprised of five homologous subunits arranged pseudosymmetrically around a central, ion-conducting pore (Figure 1.2). The large N-terminal domain of each subunit has a predominantly beta sheet structure with short loops connecting the beta strands. The primary sequence leads directly from beta strand 10 to four membrane-spanning helices, termed M1-M4, followed by a short, extracellular, carboxy terminus. The M2 helix of each subunit lines the channel pore. Neurotransmitter binding sites are located at select subunit interfaces in the extracellular domain, while the channel gate is located ~60Å away in the transmembrane region.

These large, membrane-spanning proteins do not readily lend themselves to crystallization techniques. As such, there are no crystal structures of mammalian Cys-loop neurotransmitter gated ion channels. Instead, structural information about these receptors relies heavily on biochemical studies as well as X-ray crystallography data from the acetylcholine binding protein (AChBP) and cryo-EM images of the nAChRs found in the electroplaques of the *Torpedo californica* ray. AChBP is a soluble pentameric protein isolated from snails which is highly homologous to the extracellular portion of Cys-loop neurotransmitter gated ion channels. Unlike the Cys-loop receptors, the role of AChBP is to bind acetylcholine, not to open an ion pore. Thus, while structural information from AChBP is useful in determining residues involved in neurotransmitter binding, the structure provides no information about the activation or gating pathway of the

mammalian ion channels. Cryo-EM is an inherently lower resolution methodology than X-ray crystallography, thus the amino acid side chains cannot be resolved. However, the cryo-EM image is the only structure of a full mammalian Cys-loop ligand gated ion channel, and has a higher sequence homology to nAChRs than AChBP. As such, the cryo-EM structure (Protein Data Bank code 2BG9) can guide studies relating to the gating pathway of these receptors more readily than AChBP structures.

1.3 Unnatural Amino Acid Methodology

1.3.1 *Advantage of Unnatural Amino Acids*

To study neuroreceptors on the chemical-scale, we need a precise methodology that allows us to investigate these proteins as we would small organic molecules on a bench top. The analogous experiments for neuroreceptors and their ligands are structure-function studies. Manipulation of the neurotransmitter can be carried out synthetically and has been done so extensively by medicinal chemists and pharmacologists. Derivatizing and making analogues of the neurotransmitters provides information regarding the action of neurotransmitter on neurons, and can elucidate the neurotransmitter pharmacaphore, but does not provide data on the structural rearrangements within the neuroreceptor. Conducting similar studies where the structural perturbations are restricted to the neuroreceptor allows the nature of the interactions with the receptor to be illuminated.

Cys-loop neurotransmitter-gated ion channels are multimeric membrane proteins of over two-thousand amino acids, and thus cannot be made synthetically. Furthermore, accurate evaluation of receptor function requires the proteins to be membrane bound. Mutagenesis of the receptor and expression in a heterologous system provide a means to

both perturb protein structure and preserve an *in vivo* context for channel function. However, mutagenesis restricts the structural perturbations to those contained within the twenty naturally occurring amino acids (Figure 1.3).

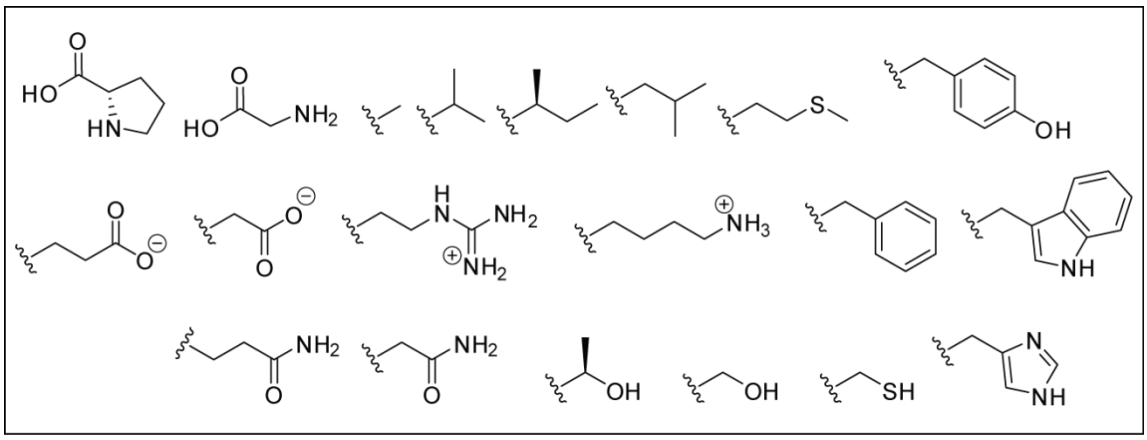

Figure 1.3 Side chains of the natural amino acids. From left to right: top row: proline, glycine (shown as full amino acid), alanine, valine, isoleucine, leucine, methioninine, tyrosine. Middle row: glutamate, aspartate, arginine, lysine, phenylalanine, tryptophan. Bottom row: glutamine, asparagine, threonine, serine, cysteine, histidine

The twenty naturally occurring amino acids have limited chemical functionality in their side chains. For example, there are no side chains with ketones, alkenes, or nitro groups. Even within the chemical functionality provided by these twenty amino acids, the overall shape, size, and length of the side chain is predetermined for a given functionality. For example, mutation from serine to cysteine replaces a hydroxyl group with a sulfhydryl group, yet there is no corresponding mutation for a threonine residue. Additionally, the interaction of two amino acids within the neuroreceptor may require augmenting side chain length or polarity or conversion of the amide peptide bond to an ester linkage. None of these objectives are accurately achieved using conventional mutagenesis. Incorporation of unnatural amino acids, however, allows the introduction of novel side chains to precisely determine the role of a specific amino acid.

While unnatural amino acids provide a virtually limitless pool of structural perturbations (Figure 1.4), how can we incorporate them into our proteins? Synthetic incorporation is not feasible for large, transmembrane bound proteins such as Cys-loop neurotransmitter gated ion channels. Instead we rely on the site-specific nonsense suppression methodology.

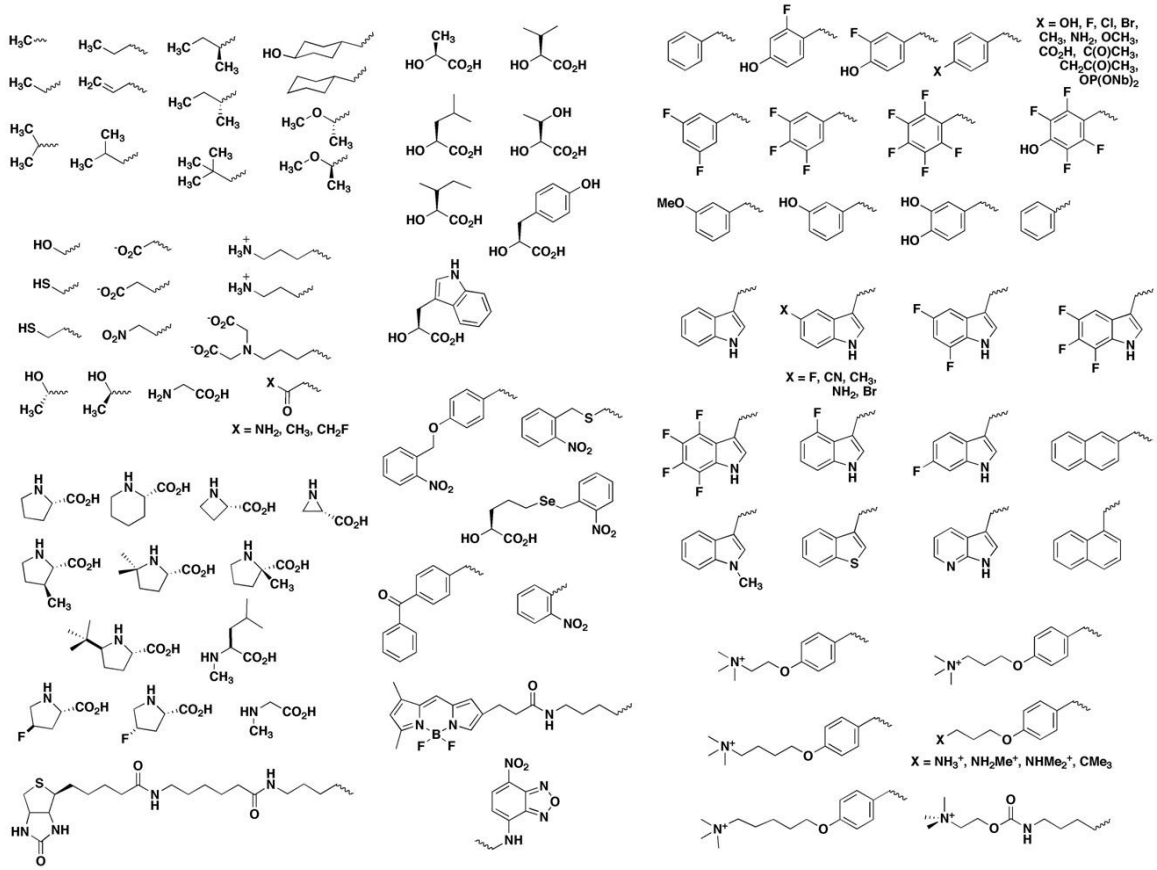

Figure 1.4 A subset of unnatural amino acid side chains and alpha hydroxy acids incorporated via the nonsense suppression methodology[1]

1.3.2 *Nonsense Suppression Methodology*

The ability to site-specifically incorporate unnatural amino acids into proteins was developed by Schultz and co-workers in 1989.[2-11] To achieve incorporation at a specific site, a codon that is not recognized by any of the native tRNAs must be utilized, a tRNA molecule recognizing this codon must be made, and the unnatural amino acid must be

chemically attached to the tRNA molecule. Only three codons, UAG, UAA, and UGA, do not code for one of the twenty naturally occurring amino acids. These three codons are STOP codons and normally mark the termination of translation. We incorporate a STOP codon at the site of interest and engineer a tRNA molecule with the appropriate anticodon. Instead of terminating protein translation when the STOP codon is reached, the ribosome incorporates the unnatural amino acid at this site as it would incorporate any of the naturally occurring amino acids (Figure 1.5).

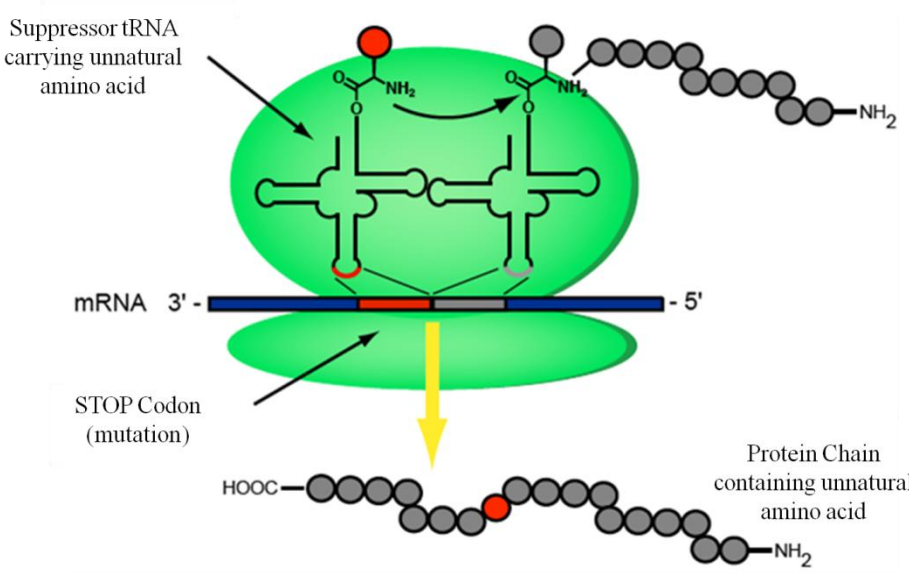

Figure 1.5 Overview of unnatural amino acid incorporation using nonsense suppression

Nonsense suppression requires a combination of molecular biology and chemical synthesis.[9,12-15] Most often, the amber codon, UAG, is used as the STOP codon because it was the first developed[8] and the suppressor tRNA engineered to recognize this codon has been shown to be more efficient.[16,17] The UAG mutation is first incorporated into the gene via quickchange PCR. *In vitro* transcription is used to make mRNA based on the DNA template. The suppressor tRNA without the last two nucleotides (C and A) of the acceptor stem are transcribed *in vitro.* The last two ribonucleotides of all tRNA

molecules are CA. Deoxy-CA (dCA) is chemically synthesized and the unnatural amino acid is attached chemically to give Uaa-dCA. The unnatural amino acids are prepared by addition of a photo- (NVOC) or iodine- (4-PO) labile amino protecting group. The carboxylic acid is activated as the cyanomethyl ester prior to acylation of the dCA molecule (Figure 1.6) to give Uaa-dCA. Once acylated, the dCA is ligated to the truncated suppressor tRNA using T4 RNA ligase to yield the full length amino-acylated tRNA. The amino group of the Uaa is left protected to stabilize the acylated tRNA.

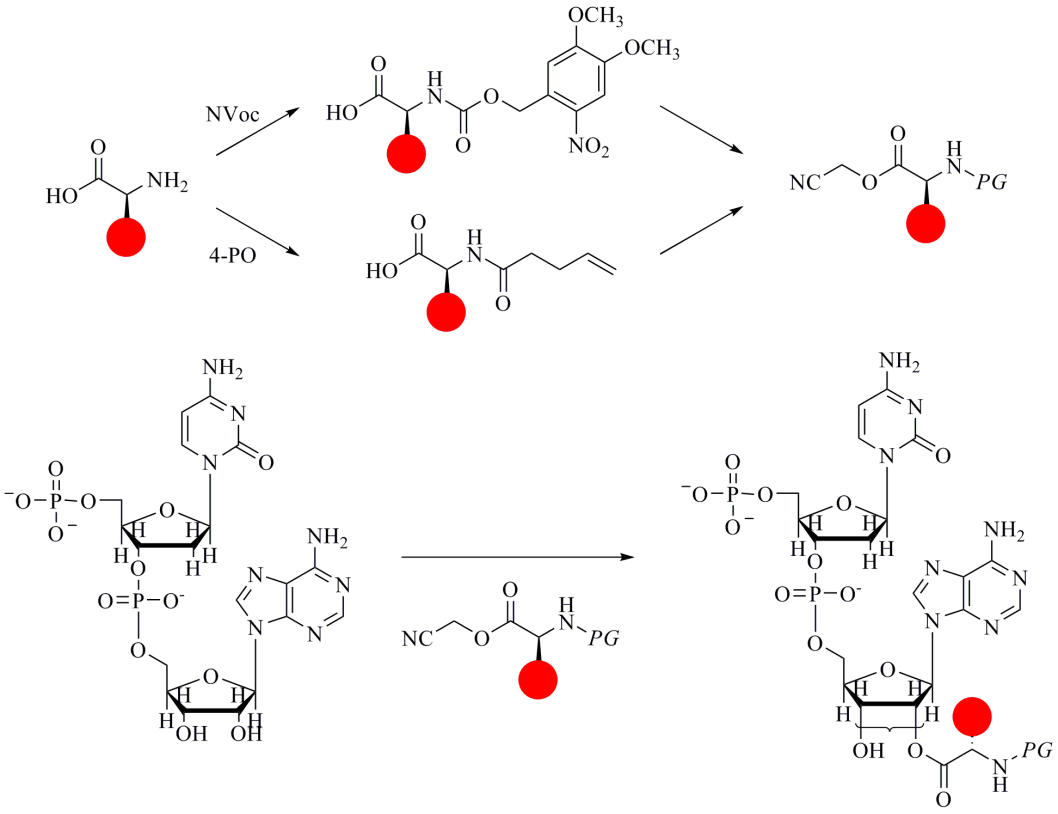

Figure 1.6 Standard preparation of unnatural amino acid (Uaa) coupled to deoxy-Cytosine, Adenine (dCA)

Immediately prior to injection into *Xenopus laevis* oocytes (Figure 1.7), the amino group of the unnatural amino acid is deprotected, and tRNA-Uaa is mixed with mRNA. Each oocyte is injected with 50 nL of RNA mix and then allowed to incubate for twenty-four to forty-eight hours. During this time, the Cys-loop neurotransmitter gated ion

channels are transcribed, folded, processed, assembled, and transported to the cell surface. Once an unnatural amino acid is incorporated into the nascent protein chain, the tRNA is released back into the cell. However, there is not a way to put more Uaa on the tRNA molecule, thus the Uaa-tRNA is used as a stoichiometric reagent, thereby limiting the amount of protein made. Fortunately, these ion channels can be evaluated by electrophysiology, a highly sensitive assay that detects currents through the whole cell.

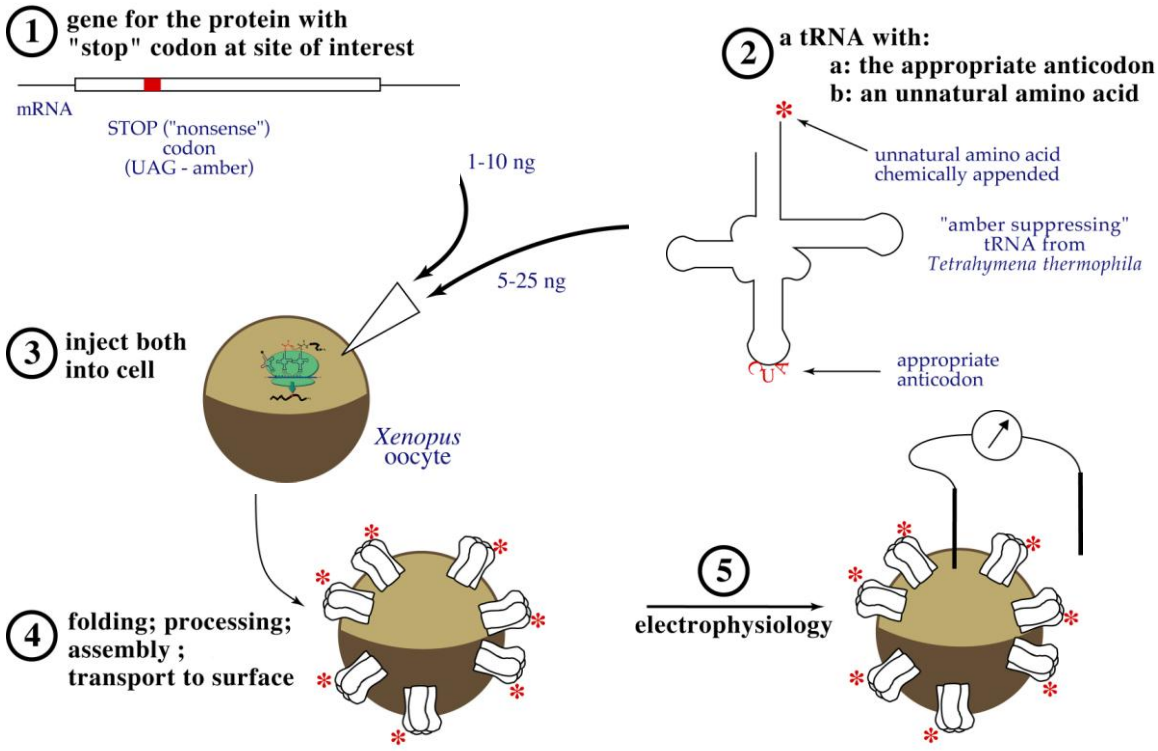

Figure 1.7 Implementation of nonsense suppression methodology using *Xenopus laevis* oocytes

Direct application of neurotransmitter to the oocytes results in neurotransmitter binding to the surface-expressed receptors followed by activation to the open state. The flow of ions across the cell membrane produces a macroscopic whole cell current that can be measured (Figure 1.8) by the two-electrode voltage clamp method. The amount of current is dependent on the number of surface expressed receptors, the proportion of the

receptors binding neurotransmitter, and the ability of the drug to activate the receptor. Applying increasing concentrations of agonist results in larger whole cell currents (Figure 1.8B). The relationship between the concentration of neurotransmitter, or drug, and the current size is the dose response relationship (Figure 1.8C). The EC_{50}, or effective concentration to induce the half-maximal response, is used as a metric of ion channel function. A leftward shift in EC_{50} is termed gain of function because less neurotransmitter is required to achieve the same level of activation. A rightward shift in EC_{50} is a loss of function mutation because more neurotransmitter is required to achieve the same level of activation. The EC_{50} is an equilibrium measurement dependent on both neurotransmitter binding and the potency (ability to activate the neuroreceptor) of the neurotransmitter.

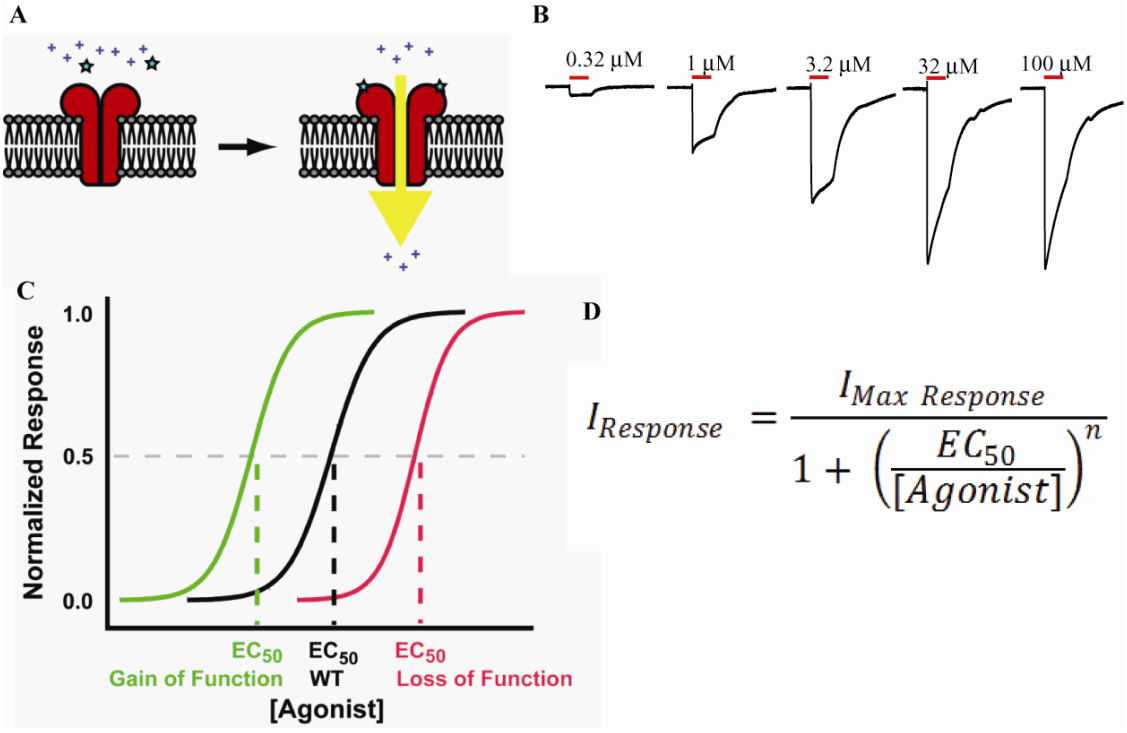

Figure 1.8 Typical electrophysiology assay. (**A**) Neurotransmitter, or agonist, (stars) binds to the neurotransmitter gated ion channels which leads to receptor gating and ion flow. (**B**) The current size increases as the concentration of agonist is increased until all receptors are saturated. (**C**) The dose response relationship is determined and fit to the Hill equation (**D**) to give the EC_{50} and Hill coefficient (n).

1.4 Dissertation Work

This dissertation describes multiple studies that utilize conventional mutagenesis as well as unnatural amino acid incorporation combined with electrophysiology. These studies focused on individual members of the Cys-loop ligand gated ion channel (LGIC) superfamily, specifically the muscle-type nAChR, the $\alpha_1\beta_2$ and $\alpha_1\beta_2\gamma_2$ $GABA_AR$, and the α_1 GlyR.

Chapters 2 through 4 describe research investigating the role of loop 2 residues in the α_1 subunit of nAChRs during channel activation. The highly charged nature of the loop is investigated through conventional mutagenesis in Chapter 2.[18] Mutation of loop 2 residues to histidine followed by pH experiments to change the protonation state of the loop are the subject of Chapter 3. In Chapter 4, site-specific incorporation of unnatural amino acids is used to evaluate a proposed interaction[19-23] between a loop 2 residue and the transmembrane domain of the receptors. Due to the precision of the nonsense suppression methodology, this study[24] is more conclusive than any previous study[25,26] investigating this interaction.

In Chapter 5, our focus shifts to the binding site of two inhibitory members of the Cys-loop family; the $\alpha_1\beta_2$ $GABA_AR$, and α_1 GlyR. Herein we identify the location and strength of a cation-π interaction formed between the cognate neurotransmitter and neuroreceptor by introduction of fluorinated phenylalanine residues.

Finally, Chapters 6 and 7 discuss our efforts to identify the role of an unstructured linker in the α_1 subunit of $GABA_ARs$ in channel activation and benzodizapine potentiation. We investigate both side chain and backbone mutations which affect the gating pathway of these receptors.

1.5 References

(1) England, P. M. *Biochemistry* **2004**, *43*, 11623-9.
(2) Chapman, E.; Thorson, J. S.; Schultz, P. G. *J. Am. Chem. Soc.* **1997**, *119*, 7151-7152.
(3) Chung, H. H.; Benson, D. R.; Schultz, P. G. *Science* **1993**, *259*, 806-809.
(4) Cornish, V. W.; Benson, D. R.; Altenbach, C. A.; Hideg, K.; Hubbell, W. L.; Schultz, P. G. *Proc. Natl. Acad. Sci. USA* **1994**, *91*, 2910-2914.
(5) Cornish, V. W.; Mendel, D.; Schultz, P. G. *Angew. Chem.* **1995**, *34*, 621-633.
(6) Ellman, J. A.; Mendel, D.; Schultz, P. G. *Science* **1992**, *255*, 197-200.
(7) Judice, J. K.; Gamble, T. R.; Murphy, E. C.; Devos, A. M.; Schultz, P. G. *Science* **1993**, *261*, 1578-1581.
(8) Noren, C. J.; A. Cahill, S. J.; Griffith, M. C.; Schultz, P. G. *Science* **1989**, *244*, 182-188.
(9) Nowak, M. W.; Kearney, P. C.; Sampson, J. R.; Saks, M. E.; Labarca, C. G.; Silverman, S. K.; Zhong, W.; Thorson, J. S.; Abelson, J. N.; Davidson, N.; Schultz, P. G.; Dougherty, D. A.; Lester, H. A. *Science* **1995**, *268*, 439-442.
(10) Thorson, J. S.; Chapman, E.; Schultz, P. G. *J. Am. Chem. Soc.* **1995**, *117*, 9361-9362.
(11) Koh, J. T.; Cornish, V. W.; Schultz, P. G. *Biochemistry* **1997**, *36*, 11314-11322.
(12) Beene, D. L.; Dougherty, D. A.; Lester, H. A. *Curr Opin Neurobiol* **2003**, *13*, 264-70.
(13) Kearney, P. C.; Nowak, M. W.; Zhong, W.; Silverman, S. K.; Lester, H. A.; Dougherty, D. A. *Mol Pharmacol* **1996**, *50*, 1401-12.
(14) Nowak, M. W.; Gallivan, J. P.; Silverman, S. K.; Labarca, C. G.; Dougherty, D. A.; Lester, H. A. *Methods Enzymol* **1998**, *293*, 504-29.
(15) Dougherty, D. A. *Curr Opin Chem Biol* **2000**, *4*, 645-52.
(16) Rodriguez, E. A.; Lester, H. A.; Dougherty, D. A. *RNA* **2007**, *13*, 1703-14.
(17) Rodriguez, E. A.; Lester, H. A.; Dougherty, D. A. *RNA* **2007**, *13*, 1715-22.
(18) Xiu, X.; Hanek, A. P.; Wang, J.; Lester, H. A.; Dougherty, D. A. *J Biol Chem* **2005**, *280*, 41655-66.
(19) Unwin, N. *J Mol Biol* **2005**, *346*, 967-89.
(20) Unwin, N. *FEBS Lett* **2003**, *555*, 91-5.
(21) Miyazawa, A.; Fujiyoshi, Y.; Unwin, N. *Nature* **2003**, *423*, 949-55.
(22) Unwin, N.; Miyazawa, A.; Li, J.; Fujiyoshi, Y. *J Mol Biol* **2002**, *319*, 1165-76.
(23) Unwin, N. *Novartis Found Symp* **2002**, *245*, 5-15; discussion 15-21, 165-8.
(24) Hanek, A. P.; Lester, H. A.; Dougherty, D. A. *J Am Chem Soc* **2008**, *130*, 13216-8.
(25) Chakrapani, S.; Bailey, T. D.; Auerbach, A. *J Gen Physiol* **2004**, *123*, 341-56.
(26) Lee, W. Y.; Sine, S. M. *Nature* **2005**, *438*, 243-7.

Chapter 2

A Unified View of the Role of Electrostatic Interactions in Modulating the Gating of Cys-Loop Receptors

Reproduced in part from:
X.Xiu, A.P. Hanek, J. Wang, H.A. Lester, and D.A. Dougherty
J. Biol. Chem. **2005**, 280 (50), 41655-41666

2.1 Introduction

The Cys-loop superfamily of neurotransmitter-gated ion channels plays a prominent role in mediating fast synaptic transmission. Receptors for acetylcholine (nicotinic ACh receptor, nAChR), serotonin (5-HT_3 receptor), γ-aminobutyric acid (GABA, types A and C receptors), and glycine are known, and the receptors are classified as excitatory (cation-conducting; nAChR and 5-HT_3) or inhibitory (anion-conducting; GABA and glycine). Malfunctions in these receptors are responsible for a number of "channelopathies," and the receptors are targets of pharmaceutical efforts toward treatments for a wide range of neurological disorders, including Alzheimer's disease, Parkinson's disease, addiction, schizophrenia, and depression.[1,2] The receptors share a common architecture, are significantly homologous, and are known to have evolved from a single ancestral gene that coded for an ACh receptor.

The gating mechanism for the Cys-loop superfamily is one of the most challenging questions in molecular neuroscience. At issue is how the binding of a small molecule neurotransmitter can induce a structural change in a large, multisubunit, integral membrane protein sufficient to open (gate) a previously closed ion channel contained within the receptor.[3,4] All evidence indicates that the neurotransmitter-binding site is

quite remote (50–60 Å) from the channel gate, the region that blocks the channel when the neurotransmitter is absent and that must move to open the channel.

The quest for a gating mechanism has been greatly aided by several recent structural advances. First, crystal structures of the soluble acetylcholine-binding protein (AChBP),[5-7] which is homologous to the extracellular domain of the nAChR and, by extension, other members of the superfamily, provide a good sense of the layout of the agonist-binding site and its relationship to the rest of the receptor. Second, continued refinement of cryo-EM images of the *Torpedo* nAChR by Unwin and co-workers,[8-11] incorporating insights gained from the AChBP structure, has produced a full atomic scale model (Protein Data Bank code 2BG9) of the nAChR. It is important to appreciate that 2BG9, although heuristically quite valuable, is not a crystal structure of the nAChR. Rather, it is a model built from low resolution data and homology modeling. Nevertheless, it represents a substantial advance for the field, and all modern attempts to obtain molecular scale information on the structure and function of Cys-loop receptors must consider this as a starting point.

The full 2BG9 model of the nAChR[11] immediately suggested ways in which the agonist-binding site could couple to the transmembrane region and thus initiate gating. As summarized in Figure 2.1, loops 2, 7, and 9 from the AChBP structure are oriented toward the transmembrane region, and indeed, in 2BG9 these loops make contacts with parts of the transmembrane domain. Note that loop 7 is the eponymous Cys-loop. The transmembrane region consists of four α-helices per subunit, labeled M1–M4. It is accepted that M2 lines all or most of the channel. Helix M1 extends out of the transmembrane region toward the extracellular domain, creating a segment termed pre-

M1. Although M4 is somewhat separated from the rest of the protein in 2BG9, recent modeling studies produce a more compact structure in which M4 is more intimately involved.[12] In particular, the carboxy terminus of M4, a region we will term post-M4, can contact the extracellular domain. A key structure is the M2–M3 loop, a short connector between the two transmembrane helices. Topological considerations have long placed this loop at the interface between the transmembrane and extracellular domains. That expectation was resoundingly confirmed by Protein Data Bank code 2BG9, and many workers have anticipated that this loop could play an important role in gating. Indeed, recent work[13] has established that a key proline at the apex of the M2–M3 loop provides the conformational switch that gates the channel in the 5-HT_3 receptor.

Several groups have attempted to identify key interactions in the interface between the extracellular domain and the transmembrane domain, and we discuss some of these results below. This interface contains a number of charged residues, and most efforts have focused on these, attempting to find crucial electrostatic interactions that regulate gating. Specific hydrophobic interactions have also been proposed.[8,14] Several interacting pairs have been identified in various receptors,[15,16] and specific gating models based on critical electrostatic interactions have been proposed.[17-20] We note from the start, however, that *none* of the proposed interactions are conserved across the superfamily. We have been puzzled by the notion that in this closely related family of receptors, the mechanism of action of the essential function of the receptors seems to vary from system to system.

In the present work we argue that specific, pairwise electrostatic interactions at the interface between the transmembrane and extracellular domains are not critical to

gating. Rather, we argue it is the global charging of this region and the network of interacting ionic residues that are critical to receptor function. We present an overall analysis of charged interfacial residues in the Cys-loop superfamily, extensive mutagenesis studies of loop 2 residues involved in potential electrostatic interactions in the nAChR, and a reconsideration of previously published data on other receptors to support the model.

2.2 Results

2.2.1 Statistical analysis of the gating interface

For the purposes of discussion and analysis, we have defined a "gating interface" between the extracellular domain and the transmembrane domain. It is comprised of the following six segments: three from the extracellular domain (all or parts of loops 2, 7, and 9) and three from the transmembrane domain (pre-M1, M2–M3, and post-M4). The precise residues considered are given in Table 2.1. Unless otherwise noted, we will use the residue numbering system accepted for the nAChR α_1 subunit. The selection criterion for the gating interface was geometric; only residues that could reasonably be considered to experience a meaningful electrostatic interaction with another component of the gating interface were included. Because of the low resolution of the nAChR structure and the further uncertainty introduced by extrapolating to other Cys-loop receptors, precise distance constraints were not applied. Rather, as illustrated in Figure 2.1, we chose a contiguous band of residues in the region where the extracellular and transmembrane domains meet. Some leeway must be given in selecting possible interactions, as residues that are not in direct contact in 2BG9 could become so on transit from the closed state to the open state or when considering another receptor. Extending

the definition further out from the interface did not significantly impact the analysis. We will refer to the extracellular component (from loops 2, 7, and 9) and the transmembrane component (from pre-M1, M2–M3, and post-M4) when discussing the gating interface.

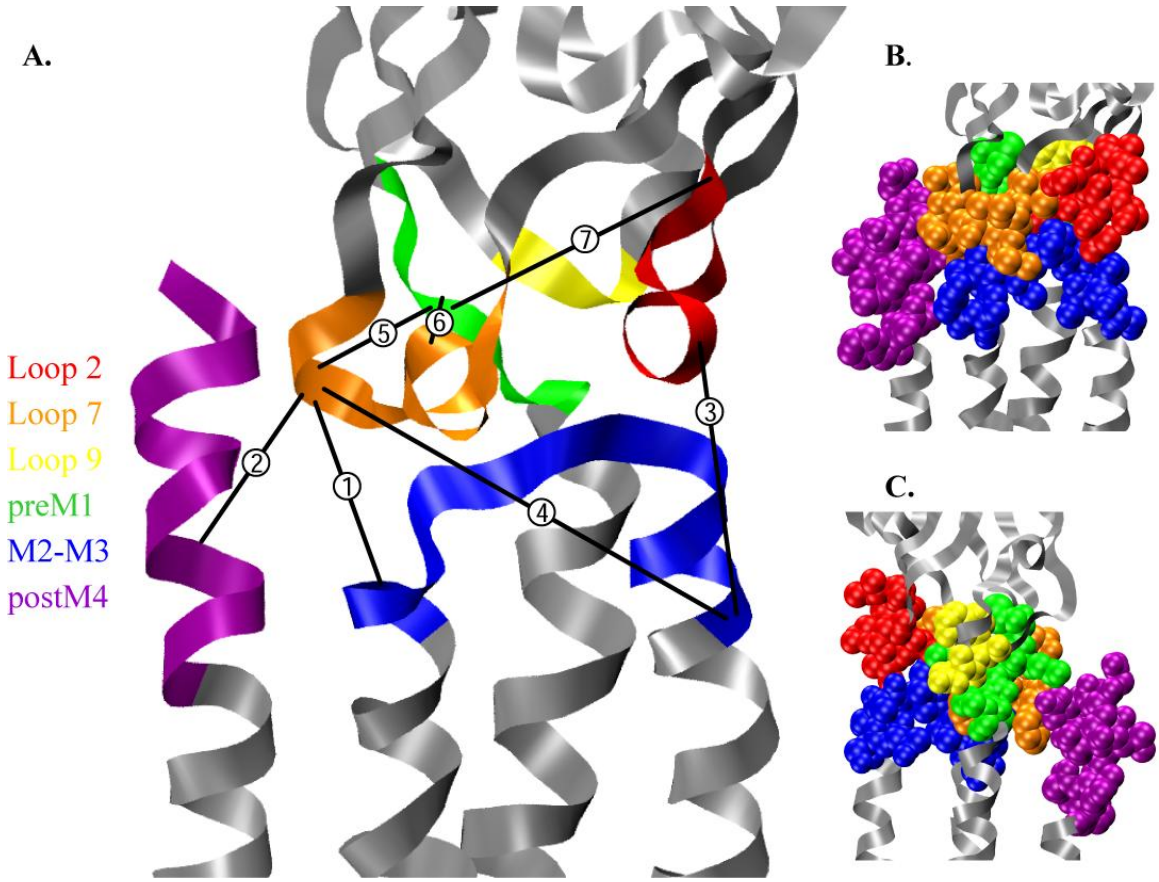

Figure 2.1 Views of the gating interface. Structure is the full model of an α subunit of the *Torpedo* nAChR developed by Unwin[11] (Protein Data Bank code 2BG9). Regions of the gating interface, as defined in text, are color-coded. **A**, ribbon diagram, also including pairwise interactions from various studies that have been proposed to contribute to the gating mechanism. Even though they are from different receptors and could be important in different states of the receptor, they are mapped onto the *Torpedo* structure to provide some sense of relative spatial relationships. Distances range from ~6 to ~20 Å. Interactions are as follows: *1*, D138 to K276 of muscle nAChR α_1 subunit ; *2*, D138 to R429 of muscle nAChR α_1 subunit; *3*, D57 to K279 of $GABA_A$ α_1 subunit; *4*, D149 to K279 of $GABA_A$ α_1 subunit; *5*, K215 to D146 of $GABA_A$ β_2 subunit; *6*, K215 to D139 of $GABA_A$ β_2 subunit; and *7*, K215 to D56 of $GABA_A$ β_2 subunit. **B**, same view as **A** with gating interface residues in space filling. **C**, view in B rotated 180° around vertical axis.

To search for patterns of charged residues, we considered the sequences of 124 subunits from the Cys-loop superfamily, 74 cationic and 50 anionic channel subunits (data not shown). Table 2.1 shows 22 representative subunits, 11 cationic (excitatory)

channels and 11 anionic (inhibitory) channels, and also serves to define the various segments. Table 2.2 summarizes the analysis of the full collection of the 124 subunits. Shown for each segment of the interface are the number of cationic residues (Lys and Arg), the number of anionic residues (Asp and Glu), the net charge (Z), and the number of charged residues (N).

Table 2.1 Selected sequences in the gating interface, highlighting cationic (blue) and anionic (red) residues

	Loop 2	Loop 7	L9	Pre-M1	M2-M3 Linker	Post-M4
Tor α	DEVNQI	IIVTHFPFDQ	EW	MQIRP	STSSAVPLIGKY	FAGRLIELSQEG
Tor β	NEKIEE	IKVMYFPFDW	QW	IQRKP	ETSLSVPIIIRY	FLDASHNVPPDN
Tor δ	NEKEEA	IAVTYFPFDW	EW	IQRKP	ETSLNVPLIGKY	FLTGHFNQVPEF
Tor γ	KETDET	INVLYFPFDW	EW	IRRKP	ETALAVPLIGKY	FVMGNFNHPPAK
nACh α_1	DEVNQI	IIVTHFPFDE	EW	MQRLP	STSSAVPLIGKY	FAGRLIELHQQG
nACh β_1	NEKDEE	IQVTYFPFDW	QW	IRRKP	ETSLAVPIIIKY	FLDATYHLPPPE
nACh δ	NEREEA	ISVTYFPFDW	EW	IQRKP	ETSQAVPLISKY	FLMAHYNQVPDL
nACh γ	KEVEET	ISVTYFPFDW	EW	IRRKP	ATSMAIPLVGKF	FLQGVYNQPPLQ
nACh α_4	DEKNQM	IDVTFFPFDQ	EW	IRRLP	STSLVIPLIGEY	FLPP--WLAGMI
nACh α_7	DEKNQV	IDVRWFPFDV	EW	MRRRT	ATSDSVPLIAQY	LMSAPNFVEAVS
5HT$_3$A	DEKNQV	LDIYNFPFDV	EW	IRRRP	ATAIGTPLIGVY	VMLWSIWQYA--
GABA α_1	SDHDME	MHLEDFPMDA	QY	LKRKI	KVAYATAM-DWF	LNREPQLKAPTP
GABA α_2	SDTDME	MHLEDFPMDA	QY	LKRKI	KVAYATAM-DWF	LNREPVLGVSP-
GABA α_3	SDTDME	MHLEDFPMDV	QY	LKRKI	KVAYATAM-DWF	VNRESAIKGMIR
GABA α_4	SDVDME	MRLVDFPMDG	QY	LKRKM	KVSYLTAM-DWF	LSKDTMEKSESL
GABA α_5	SDTEME	MQLEDFPMDA	QY	LKRKI	KVAYATAM-DWF	LNREPVIKGAAS
GABA α_6	SDVEME	MRLVNFPMDG	QY	LQRKM	KVAYATAM-DWF	LSKDTMEVSSSV
GABA β_1	SEVNMD	MDLRRYPLDE	QF	LKRNI	KIPY-VKAIDIY	VN----------
GABA β_2	SEVNMD	MDLRRYPLDE	QF	LKRNI	KIPY-VKAIDIY	VN----------
GABA β_3	SEVNMD	MDLRRYPLDE	QF	LKRNI	KIPY-VKAIDIY	VN----------
Gly α_1	AETTMD	MDLKNFPMDV	QF	LERQM	KVSY-VKAIDIW	KIVRREDVHNQ-
Gly α_2	TETTMD	MDLKNFPMDV	QF	LERQM	KVSY-VKAIDIW	KIVRHEDVHKK-
	44 49	130 139	175	207211	266 277	426

The abbreviations used are as follows: Tor, nAChR from *Torpedo californica*; nACh, nicotinic ACh receptor; 5-HT$_3$A, 5-HT$_3$ receptor, type A. All sequences were from human receptors except Tor and nACh α_1, β_1, δ, γ, which were from mouse muscle.

Although there is some variation, the typical gating interface contains 47 residues: 18 in the extracellular component and 29 in the transmembrane component. On average, 11.1 or 24% of these residues are charged. This is not significantly different from expectation based on the overall frequencies of occurrence of Asp, Glu, Arg, and Lys in

proteins (July, 2004, Swiss Protein Database). Most of the residues of the gating interface are or can be easily imagined to be water-exposed to some extent; therefore, this global result is not surprising. Of the ~11 charged residues found in the gating interface, only two are universally conserved, Asp-138 and Arg-209. So, although all Cys-loop receptors have a large number of ionic residues in the gating interface, their locations and absolute charges are variable.

Table 2.2 Charge characteristics of the gating interface

	+	-	Z	N
Loop 2	0.5	2.3	-1.8	2.8
Loop 7	0.4	1.9	-1.5	2.4
Loop 9	0.0	0.5	-0.5	0.5
Pre-M1	2.3	0.1	2.2	2.3
M2-M3	1.0	0.8	0.2	1.8
Post-M4	0.6	0.7	-0.1	1.3
Extracellular	0.9	4.8	-3.9	5.7
Transmembrane	3.9	1.6	2.3	5.5
Gating Interface	4.8	6.4	-1.6	11.1

The abbreviations used are as follows: + indicates number of cationic residues (K and R); - indicates number of anionic residues (D and E); Z indicates overall charge; and N indicates the number of ionic residues.

Although the two components of the gating interface do not have the same number of amino acids, the total number of charges is essentially the same (5.7 versus 5.5) for the two. There is, however, a dramatic difference in the net charge of the two components. The extracellular component has an overall negative charge, averaging -3.9 over the 124 subunits considered. The transmembrane component has an overall positive charge, averaging +2.3. Thus, there is a *global* electrostatic attraction in the interface, holding together the extracellular component and the transmembrane component. This interfacial electrostatic interaction is not created by simply putting anions in the extracellular component and cations in the transmembrane component; typically, there

are one cationic and five anionic side chains in the extracellular component but four cationic and two anionic side chains in the transmembrane component. We propose that it is the balance among all these charges that controls receptor function. With all these charges packed into a fairly compact space, we felt it more reasonable to consider a network of electrostatic interactions, rather than emphasizing any particular charged pair, as discussed below.

There is variability in the charging pattern of the gating interface. Considering only $GABA_A$ subunits, α_1 shows Z = -6 in the extracellular component and Z = +4 in the transmembrane component. In contrast, the α_4 subunit shows Z = - 4 in the extracellular component and Z = +2 in the transmembrane component. Despite the smaller Z values, the α_4 subunit actually has more ionic residues overall than α_1 (*n* =16 versus 14).

Looking more closely at the superfamily as a whole, it is clear that loop 2 carries the most negative charge per residue, followed by loop 7. The largest net positive charge is associated with pre-M1. The total number of charges (*N*) is slightly larger for the inhibitory channels (average of 11.8 versus 10.7). The "additional charge" is usually cationic, as the net charge is slightly more positive for the inhibitory channels (-1.1 versus -1.9).

We propose that Cys-loop receptors can function as long as the essential features of the electrostatic network are intact. Herein we present results concerning our study of the residues in the short, highly charged loop 2 of the nAChR α_1 subunit. As shown below, mutations that alter the charge balance are often well tolerated, apparently because they can be absorbed by the larger collection of charges. In fact, full charge reversals are quite acceptable. It appears that the essential criteria for maintaining channel function is

to conserve the number of charges in the gating interface, rather than any specific interaction involving loop 2 residues.

2.2.2 Mutations in loop 2 of the nAChR α_1 subunit

We have evaluated three residues, D44, E45, and V46, in loop 2 of the nAChR α_1 subunit.[21] These studies are both complementary to other studies in the nAChR[22] and parallel to those in other receptors,[14-16] though conservation is not strong across the superfamily. We studied the embryonic mouse muscle nAChR with a subunit composition of $(\alpha_1)_2\beta_1\delta\gamma$. This receptor shows extremely high homology with and is thus directly comparable to the *Torpedo* receptor modeled by 2BG9. We report the results of two-electrode voltage clamp determinations of EC_{50}, a measure of channel function reflecting contributions from agonist binding and gating. These residues are distinct from the agonist-binding site and therefore seem unlikely to contribute directly to binding. Furthermore, we show that representative mutations in the gating interface alter the relative efficacy of succinylcholine, a partial agonist of the receptor.[23] Extensive mutagenesis studies of loop 2 residues by Auerbach and co-workers[22] demonstrate that these residues contribute to channel gating rather than binding events. As such, we conclude that shifts in EC_{50} for the mutations reported here reflect alterations in channel gating behavior.

The loop 2 residues are DEVNQI. The neutral residues have been extensively studied by others,[22] thus we focused our efforts on the charged residues D44 and E45, and on V46, which is the loop 2 residue closest to the cell membrane in the 2BG9 structure and thus seems most likely to interact with the transmembrane domain. D44 is conserved in nicotinic α subunits and this position is generally a polar residue in other

nicotinic subunits as well as in other receptors. Charge neutralization (N) and charge reversal (K) lowered EC_{50} slightly, suggesting these mutations are well tolerated (Table 2.3).

Table 2.3 Mutations in loop 2 nAChR α_1 subunit

Mutant	EC_{50} (μM)	n_H	Mutant	EC_{50} (μM)	n_H
Wild Type	50 ± 2	1.6 ± 0.1	V46A	>1000	
D44K	14.3 ± 0.6	1.4 ± 0.1	V46I	59 ± 7	1.1 ± 0.1
D44N	20 ± 4	0.80 ± 0.08	V46T	>1000	
E45A	210 ± 20	1.1 ± 0.1	V46K	0.94 ± 0.07	1.5 ± 0.1
E45W	117 ± 7	1.3 ± 0.1	V46R	120 ± 10	1.4 ± 0.1
E45V	49 ± 4	1.9 ± 0.2	V46D	>1000	
E45D	19.2 ± 0.5	1.4 ± 0.1	V46E	>1000	
E45N	6.3 ± 0.1	1.4 ± 0.1	E45K/V46D	>1000	
E45K	6.5 ± 0.3	1.4 ± 0.1	E45K/V46E	>1000	
E45Q	1.9 ± 0.1	1.3 ± 0.1	E45R/V46D	N.E.	
E45R	1.6 ± 0.1	1.0 ± 0.1	E45R/V46E	N.E.	

The abbreviations used are as follows, N.E. = no expression as determined by radiolabelled bungarotoxin binding. EC_{50} > 1000 μM indicates sufficient surface expression and current to determine EC_{50} but that saturation had not been achieved with application of 1000 μM Ach.

Glutamate 45 (E45) is very highly conserved as an anionic (D or E) residue across the superfamily. Quite surprisingly, we find that full charge reversal (E45K or E45R) substantially lowers EC_{50} (Table 2.3), as does substitution by a neutral but polar residue (E45Q or E45N). Conversion to a hydrophobic residue (E45V) gives a wild type EC_{50}, while incorporation of a bulkier hydrophobic side chain (E45W) or reduction in the size of the side chain (E45A) result in only small increases in EC_{50}. There is no correlation between the side chain volume or hydrophobicity of the mutations at E45 (Figure 2.2).

Although the next residue in loop 2 is a neutral residue, V46, we made mutations here as well for the following reasons: (1) a proposal[8-11] based on the 2BG9 structure indicates that the V46 side chain interacts with the M2-M3 linker and is crucial to communication between the extracellular and transmembrane domains, and (2) the

surprising effect of charge reversal and charge neutralization at the preceding two residues caused us to wonder what the effects of introducing a charged side chain at V46 would be. The proposed interaction between the V46 side chain and the M2-M3 linker is discussed in depth in Chapter 4. In the present chapter we will restrict our presentation of results and discussion to the conventional mutations in Table 2.3.

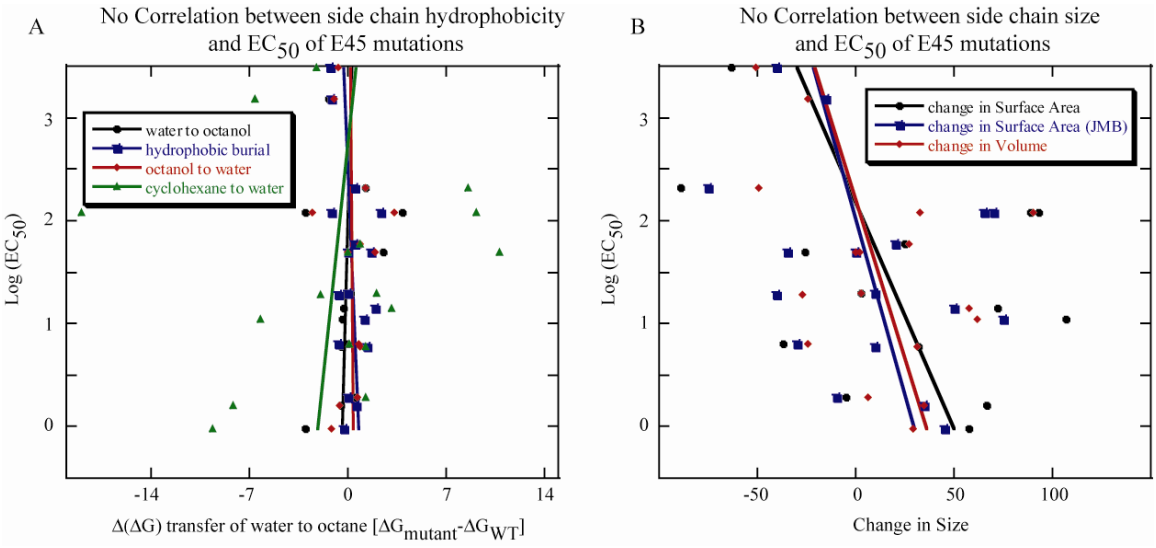

Figure 2.2 Shifts in EC_{50} of E45 mutations are not correlated with changes in side chain hydrophobitiy (**A**) or size (**B**). Four hydrophobicity scales (**A**) were used giving R=0.10 for transfer from water to octanol; 0.26 for hydrophobic burial; 0.03 for transfer from octanol to water; and 0.01 for transfer from cyclohexane to water. Three measures of size (**B**) give R=0.38, and 0.32 for surface area, respectively, and R=0.40 for volume measurements.

We reasoned that if interaction (1) is true, mutation to alanine should be highly deleterious to channel function, as was the case. Furthermore, we predicted that mutation to isoleucine would be essentially wild type, and that mutation to threonine, which is isosteric to valine, would affect EC_{50} only if the hydrophobicity of the side chain were important. The results validate our predictions and indicate that the hydrophobicity of the V46 side chain may be important, as mutation to threonine significantly impaired receptor function.

Given these results, it is surprising that introduction of a positively charged side chain (V46R) has little effect on EC_{50} or (V46K) lowers the EC_{50} ~50 fold. Conversely, introduction of a negatively charged side chain (V46D and V46E) results in a large shift in EC_{50} that cannot be measured. Attempts to rescue the effects of V46D and V46E by coupling with an EC_{50} lowering mutation at E45 (E45R or E45K) failed, and in the case of E45R resulted in loss of surface expression.

N47 in loop 2 of the nAChR α_1 subunit aligns with D57 in the $GABA_A$ α_1 subunit, which has been proposed to experience important electrostatic interactions in the $GABA_AR$.[16] Auerbach and co-workers[22] found that N47K shows a decrease in EC_{50} values while N47D shows an increase. Therefore at four consecutive residues in loop 2, introduction of a positive charge lowers the EC_{50}. Additionally, at the two neutral residues, V46 and N47, introduction of a negative charge has the opposite effect. These various side chains point in quite different directions in 2BG9. Although it is possible that all these side chains make specific electrostatic contacts that are being modulated in similar ways by the mutations introduced, it is far more likely that the global charge of loop 2, not a specific interaction, is essential to proper receptor function.

2.2.3 Studies of a Partial Agonist

To support our contention that mutations at the gating interface perturb the gating of the receptor rather than the agonist-binding site, we measured the relative efficacy (ε) of succinylcholine (SuCh), an nAChR partial agonist,[23] for wild type receptor as well as for several representative mutants. The relative efficacy is defined as the ratio of the maximal current elicited by the partial agonist to the maximal current elicited by a full agonist (ACh) (Equation 2.1). Equation 2.2 shows a highly simplified model of the

agonist binding and receptor gating processes, where R is receptor; c is closed; o is open; A is agonist; and β and α are the opening and closing rate constants, respectively. At saturating doses of agonist, all the receptors are forced into a di-liganded state (RA_2), so differences in I_{max} for the two agonists are due to differences in P_{open}. As such, ε reflects the ratio of P_{open} (the open channel probability) values for the partial and full agonists (Equation 2.1). Changes in P_{open} for an agonist are dependent only on changes in the gating rate constants (Equation 2.3). If a mutation has not altered the gating, but only the ligand binding of the receptor, the relative efficacies should be identical for the wild type and mutant receptors.[15,24]

$$\varepsilon = \frac{I_{max,PA}}{I_{max,FA}} = \frac{P_{open,PA}}{P_{open,FA}} \qquad \textbf{Equation 2.1}$$

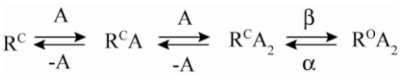

Equation 2.2

$$P_{open} = \frac{\beta}{\alpha + \beta} \qquad \textbf{Equation 2.3}$$

For the wild type nAChR, P_{open} for ACh is very nearly 1 but P_{open} for succinylcholine is only 7.5% that for acetylcholine (ε = 0.075). As a control, we examined a previously studied mutant known to affect gating. Mutation of a universally conserved leucine at the 9' position of M2 to a more polar residue such as serine (βL251S) substantially reduces EC_{50} values.[24-26] This residue forms part of the hydrophobic gate of the channel and is quite remote from the agonist-binding site, establishing it as a gating residue. As shown in Figure 2.3, the SuCh ε of the βL251S mutant is substantially increased over that of wild type. This indicates that P_{open} for SuCh has increased in the mutant, as expected for a mutation that substantially affects gating. In the α subunit, the loop 2 mutations E45R and E45Q decrease EC_{50} more than 25-fold.

All three mutations greatly increase ε, for SuCH, giving values near 1 (Figure 2.3). This indicates that these mutations ease receptor opening, allowing SuCh to act as a full agonist. More importantly, the mutation E45V, which has no affect on EC_{50}, does not alter the ε of SuCh.

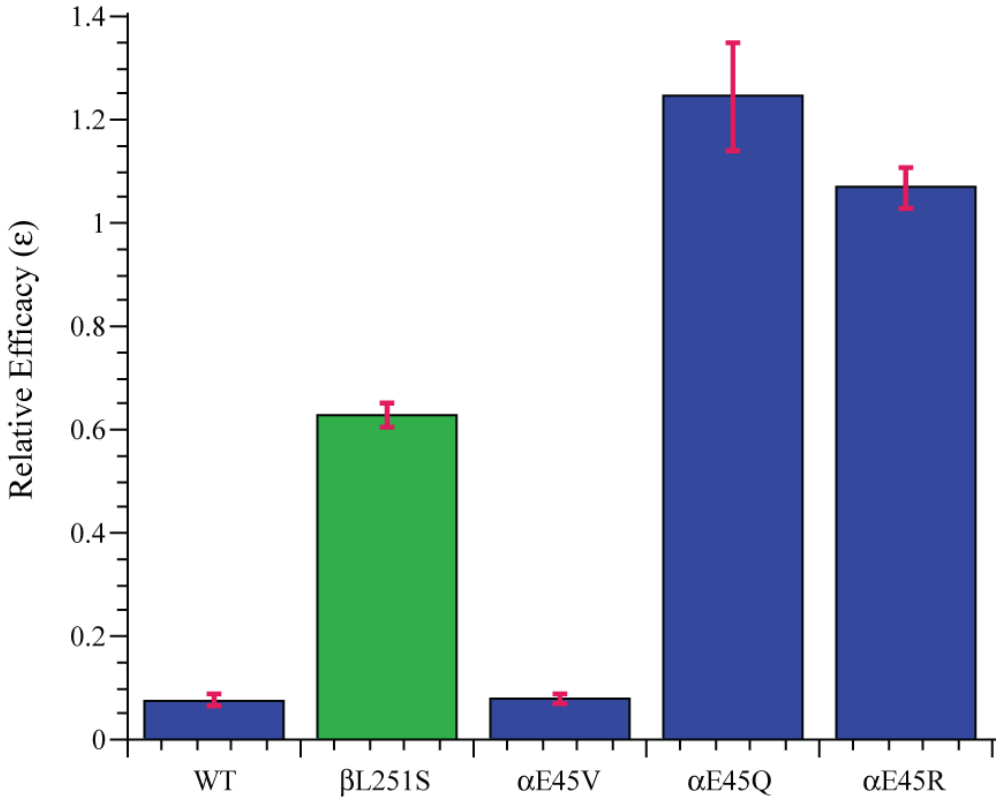

Figure 2.3 Relative efficacy of succinylcholine for representative mutations. Mutations that lower EC_{50} by affecting gating (βL251S, αE45Q, and αE45R) substantially increase the relative efficacy (ε).

2.3 Discussion

We have defined for the Cys-loop superfamily of receptors a gating interface that is composed of segments from the extracellular domain and the transmembrane domain that can reasonably be assumed to be juxtaposed, based on mutagenesis data and the best available structural information. Analysis of representative subunits from the superfamily indicates that there are a large number of ionic residues in the interface, but

for the most part their precise locations and particular charges are not conserved. Many workers, including ourselves, have sought specific ion pair interactions that exert precise control over the gating process. However, we have come to believe that, with such a large number of charges clustered in a fairly compact region, it is not meaningful to isolate specific ion pairs. Rather, the global charging pattern of the gating interface is what controls gating. Receptors have evolved to create a compatible collection of charged residues that allow the receptor to assemble and also facilitates the existence of and interconversions among multiple states.

In the current work we have presented data on charge reversal, charge neutralization, and charge introduction at three loop 2 residues. Similar mutations in other regions of the gating interface of nAChR α_1 are shown in Table 2.4.[1] Although specific ionic residues are generally not conserved, overall charging patterns are. Within the gating interface the extracellular component carries a net negative charge, and the transmembrane component carries a net positive charge. This creates a global electrostatic attraction at the interface that maintains the integrity of the receptor as it transitions from the mostly β-sheet, relatively polar extracellular domain to the α-helical, nonpolar transmembrane domain.

Several lines of evidence support this way of thinking about the gating interface. Typically, charge reversals are considered to be dramatic mutations, and they might be expected to disrupt a functionally important interface. However, one of the more remarkable features of the mutagenesis data of Tables 2.3 and 2.4 is the tolerance of the gating region to such charge disruptions. In fact, very often the EC_{50} value is *lowered* by

[1] These data were collected by Xinan Xiu and are presented here for the purpose of discussion of a global electrostatic gating interface.

such strong perturbations. It seems implausible that such dramatic mutations involving the introduction or reversal of charge just happen to lead to a viable ion pair that is tolerated by the receptor. Rather, we believe the entire gating interface is tolerant of charge up to a threshold. By distributing a large number of charges across an interface, it is possible to have movement along that interface without creating adverse situations of like charges interacting strongly or a single charge in isolation in a poorly solvated environment.

Table 2.4 Mutations in loop 7, loop 9, pre-M1, M2-M3 linker, and post M4 nAChR α_1 subunit

Mutant	EC_{50} (μM)	n_H	Mutant	EC_{50} (μM)	n_H
Wild type	50 ± 2	1.6	S266K	62 ± 6	1.54
D138A	NF		T267A	36 ± 5	1.94
D138R	NF		T267D	24 ± 2	1.21
D138K	NF		T267K	26 ± 2	1.35
D138S	NF		S268D	0.59 ± 0.02	1.82
D138N	NF		S268E	0.18 ± 0.01	1.56
D138E	28 ± 2	1.45	S268K	7.5 ± 1	1.36
D138K/K276D	66 ± 10	1.01	S269D	12 ± 0.5	1.56
D138K/R429D	50 ± 3	1.45	S269E	0.08 ± 0.01	1.34
D138R/R429E	LE		S269K	9 ± 0.6	1.22
D138E/R429K	63 ± 9		R209A	NE	
D138K/K276D/R429D	67 ± 10		R209D	NF	
K276D	45 ± 6	1.39	R209E	NF	
K276E	38 ± 2	1.28	R209K	18 ± 1	1.66
K276D/R429D	51 ± 3	1.52	D138K/R209D	NF	
R429D	57 ± 5	1.46	D138R/R209D	NS	
R429E	69 ± 5	1.29	E175R	120 ± 7	1.35
R429K	83 ± 4	1.48	E175R/R209E	NS	
R429A	90 ± 4	1.48			

The abbreviations used are as follows: NF, nonfunctional, no response to applied ACh but surface expression of receptor confirmed by α-bungarotoxin binding; L.E., functional, response to applied ACh are seen but are too weak to obtain EC_{50}; NS, no signal, no response to applied ACh, surface expression not independently verified; NE, no expression as determined by lack of α-bungarotoxin binding.

Across the superfamily, loop 2 always carries a net negative charge. When another negative charge is introduced, as in V46D, V46E, or N47D,[22] receptor function is hindered, suggesting there is an excess of negative charge in the region. In contrast,

introduction of a positive charge at the same sites, thereby decreasing the net charge of loop 2 from -2 to -1, improves (V46K, N47K) or barely impacts (V46R) receptor function. Overall these changes decrease the average extracellular charge from -3.9 to -2.9, which is still a higher magnitude charge than the positive charge of the transmembrane domain. Charge neutralization at D44 and E45 (D44N and E45Q, respectively) has the same overall effect on the region and produces a similar result of lowering the EC_{50}. Charge reversal at D44 and E45 changes the loop 2 charging pattern in the nACh α_1 subunit to a net charge of zero, yet this change is well tolerated, likely because the extracellular domain still carries a net negative charge. It thus appears that the native negative charge stabilizes the closed state of the nicotinic receptor by interacting with a positive region.

A few charge reversals in the gating interface have been shown to be deleterious, and they can often be rescued by compensating charge reversals. For example, the universally conserved D138 is one such residue. In the nAChR α_1, the $GABA_A$ α_1[16] (where it is D149) and $GABA_A$ β_2[15] (where it is D146) compensating charge reversals can rescue the initial mutant (pairwise interactions *1, 2, 4,* and *5* in Figure 2.1, A). However, the systems use completely different residues from apparently very different regions of the interface. There is certainly no universal pattern, and it appears that rather than conserving some specific pairwise interaction, it is the global charging pattern of the trio of residues that is most important. At another site, D139 of $GABA_A$ β_2[15] (I131 of nAChR α_1), as many as five different sites can contribute to compensating a charge reversal, with a gradation of efficiencies.

We conclude that no one ion pair interaction is crucially important to receptor gating across the entire Cys-loop superfamily; clearly each receptor is different. However, it may be that there is a consistent mechanism across the superfamily, but one that does not single out any particular ion pair. Several groups have suggested that the extracellular domain and the transmembrane domain change relative positions going from the closed to the open state. Harrison and co-workers[16] propose that a residue on loop 7 moves closer to a residue on M2–M3 in the $GABA_A$ receptor α_1 subunit (D149 and K279, $GABA_A$ numbering; pairwise interaction 4 in Figure 2.1, A). The detailed gating model from Unwin[11] emphasizes differential interactions between loops 2/7 (extracellular domain) and M2–M3 (transmembrane domain) along the gating pathway. We have proposed recently[13] that loop 2 and especially loop 7 interact with a specific proline on M2–M3 differentially in the open and closed states. In order to accommodate the structural rearrangement at the gating interface, the many charges involved must be comfortable in the environments provided by both the open and closed states as well as avoid any highly adverse interactions in the transition state separating the two. With a large number of charges distributed throughout the interface, the extracellular domain and the transmembrane domain can slide past one another (or twist or turn or unclamp . . .) while maintaining an acceptable network of compensating charges throughout the process. During the movement, some ion pair interactions will strengthen and some will weaken, but crucial on/off interactions seem less critical. There are clearly many ways to achieve the proper balance, and each system has evolved an ionic array that supports the desired gating behavior. The essential mechanism is universal across the Cys-loop superfamily, but the precise details vary from system to system.

2.4 Materials and Methods

Mutagenesis and mRNA Synthesis: The mRNA that codes for the muscle type nAChR subunits (α, β, δ, and γ) was obtained by linearization of the expression vector (pAMV) with NotI (Roche), followed by *in vitro* transcription using the mMessage mMachine kit purchased from Ambion (Austin, TX). The mutations in all subunits were made following the QuickChange mutagenesis protocol (Stratagene).

Electrophysiology and Data Analysis: mRNAs of α, β, δ, and γ subunits were mixed in the ratio of 2:1:1:1 and microinjected into stage VI oocytes of *Xenopus laevis*. Electrophysiology recordings were performed 24–48 h after injection in two-electrode voltage clamp mode using the OpusXpress 6000A (Axon Instruments, Molecular Devices). The holding potential was -60 mV and agonist was applied for 15 seconds.[27] Acetylcholine chloride and succinylcholine chloride dihydrate were purchased from Sigma. All drugs were diluted to the desired concentrations with calcium-free ND96 buffer. Dose-response data were obtained for at least eight concentrations of agonists and for a minimum of five oocytes. Mutants with I_{max} equal to or greater than 100 nA were defined as functional. EC_{50} and Hill coefficients (n) were calculated by fitting the dose-response relation to the Hill equation (Equation 2.4). All data are reported as mean ± standard error.

$$I = \frac{I_{\max}}{1 + EC_{50}/[A]^n} \qquad \textbf{Equation 2.4}$$

If saturation was not reached at 1000 μM concentrations of acetylcholine, the EC_{50} value could not be calculated. For two mutations, αV46A and αV46T, a second mutation was incorporated at the 9' position of the β subunit (βL251S). This mutation is

known to reduce the wild type EC_{50} to 1.2 μM.[25] The EC_{50} of the double mutant was then determined as described. For scatter plots the EC_{50} value of the double mutant was multiplied by 41.7 (50/1.2) to get a corrected EC_{50} value. The corrected EC_{50} value was used for the linear regression analysis.

EC_{50} values for succinylcholine were measured in the same manner. Maximal currents elicited by acetylcholine, $I_{max(acetylcholine)}$, and by succinylcholine, $I_{max(succinylcholine)}$, were measured sequentially at saturating concentrations on the same cell. The ratio of maximal current of succinylcholine to acetylcholine ($I_{max(succinylcholine)}/I_{max(acetylcholine)}$) was calculated for each cell and is reported as the mean ± standard error.

Bungarotoxin Binding: 48–72 hours after injection, oocytes were prewashed with calcium-free ND96 buffer with 1 mg/ml bovine serum albumin, then transferred to the same buffer with the addition of 10 nM ^{125}I-α-bungarotoxin (PerkinElmer Life Sciences), and incubated for 1 h at room temperature.[28] Oocytes were then washed four times and counted individually in a gamma counter. Oocytes injected with 50 nl of water were used to determine background. Mutants with more than five times the background reading are regarded to have sufficient expression.

2.6 References

(1) Leite, J. F.; Rodrigues-Pinguet, N.; Lester, H. A. *J Clin Invest* **2003**, *111*, 436-7.
(2) Paterson, D.; Nordberg, A. *Prog Neurobiol* **2000**, *61*, 75-111.
(3) Changeux, J.; Edelstein, S. J. *Curr Opin Neurobiol* **2001**, *11*, 369-77.
(4) Lester, H. A.; Dibas, M. I.; Dahan, D. S.; Leite, J. F.; Dougherty, D. A. *Trends Neurosci* **2004**, *27*, 329-36.
(5) Brejc, K.; van Dijk, W. J.; Klaassen, R. V.; Schuurmans, M.; van Der Oost, J.; Smit, A. B.; Sixma, T. K. *Nature* **2001**, *411*, 269-76.
(6) Celie, P. H.; Klaassen, R. V.; van Rossum-Fikkert, S. E.; van Elk, R.; van Nierop, P.; Smit, A. B.; Sixma, T. K. *J Biol Chem* **2005**, *280*, 26457-66.
(7) Celie, P. H.; van Rossum-Fikkert, S. E.; van Dijk, W. J.; Brejc, K.; Smit, A. B.; Sixma, T. K. *Neuron* **2004**, *41*, 907-14.
(8) Miyazawa, A.; Fujiyoshi, Y.; Unwin, N. *Nature* **2003**, *423*, 949-55.
(9) Unwin, N. *Novartis Found Symp* **2002**, *245*, 5-15; discussion 15-21, 165-8.
(10) Unwin, N. *FEBS Lett* **2003**, *555*, 91-5.
(11) Unwin, N. *J Mol Biol* **2005**, *346*, 967-89.
(12) Taly, A.; Delarue, M.; Grutter, T.; Nilges, M.; Le Novere, N.; Corringer, P. J.; Changeux, J. P. *Biophys J* **2005**, *88*, 3954-65.
(13) Lummis, S. C.; Beene, D. L.; Lee, L. W.; Lester, H. A.; Broadhurst, R. W.; Dougherty, D. A. *Nature* **2005**, *438*, 248-52.
(14) Kash, T. L.; Kim, T.; Trudell, J. R.; Harrison, N. L. *Neurosci Lett* **2004**, *371*, 230-4.
(15) Kash, T. L.; Dizon, M. J.; Trudell, J. R.; Harrison, N. L. *J Biol Chem* **2004**, *279*, 4887-93.
(16) Kash, T. L.; Jenkins, A.; Kelley, J. C.; Trudell, J. R.; Harrison, N. L. *Nature* **2003**, *421*, 272-5.
(17) Absalom, N. L.; Lewis, T. M.; Kaplan, W.; Pierce, K. D.; Schofield, P. R. *J Biol Chem* **2003**, *278*, 50151-7.
(18) Kash, T. L.; Trudell, J. R.; Harrison, N. L. *Biochem Soc Trans* **2004**, *32*, 540-6.
(19) Schofield, C. M.; Jenkins, A.; Harrison, N. L. *J Biol Chem* **2003**, *278*, 34079-83.
(20) Schofield, C. M.; Trudell, J. R.; Harrison, N. L. *Biochemistry* **2004**, *43*, 10058-63.
(21) Xiu, X.; Hanek, A. P.; Wang, J.; Lester, H. A.; Dougherty, D. A. *J Biol Chem* **2005**, *280*, 41655-66.
(22) Chakrapani, S.; Bailey, T. D.; Auerbach, A. *J Gen Physiol* **2004**, *123*, 341-56.
(23) Placzek, A. N.; Grassi, F.; Papke, T.; Meyer, E. M.; Papke, R. L. *Mol Pharmacol* **2004**, *66*, 169-77.
(24) Filatov, G. N.; White, M. M. *Mol Pharmacol* **1995**, *48*, 379-84.
(25) Kearney, P. C.; Zhang, H.; Zhong, W.; Dougherty, D. A.; Lester, H. A. *Neuron* **1996**, *17*, 1221-9.
(26) Labarca, C.; Nowak, M. W.; Zhang, H.; Tang, L.; Deshpande, P.; Lester, H. A. *Nature* **1995**, *376*, 514-6.
(27) Cashin, A. L.; Petersson, E. J.; Lester, H. A.; Dougherty, D. A. *J Am Chem Soc* **2005**, *127*, 350-6.
(28) Yoshii, K.; Yu, L.; Mayne, K. M.; Davidson, N.; Lester, H. A. *J Gen Physiol* **1987**, *90*, 553-73.

Chapter 3

Investigations of pH dependence of Loop 2 of the nAChR α_1 subunit

3.1 Introduction

Cys-loop ligand gated ion channels mediate rapid synaptic transmission in the central and peripheral nervous systems. Receptors for acetylcholine (nicotinic acetylcholine, nACh) and serotonin (5-HT_3) are classified excitatory (cation conducting) while receptors for γ-aminobutyric acid (GABA) and glycine (Gly) are termed inhibitory (anion conducting). Proper functioning of these receptors is crucial to normal brain function. As such, malfunctions in these receptors lead to a number of "channelopathies" making the receptors a target of pharmaceutical efforts for a range of neurological disorders, including addiction, Parkinson's disease, Alzheimer's disease, schizophrenia, and depression.[1,2]

At rest Cys-loop receptors are in a closed non conducting state. Upon binding of their cognate neurotransmitter (agonist), the channels undergo a conformational change to an open ion-conducting state. The conformational change is analogous to the opening of a gate, and the process of going from a closed channel to an open one is often referred to as channel gating. The gating mechanism for this superfamily of receptors is one of the most challenging questions in molecular neuroscience. The neurotransmitter binding site is located 50-60 Å from the channel gate, and it remains unclear how binding of a small organic molecule can induce a structural change in a large, multisubunit, integral membrane protein.

The superfamily shares a common topology of five homologous subunits arranged pseudo-symmetrically around a central ion-conducting pore. Each subunit (Figure 3.1) contains a large amino-terminal extraceullular domain comprised of two beta sheets, followed by four membrane-spanning helices (M1-M4) and a short extracellular carboxy tail. The M2 helix of each subunit lines the channel pore and contains the channel gate. Ligand binding sites are located in the extracellular domain at select subunit interfaces. Numerous biochemical studies have established the importance of loops 2 and 7 (Figure 3.1 C, D) in the extraceullular domain and the M2-M3 linker as critical to channel gating.[3-9]

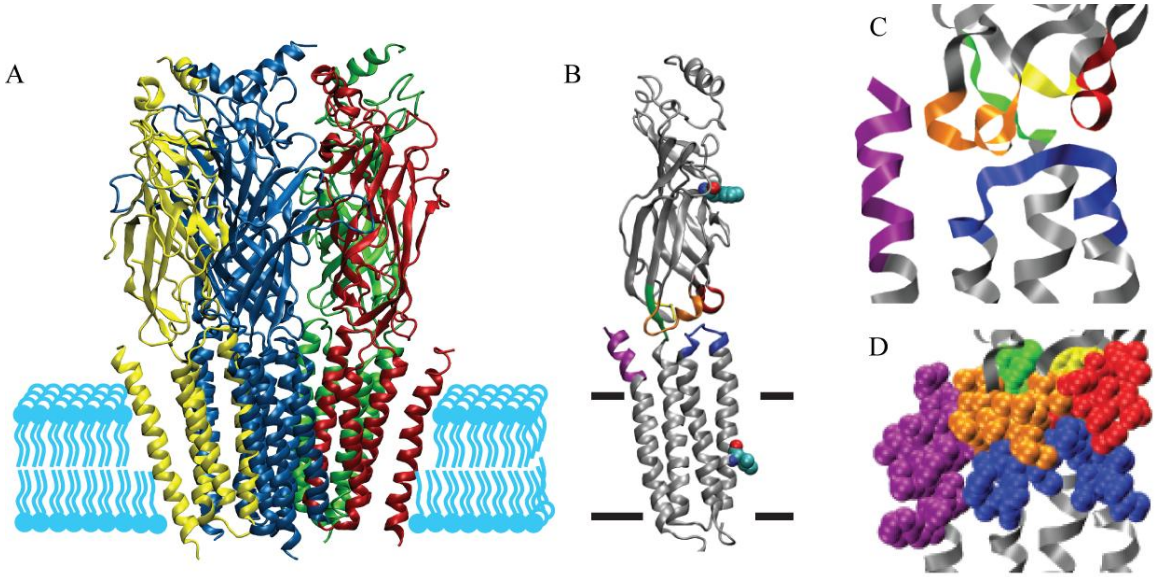

Figure 3.1 Cys-loop ligand gated ion channel structure. (**A**) The *Torpedo* nAChR from PDB 2BG9 is nearly identical to the mouse muscle nAChR. α subunits are shown in blue, β in green, δ in red, and γ in yellow. A single subunit (**B**) with the ligand binding site and channel gate highlighted as Van der Waals residues. A geometrically defined gating interface (**C**) in ribbon and space fill models (**D**) from the 2BG9 structure. Loop 2 is shown in red, loop 7 in orange, and the M2-M3 linker in blue.

As discussed in Chapter 2,[10] studies in the mouse muscle nAChR have demonstrated the important balance of charged residues at the gating interface of Cys-loop receptors. Loop 2 was of particular interest to us as introduction of positive charge

at four consecutive residues (D44, E45, V46, and N47) in this loop lowered EC_{50}.[3,10] In the nAChR α_1 subunit the first two residues of Loop 2 are aspartate and glutamate (positions 44 and 45, respectively). D44 is conserved among the nACh α subunit and E45 is highly conserved as a negatively charged residue among the superfamily. The short length of loop 2 and high degree of conservation of charge (Table 2.1) suggested there may be a perturbed pK_a in this region of the protein. Therefore, we hypothesized that the region may be sensitive to changes in pH and that this sensitivity results from changes in the protonation state of the side chains.

3.2 Results

On average the pK_a of the side chain carboxylic acid of aspartate and glutamate in a protein are 3.65 and 4.25, respectively,[11] and thus the residues are in the carboxylate form at physiological pH. If, however, loop 2 has an altered pK_a due to the number of charged species, it is possible that one of the D44 and E45 side chains is protonated. To address this possibility, we both lowered and raised the pH of the extracellular recording solution, normally a pH of 7.5, by two pH units (pH=5.5 and 9.5, respectively). The change in pH did not significantly impact EC_{50} (Table 3.1) indicating that the receptor is not highly sensitive to pH and that a perturbed pK_a at loop 2 is unlikely.

Table 3.1 EC_{50} (μM) of loop 2 histidine mutations grouped by pH

	pH = 5.5		**pH=7.5**		**pH=9.5**	
	EC_{50}	n_H	EC_{50}	n_H	EC_{50}	n_H
Wild Type	64 ± 2	1.4 ± 0.1	50 ± 2	1.6 ± 0.1	71 ± 1	1.5 ± 0.1
D44H	45 ± 1	1.5 ± 0.1	41 ± 2	1.6 ± 0.1	48 ± 1	1.5 ± 0.1
E45H	4.3 ± 0.1	1.5 ± 0.1	5.8 ± 0.3	1.4 ± 0.1	5.3 ± 0.2	1.5 ± 0.1
V46H	75 ± 0.2	1.4 ± 0.1	61 ± 3	1.5 ± 0.1	94 ± 6	1.3 ± 0.1

Ideally, the pH would be lowered even further to modulate the protonation state of the D44 and E45 side chains. However, the health of the oocytes degrades at pH < 5.5. Thus we needed to incorporate a side chain that would change from neutral to positively charged when the pH was lowered to 5.5 from 7.5. In Chapter 2,[10] we found that introduction of a positive charge at D44, E45, and V46 decreased EC_{50}, thus these residues were selected for further study. At physiological pH, the imidazole side chain of histidine is neutral (Figure 3.2), but at pH<6.0 the imidazole ring is charged. By first incorporating histidne at the site of interest, we would thus be able to alter the protonation state, and thus the charge of the side chain by changing the pH of the extracellular media.

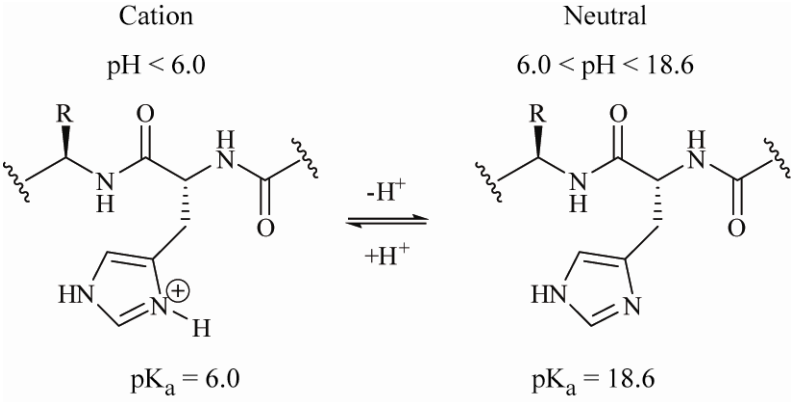

Figure 3.2 Protonation states of a histidine residue. At physiological pH, the imidazole side chain is neutral.

The EC_{50} of D44H was essentially that of wild type at physiological pH. Neither decreasing nor increasing the pH altered this EC_{50} (Table 3.1). In contrast, incorporation of histidine at position 45, greatly impacted channel function, lowering the EC_{50} ~10 fold. Lowering the pH had a small affect on EC_{50} while raising the pH did not. At the third postion, V46, mutation to histidine gave an EC_{50} similar to wild type. Both lowering and raising the pH increased EC_{50} slightly (1.5-fold and 2-fold, respectively) similar to wild type. The shape of the dose-response relationships for wild type and the mutant receptors

remains unchanged with varying pH (Figure 3.3), indicating the receptor is able to function properly.

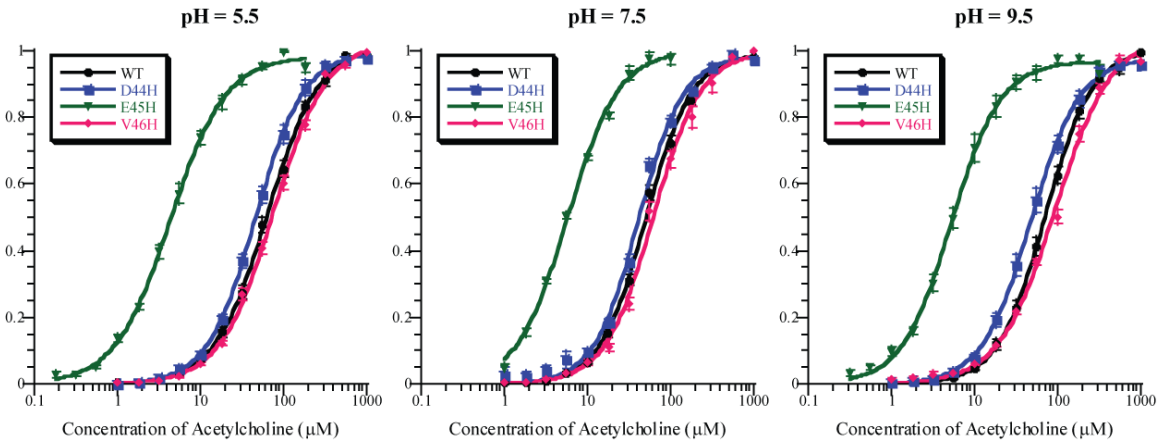

Figure 3.3 Dose response relationship for wild type (black), D44H (blue), E45H (green), and V46H (pink) mutants at varying pH. The y-axis corresponds to the whole cell current of each cell after normalizing to the maximal current for the given cell.

3.3 Discussion

Shifts in the EC_{50} of the wild type muscle nAChR do not show a one-directional trend with pH (Table 3.1). Rather, the EC_{50} increases with both an increase and decrease in pH. These changes in EC_{50} could be intrinsic to the receptor or the result of changes in the concentration of acetylcholine due to hydrolysis. Increasing the time between making acetylcholine solutions and conducting electrophysiology recordings resulted in higher EC_{50} values, suggesting degradation of acetylcholine contributes to the changes in EC_{50}. Ester hydrolysis of acetylcholine produces choline, a much weaker agonist of the receptor. Drug solutions were prepared by identical means for both the wild type and mutant receptors. We use the changes in EC_{50} for wild type, which accounts for both the intrinsic response of the protein to pH and degradation of acetylcholine as a reference point for the mutant receptors. The ratio of the EC_{50} at low pH to that of the

physiological pH is denoted as $R_{pH,5.5}$ and has a value of 1.28±0.06 for wild type. For the higher pH, the wild type receptor has an $R_{pH,9.5}$ equal to 1.42±0.06.

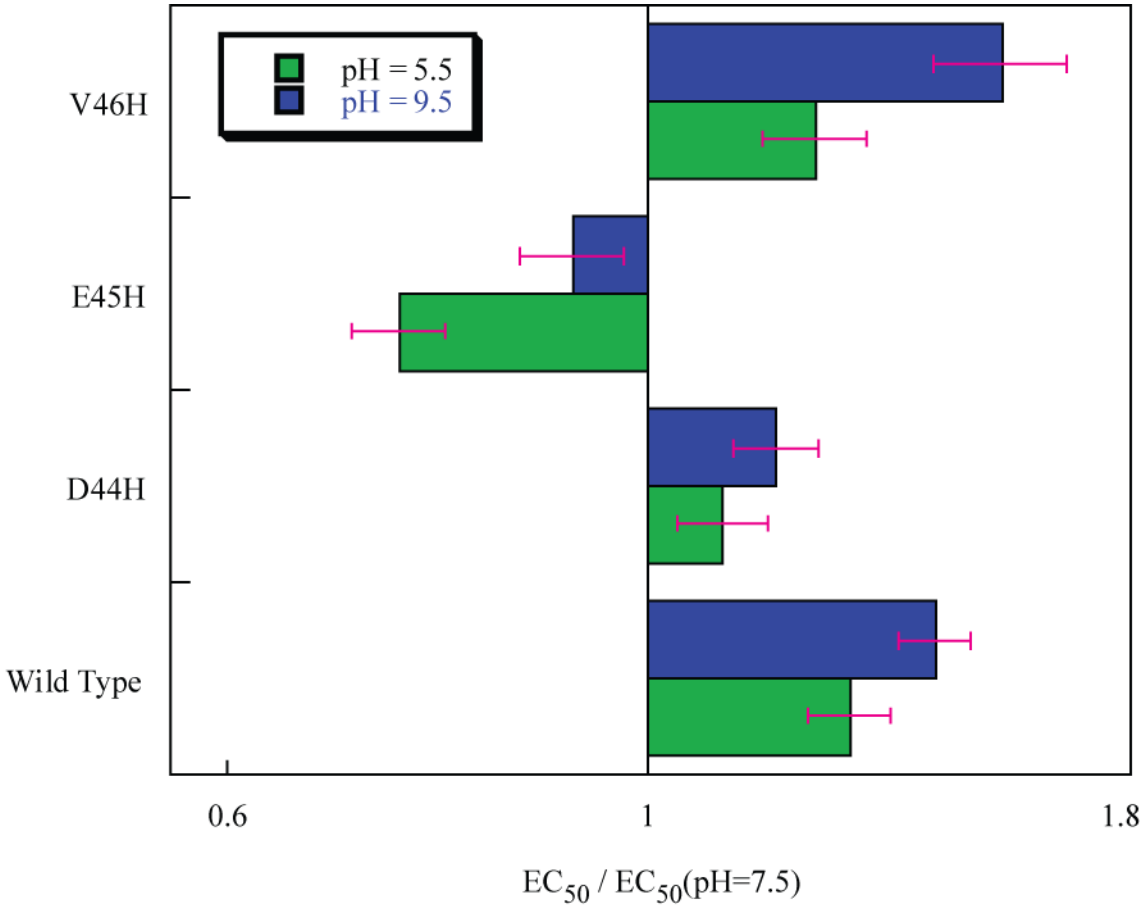

Figure 3.4 Shift in EC_{50} due to pH. Physiological pH (7.5) is used as the reference point. E45H, and to a lesser extent D44H, differ from wild type. A log scale is used for the x-axis.

In all cases the changes in EC_{50} due to altering the pH are small, but not meaningless. Of the three mutations, V46H is most similar to wild type while E45H differs to the greatest extent. The pH range used in these experiments is sufficient to form the positively charged histidine species (Figure 3.2), therefore we will focus our further discussion to the low pH experiments. Previous studies,[10] demonstrate that neutralizing the charge by conventional mutation to D44N or E45Q lowers EC_{50} and that

the affect is greater at E45. These data are consistent with the EC_{50} values obtained for D44H and E45H at physiological pH. While the EC_{50} for D44H is essentially that of wild type, we see a l0-fold decrease in EC_{50} for E45H.

Based on the consistency of these results with other studies,[10] we expected to see a decrease in EC_{50} for all three histidine mutants when the pH was lowered, creating a bias for the positively charged histidine side chain. Only E45H shows the expected decrease in EC_{50} and the change is quite small. However, we must also account for the slight increase in EC_{50} from hydrolysis of acetylcholine as seen for wild type. To complete this analysis, it is best to take the ratio of R_{pH} for the mutant ($R_{pH,mutant}$ = $EC_{50,mutant}/EC_{50(pH=7.5),\ mutant}$) to R_{pH} for wild type to give a ratio of ratios (Figure 3.5). Once the acetylcholine hydrolysis is accounted for, the data clearly indicate that lowering the pH (Figure 3.5, green bars) has a similar affect on the E45H channel function as incorporating a positively charged residue at this site.[10] D44H follows the trend of E45H though the effects are smaller.

The results for V46H are virtually identical to that of the wild type receptor (Figure 3.5, top). Although the mutation V46K drastically lowers EC_{50}[10] indicating a positively charged species increases channel function, we were not able to affect this same result using an altered pH in the extracellular media. Our V46H data are more indicative of the V46R results (2-fold increase in EC_{50}) reported in the same study.[10] Unlike the side chains of D44 and E45 which are suggested to stick into open space in the available structural data,[12] it has been proposed that the V46 side chain is in a hydrophobic environment.[12-16] Our results are consistent with this proposal. If the V46H

side chain is in a hydrophobic environment, it would not be readily in contact with the extracellular solution and therefore would not be affected by changes in pH.

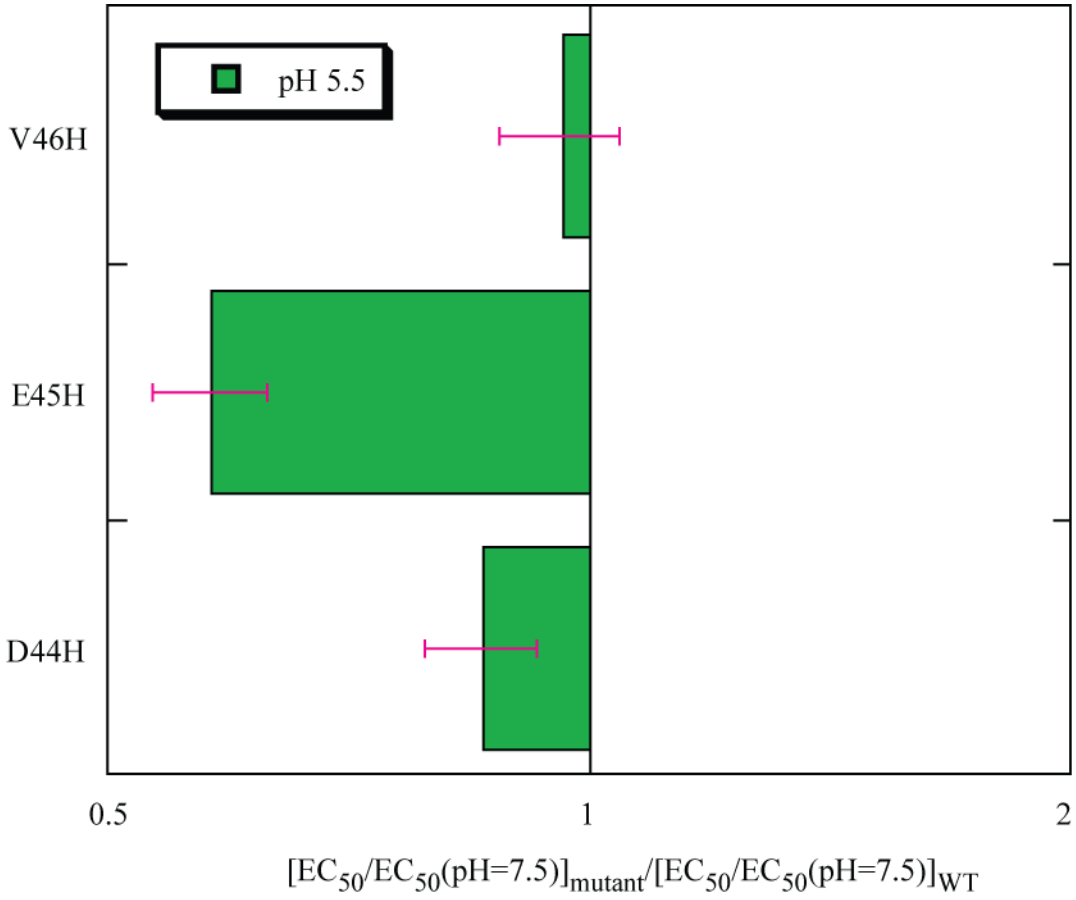

Figure 3.5 Comparison of shifts in EC_{50} from pH compared to the same shift found in wild type. Wild type is set to unity (center of graph). A log scale is used for the x-axis.

The muscle type nAChR does not show a pH dependence, indicating that despite being short and highly charged, the loop 2 region of the α_1 subunit does not experience a perturbed pK_a. Additionally, we have found that the affects of charge reversal[10] at two loop 2 residues, D44 and E45, can be mimicked by mutating these residues to histidine and varying the pH. At a third loop 2 resiude, V46, we find no alteration in channel function due to changes in pH. While these experiments do not definitively place V46 in

a hydrophobic environment, [12-16] the results suggest that unlike D44 and E45, V46H is in a sequestered environment, unable to interact with the extracellular solution.

3.4 Materials and Methods

Mutagenesis and mRNA Synthesis: Mutations in the α subunit were made following the QuickChange mutagenesis protocol (Strategene). Custom primers were purchased from Integrated DNA technologies. The mRNA that codes for the muscle type nAChR subunits (α, β, δ, and γ) was obtained by linearization of the expression vector (pAMV) with NotI (Roche), followed by *in vitro* transcription using the mMessage mMachine kit purchased from Ambion (Austin, TX). RNA concentrations were determined by UV/Vis spectroscopy.

Electrophysiology and Data Analysis: mRNAs of α, β, δ, and γ subunits were mixed in the ratio of 2:1:1:1 and microinjected into stage VI oocytes of *Xenopus laevis*. The mRNA mixes were diluted to a final concentration of 10 ng/μl. Oocytes were injected with 50 nL mRNA mix each, then stored in $ND96^{+}$ with 5% horse serum at 16-18°C. Oocytes were shaken continuously during incubation. Electrophysiology recordings were performed 24–48 hours after injection in two-electrode voltage clamp mode using the OpusXpress 6000A (Axon Instruments, Molecular Devices). The holding potential was -60 mV and agonist was applied for 15 seconds,[17] with 146 seconds of wash time between doses of agonist. For all dose-response data, agonist was applied from lowest to highest concentration. Dose-response data were obtained for at least eight concentrations of agonists and for a minimum of five oocytes with I_{max} equal to or greater than 500 nA. EC_{50} and Hill coefficients (n) were calculated by fitting the dose-response

relation to the Hill equation (Equation 3.1). All data are reported as mean ± standard error of the fit.

$$I = \frac{I_{max}}{1 + EC_{50}/[A]^n}$$ **Equation 3.1**

Acetylcholine chloride was purchased from Sigma. Stock solutions of 1M acetylcholine in water were stored at -20°C. Drug solutions were made from dilution of 1M acetylcholine using calcium-free ND96 buffer.

Drug Solutions for pH=5.5, 9.5: To prevent unnecessary hydrolysis of the acetyl group of acetylcholine, stock solutions of acetylcholine were made up in calcium free ND96 pH=7.5. No more than one hour prior to recording, the stock solutions were diluted 1- to 100-fold using calcium free ND96, previously pHed to 5.5 (using concentrated hydrocholoric acid) or 9.5 (using concentrated sodium hydroxide). This process was used for each individual experiment on the OpusXpress.

3.4 References

(1) Leite, J. F.; Rodrigues-Pinguet, N.; Lester, H. A. *J Clin Invest* **2003**, *111*, 436-7.
(2) Paterson, D.; Nordberg, A. *Prog Neurobiol* **2000**, *61*, 75-111.
(3) Chakrapani, S.; Bailey, T. D.; Auerbach, A. *J Gen Physiol* **2004**, *123*, 341-56.
(4) Kash, T. L.; Dizon, M. J.; Trudell, J. R.; Harrison, N. L. *J Biol Chem* **2004**, *279*, 4887-93.
(5) Kash, T. L.; Jenkins, A.; Kelley, J. C.; Trudell, J. R.; Harrison, N. L. *Nature* **2003**, *421*, 272-5.
(6) Kash, T. L.; Kim, T.; Trudell, J. R.; Harrison, N. L. *Neurosci Lett* **2004**, *371*, 230-4.
(7) Lummis, S. C.; Beene, D. L.; Lee, L. W.; Lester, H. A.; Broadhurst, R. W.; Dougherty, D. A. *Nature* **2005**, *438*, 248-52.
(8) Xiu, X.; Puskar, N. L.; Shanata, J. A.; Lester, H. A.; Dougherty, D. A. *Nature* **2009**.
(9) Bouzat, C.; Gumilar, F.; Spitzmaul, G.; Wang, H. L.; Rayes, D.; Hansen, S. B.; Taylor, P.; Sine, S. M. *Nature* **2004**, *430*, 896-900.
(10) Xiu, X.; Hanek, A. P.; Wang, J.; Lester, H. A.; Dougherty, D. A. *J Biol Chem* **2005**, *280*, 41655-66.
(11) Nelson, D. L.; Cox, M. M.; Worth Publishers: New York, New York, **2004**, p. 118.
(12) Unwin, N. *J Mol Biol* **2005**, *346*, 967-89.
(13) Miyazawa, A.; Fujiyoshi, Y.; Unwin, N. *Nature* **2003**, *423*, 949-55.
(14) Unwin, N. *Novartis Found Symp* **2002**, *245*, 5-15; discussion 15-21, 165-8.
(15) Unwin, N. *FEBS Lett* **2003**, *555*, 91-5.
(16) Unwin, N.; Miyazawa, A.; Li, J.; Fujiyoshi, Y. *J Mol Biol* **2002**, *319*, 1165-76.
(17) Cashin, A. L.; Petersson, E. J.; Lester, H. A.; Dougherty, D. A. *J Am Chem Soc* **2005**, *127*, 350-6.

Chapter 4

Stereochemical Requirements of nAChR αVal46 Side Chain Determined by Unnatural Amino Acid Incorporation: Support for the Pin-Into-Socket Interaction

Reproduced in part from:
Hanek, A.P.; H.A. Lester, and D.A. Dougherty; *J. Am. Chem. Soc.* **2008**, *130* (40), 13216-13218

4.1 Introduction

Understanding the gating mechanism of neurotransmitter-gated ion channels constitutes one of the most significant mechanistic challenges in chemical neurobiology. For some time we have been applying the tools of physical organic chemistry to this important problem, emphasizing strategies that can produce linear free energy relationships.[1,2] In the present work we apply another classical tool of physical organic chemistry – the stereochemical probe[3] – to address a specific proposal concerning the mechanism of ion channel gating.

The nicotinic acetylcholine receptor (nAChR), like all members of the Cys-loop neurotransmitter-gated ion channel superfamily to which it belongs, mediates rapid synaptic transmission in the mammalian nervous system. At rest the nAChR is in a closed, non-conducting conformation. Upon binding of the neurotransmitter acetylcholine, the protein undergoes a conformational change to an open ion-conducting state, thereby converting the chemical signal to an electrical one.

The muscle-type nAChR is comprised of five homologous subunits (α_1-γ-α_1-δ-β_1) arranged pseudo-symmetrically around a central ion-conducting pore. Each individual

subunit has a large extracellular N-terminal domain, four membrane-spanning helices (M1–M4), and a short extracellular carboxy-terminal tail (Figure 4.1). The extracellular domain is comprised largely of β strands connected by short loops, with the agonist binding sites located at the α/γ and α/δ subunit interfaces. The channel gate is located in the 2nd pore-lining helix (M2) some 40-60 Å from the ligand binding site. The nature of the communication between the binding site and channel gate is incompletely known.

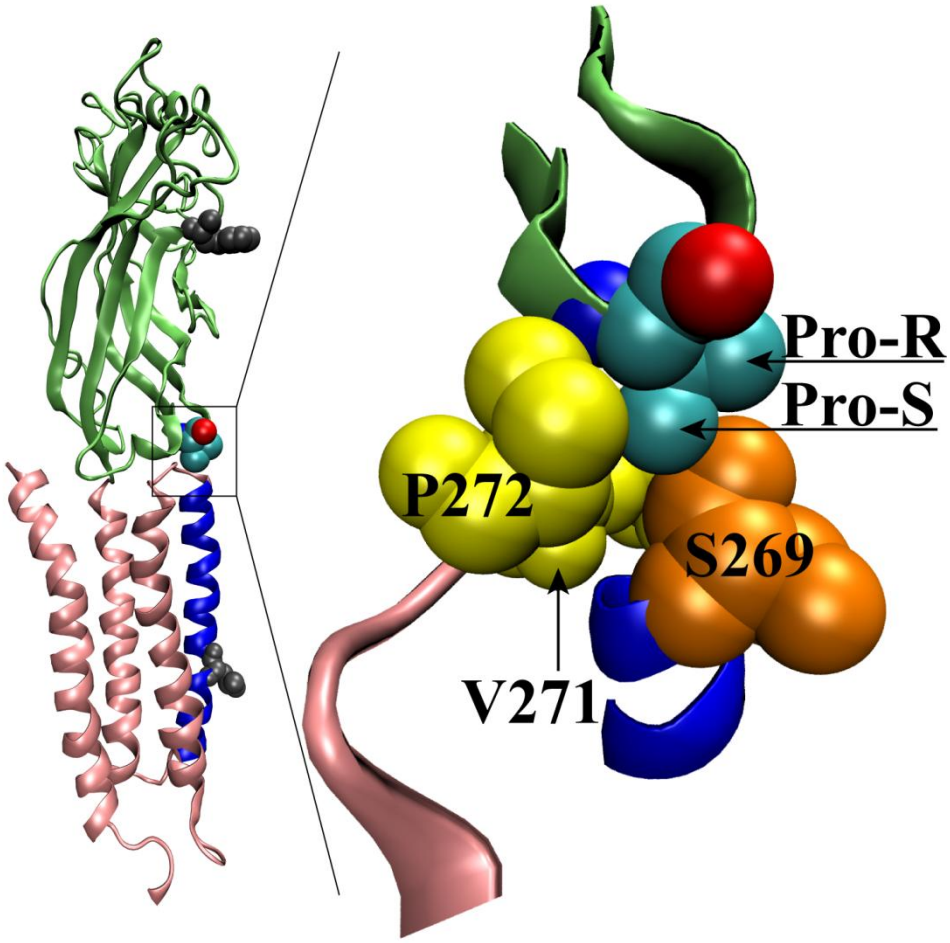

Figure 4.1 Left: Topology of a single α subunit (chain A of PDB 2BG9). The extracellular domain (green) contains the ligand binding site located at αW149 (dark gray). There are four membrane-spanning helices (M1, M3, M4 in pink) including the pore-lining M2 (blue) helix containing the channel gate at αL251 (dark gray). Right: αVal46 (side chain in cyan, backbone carbonyl in red) is oriented such that pro-S points into a pocket formed by residues 269 (orange), 270, 271 and 272 (yellow), while the pro-R methyl points away from the pocket.

Recent cryo-EM images[4-9] of nAChRs from the *Torpedo* ray show that loop 2, a short loop connecting β strands 1 and 2, lies directly over the extracellular terminus of M2 and to one side of the M2-M3 linker (Figure 4.1). Furthermore, the structure shows that the side chain of a specific loop 2 residue in the α subunit – valine 46 – points toward the top of the M2 helix.[5] αVal46 is part of the "gating interface" between the extracellular and transmembrane domains, and we and others have argued that this interface plays an important role in communicating neurotransmitter binding to the gating region.[10-18] Specifically, Unwin et al.[4-9] propose that αVal46 makes a key "pin-into-socket"[7] interaction, with the side chain of αVal46 tucked into a hydrophobic pocket formed by the top of M2. This interaction allows αVal46 to communicate changes in the structure of the extracellular domain to the M2 helix, which causes the channel gate to release. While it was immediately recognized that αVal46 of the nAChR is not conserved among Cys-loop receptors,[16,19] and therefore that this proposed mechanism of gating cannot be conserved across the superfamily, it has also been shown that the gating mechanisms of these receptors are quite varied.[11,14,16,19] Therefore the proposed pin-into-socket mechanism for the nAChR merits further scrutiny.

4.2 Results

4.2.1 Unnatural Amino Acid Incorporation

To probe the hypothesis that αVal46 makes a key pin-into-socket interaction, we used nonsense suppression methodology to incorporate unnatural amino acids in place of αVal46. In contrast to conventional mutagenesis, unnatural amino acids allow us to perturb side chain hydrophobicity while retaining the overall size and shape of the side chain. Therefore, we can unambiguously attribute changes in receptor function to the

alterations in the polarity of the side chain with minimal concern that these subtle mutations have altered the nature of communication between the binding site and channel gate.

Table 4.1 Measured EC_{50} values (μM) for αVal46 mutants

Amino Acid	EC_{50}	n_H	N	Amino Acid	EC_{50}	n_H	N
Val (WT)	50 ± 5	1.4	4				
Thr	>1000	---	8	*a*Thr	102 ± 5	1.4	19
Ile	58 ± 7	1.4	4	*a*Ile	48 ± 2	1.7	8
Omt	152 ± 5	1.4	12	*a*Omt	30 ± 1	1.7	12

Abbreviations used: Hill coefficient (n_H) and number of oocytes (N)

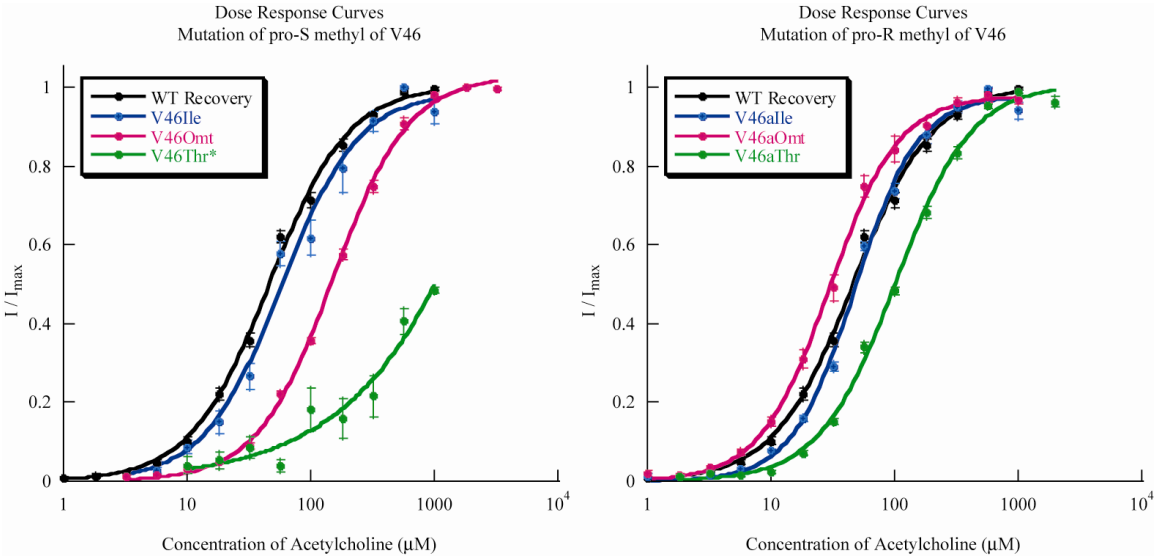

Figure 4.2 Dose response curves for mutations at αVal46. Mutations to the pro-S methyl (left panel) impact EC_{50} to a greater extent than mutations to the pro-R methyl (right panel). (*) The Thr mutation was deleterious and the EC_{50} could not be directly measured (further discussion below).

The αVal46Thr mutant was made and channel function was evaluated using whole-cell voltage clamp techniques.[19] Incorporation of Thr proved highly deleterious, causing a >20-fold rightward shift in EC_{50} to >1000 μM (Table 4.1, Figure 4.2).[18] Threonine is isosteric to valine, thus the shift in EC_{50} must be attributed to the increase in side chain polarity. Surprisingly, incorporation of the unnatural amino acid *allo*-threonine (*a*Thr) at the same position caused only a 2-fold increase in EC_{50} (Table 4.1, Figure 4.2). Thr and

*a*Thr have the same overall side chain polarity and both are isosteric to valine, yet Thr causes a large change in channel function while *a*Thr does not. Since the amino acids differ only in the side chain stereochemistry, the data clearly indicate that changing the polarity of the pro-S methyl of the αVal46 side chain affects channel gating to a much greater extent than changing the pro-R methyl. These results and the cryo-EM image of this region suggest that the pro-R and pro-S methyl groups are in distinct environments (Figure 4.1), consistent with the pin-into-socket proposal.

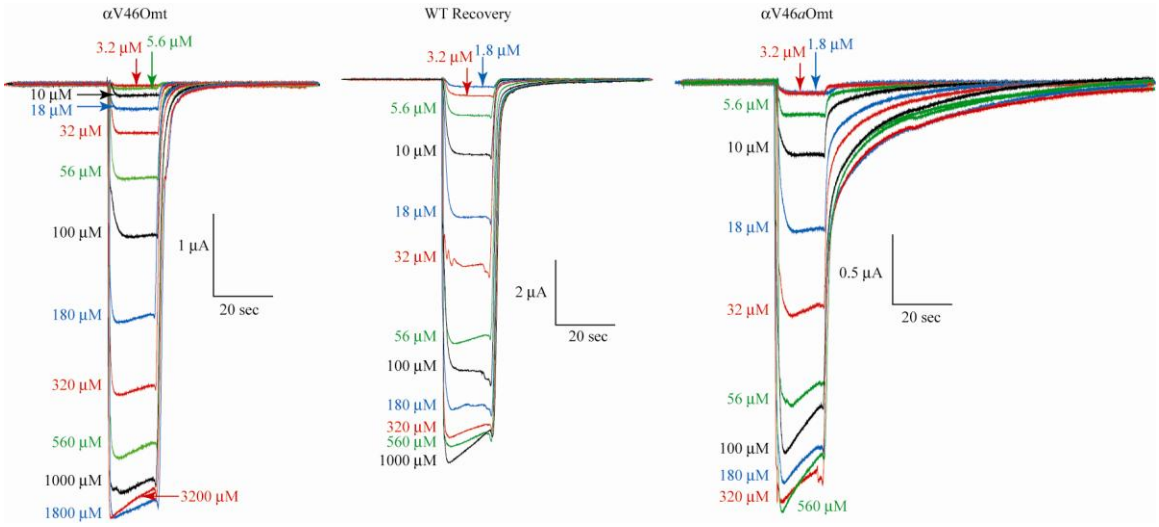

Figure 4.3 Representative traces for wild type recovery and the Omt and *a*Omt mutations are shown. All mutations have a sharp rise time and some desensitization once the concentration of acetylcholine exceeds the EC_{50}. The concentrations of acetylcholine are provided.

While minimally perturbing in a steric sense, converting a methyl to a hydroxyl is still a strong chemical disruption. Thus, we considered other mutants at αVal46 (Table 4.1). Previously, we have employed the O-methyl threonine (Omt)/*allo*-O-methyl threonine (*a*Omt) epimeric pair.[3] However, since Omt is isosteric to isoleucine, not to valine, we first incorporated isoleucine (Ile) and *allo*-isoleucine (*a*Ile) mutations as reference points. As expected, replacement of Val with the similarly hydrophobic Ile and

*a*Ile does not appreciably impact channel function (Table 4.1). Mutation to Omt produced a 3-fold increase in EC_{50} to 152 μM, indicating a decrease in channel function, while *a*Omt decreased EC_{50} slightly. Introduction of the slightly larger side chain with intermediate polarity had no effect on the macroscopic currents (Figure 4.3). These results provide an intermediate point between wild type and threonine that clearly demonstrates the importance of a hydrophobic group at the pro-S methyl of the valine side chain.

4.2.2 Coupling of αVal46 to βL251

The EC_{50} of αVal46Thr could not be directly measured since saturation of the whole-cell dose response curve was not achieved with 1000 μM acetylcholine. Concentrations of acetylcholine greater than 1000 μM block the whole-cell current, thus EC_{50} values greater than 500 μM cannot be accurately measured. Previously we have used a known gain-of-function mutation, βL251S (Table 4.2, Figure 4.4A),[3] measured the EC_{50} of the double mutant and then calculated the EC_{50} of loss-of-function mutant.[20-22] The EC_{50} of αVal46Thr/βL251S, was determined to be 74 μM (Table 4.2, Figure 4.4B). If the two mutants are independent, the EC_{50}s are multiplicative, and the EC_{50} of αVal46Thr is ~3000 μM.

Table 4.2 Measured EC_{50} (μM) for select αVal46/βL251S double mutations. The fold shift for the αVal46 single mutation is given.

Mutation	EC_{50}	Fold-shift	n_H	N
βL251S	1.2 ± 0.1	40.3	1.5	5
αVal46Thr/ βL251S	74 ± 5	N/A	1.6	9
αVal46Omt/ βL251S	17.5 ± 0.6	37.5	1.3	4
αVal46*a*Omt/ βL251S	0.80 ± 0.03	8.7	1.5	4

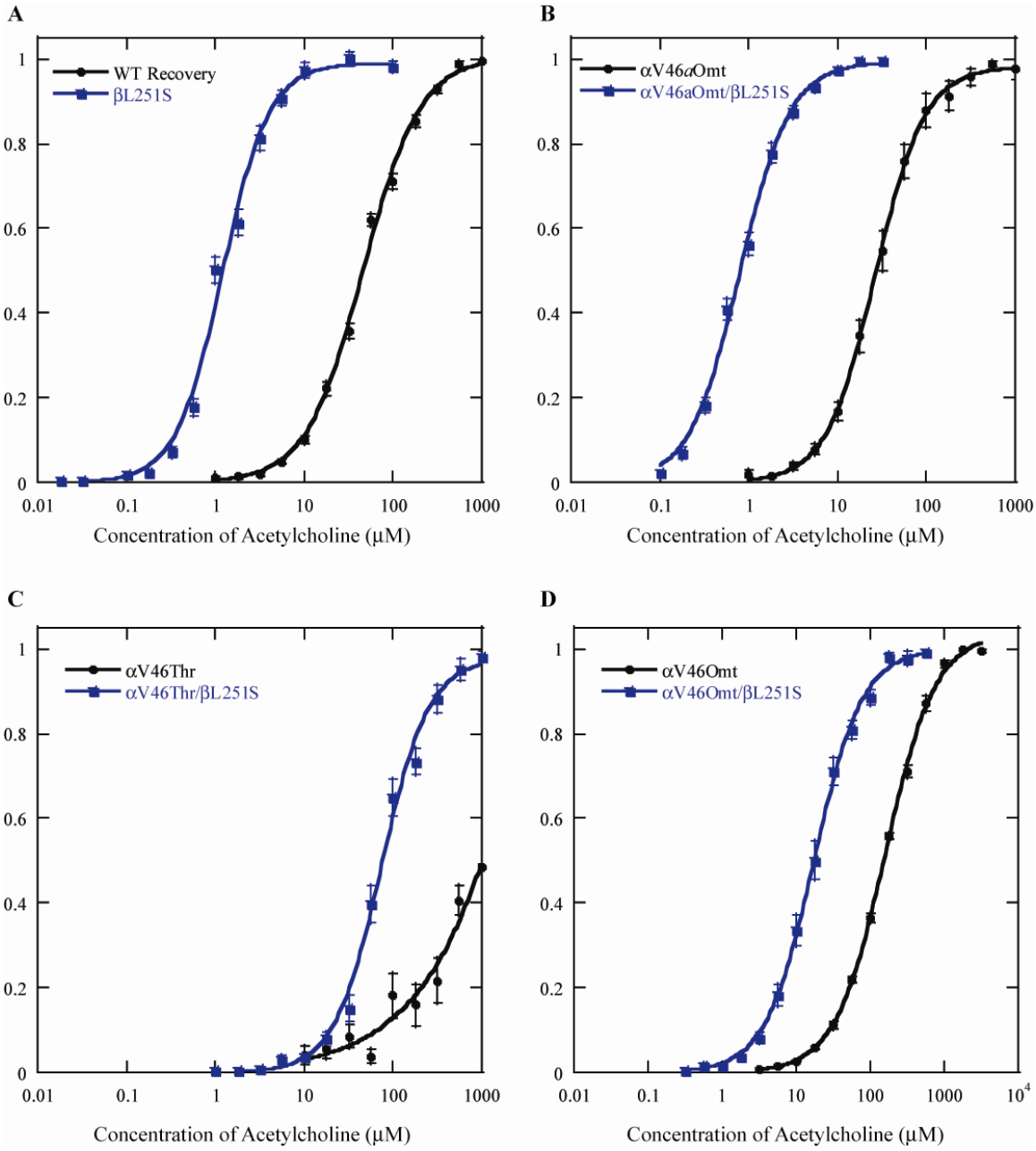

Figure 4.4 Dose response relationship for three αVal46 mutants with and without the βL251S mutation. **A**, The βL251S mutation shifts the wild type EC_{50} ~40-fold. **B,** βL251S shows a ~40-fold shift with the αVal46*a*Omt compared to the single mutation in the α subunit. **C,** αVal46Thr cannot be measured unless a second mutation (βL251S) is incorporated. **D,** βL251S does not shift the EC_{50} of αVal46Omt ~40-fold.

Before assigning the αVal46Thr mutant an EC_{50} of 3000 μM, we must consider the nature of the βL251S mutation. This mutation is known to affect channel gating[3] and it has been proposed that αVal46 is part of the gating pathway,[4-9] thus it is reasonable that

the two mutations are energetically coupled. To determine if mutations to αVal46 are coupled to βL251S, we determined the EC_{50} of the Omt and *a*Omt with the βL251S mutation (Table 4.2). The *a*Omt mutation shows the characteristic ~40-fold shift in EC_{50} between wild type and βL251S (Figure 4.4B). However, the Omt mutation shows a reduced shift in EC_{50} of 8.7-fold. These results indicate that mutations to the pro-S methyl of αVal46 are not independent of the βL251S mutation. Furthermore, these data suggest that the αVal46Thr mutant is unlikely to be independent of βL251S, thus we cannot determine the exact EC_{50} of the Thr mutant.

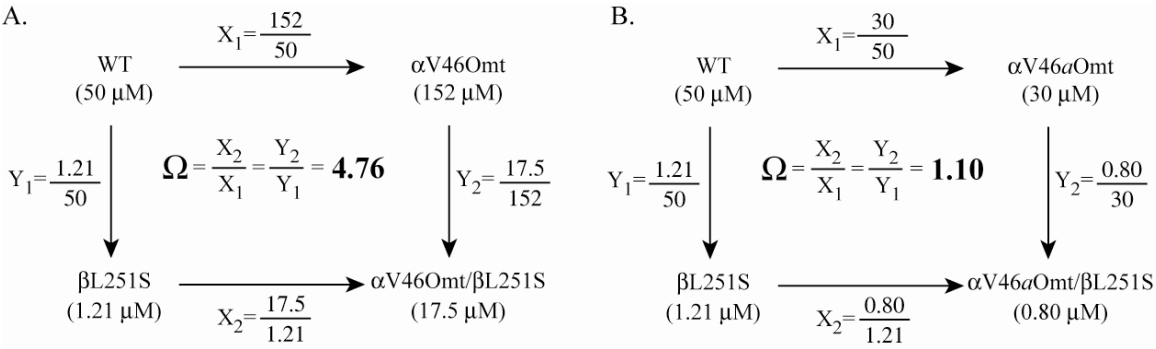

Figure 4.5 Double mutant cycle analysis. (**A**) αVal46Omt and βL251S show a coupling (i.e., Ω≠1) while (**B**) αVal46*a*Omt and βL251S do not.

The coupling constants, Ω, for the Omt and *a*Omt mutants and βL251S were calculated from the double mutant cycle analysis (Figure 4.5). Ω for two independent mutations is unity. Larger deviations from unity indicate stronger interactions, or couplings, between the two residues. The energetic coupling ($\Delta\Delta G_{int}$) was calculated (Equation 4.1) and found to be 3.87 kJ/mol and 0.24 kJ/mol for Omt and *a*Omt, respectively.

$$\Delta\Delta G_{int} = -RT\ln(\Omega) \qquad \textbf{Equation 4.1}$$

4.3 Discussion

4.3.1 The Pro-S Methyl of αVal46 is Involved in Channel Gating

Based on the location and the subtlety of the changes, it seems unlikely that these mutations could significantly impact ligand binding events, whereas αVal46 is located at the interface of the extracellular and transmembrane domains at an ideal location to influence channel gating.[10-13,16,18,23] Additionally, detailed kinetic studies of conventional mutations at αVal46 have demonstrated that changes to this residue primarily affect gating events,[11] and our own data show a coupling between a known gating residue and mutations at αVal46. Therefore we ascribe the changes in EC_{50} here to reflect changes in

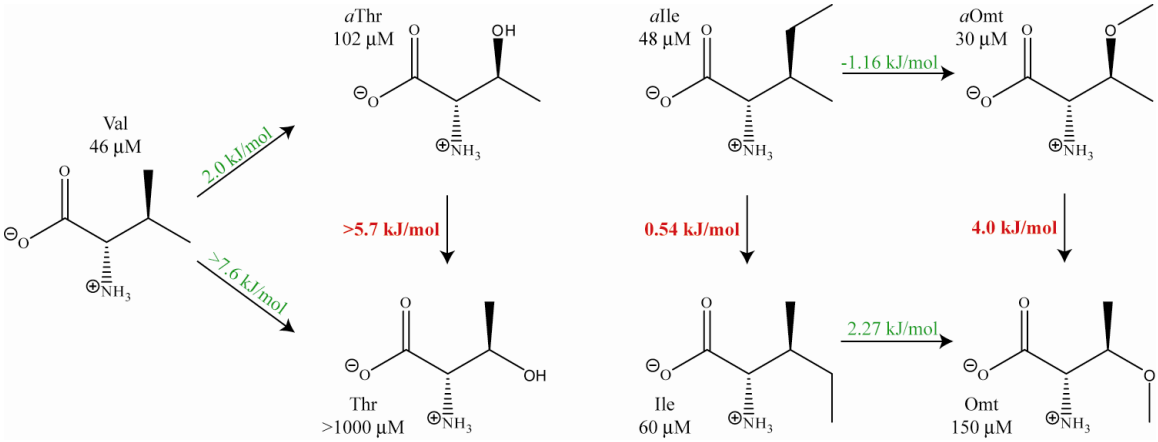

Figure 4.6 Incorporation of polar groups in the αVal46 side chain inhibits channel function to a greater extent at the pro-S position (lower row). The decreases in channel function are attributed to destabilization of the open state, stabilization of the closed state, or a combination of both. ΔΔG values in red show the difference in energy for the same functional group at the pro-S versus pro-R position. ΔΔG values in green show the difference in energy due to mutation from a hydrophobic to more polar group.

the gating equilibrium constant (k_{open}/k_{closed}) for the channel. Interpreted this way (Figure 4.6), the threonine mutation at αVal46 results in a greater than 7.6 kJ/mol change in the gating equilibrium. Introduction of this polar substituent affects channel gating by stabilizing the closed state, destabilizing the open state, or a combination of both.

Our results clearly indicate that the pro-S methyl group of αVal46 is critical to proper channel gating, while mutation of the pro-R methyl group has little impact on channel function. Additionally, mutation to Omt shows coupling to another mutation known to affect channel gating, βL251S. βL251 is located on an entirely distinct subunit and is well-removed from the interface of the extracellular and transmembrane domains. Therefore, these two residues cannot interact directly and the energetic coupling must be the result of a long range interaction, suggesting αVal46 is part of the gating pathway. Furthermore, the same interaction is not found for the *a*Omt mutant, clearly indicating the importance of the pro-S over the pro-R methyl group. We consider the present results to provide strong support for the pin-into-socket mechanism. The images of Figure 4.1 are based on cryo-EM data that are at best of 4 Å resolution. Yet, the clear prediction that the pro-R and pro-S methyl groups of αVal46 are in stereochemically distinct environments, with the pro-S tucked into a pocket, is substantially confirmed by our data.

4.3.2 Consideration of Previous Studies

Previous studies of Val46 by conventional mutagenesis[11,16,23] largely support the pin-into-socket interaction. Xiu et al.[18] found that mutation to Ala is highly deleterious, as measured by EC_{50}. A detailed kinetic analysis of the same mutation by Chakrapani et al.[11] revealed that the Ala mutation decreased k_{open} drastically, consistent with the proposed pin-into-socket mechanism.[4-9] Additionally, Xiu et al.[18] report data on mutations to Asp, Glu, Arg, and Lys. Mutations to Asp and Glu result in surface expressed but nonfunctional channels, while mutations to Arg and Lys increase the EC_{50} 2-fold and decrease the EC_{50} 30-fold, respectively. In the context of the pin-into-socket mechanism, the deleterious nature of the Asp and Glu mutations are not surprising. The

more complex issue is that of the Arg and Lys mutations. Both these residues have much longer side chains than Val and these side chains may adopt a variety of conformations such that it is possible that part of the side chain makes the same contacts necessary for channel function while keeping the positively charged portion of the side chain away from this same area of the protein. Mutations to Asp, Glu, Arg, and Lys eliminate the β-branching nature of WT Val, and change the size and polarity of the residues, making it difficult to attribute the changes in EC_{50} to only one of these alterations.

In addition to considering previous studies of conventional mutations, we must consider the nature of the interacting partner(s) for the pro-S methyl of Val46. Based on mutant cycle analysis using much more structurally perturbing conventional mutants, Lee and Sine suggest that a hydrophobic interaction between αVal46, αSer269 and αPro272 exists.[16] Single-channel analyses by Jha et al. suggest that Ser269 and Ala270 move early in the gating process – contemporaneously with Val46 – while Pro272 moves later.[23] This could be interpreted to indicate that Val46 is more likely to interact with Ser269/Ala270. We have made no effort here to identify the interacting partner of Val46. We do note, however, that assuming the image of Figure 4.1 is of the closed state, the assignment of the pocket as being hydrophobic[5,8] seems inconsistent with our data. Changing the pro-S methyl to a polar group apparently stabilizes the closed state relative to the open state (raising EC_{50}); therefore a polar pocket to receive that polar group is more consistent with our data. This pocket could be formed by backbone carbonyls and/or the side chain of S269.

As noted above, Val46 is not conserved in the Cys-loop superfamily, and so the key interaction probed here cannot play a critical gating role in all Cys-loop receptors.[14,18]

As discussed in detail elsewhere, this is more nearly the norm, rather than the exception, with most pairwise interactions in the crucial gating interface not being conserved across the family.[12-18,23] For example, Lummis et al. found that the cis-trans isomerization of a semi-conserved proline residue in the $5HT_{3A}R$ plays a key role in the gating of this channel.[17] However, in the nAChR, mutation of this same proline to serine, alanine, and glycine results in functional channels, demonstrating that *cis-trans* isomerization of this proline cannot wholly account for the gating of nAChR.[2,17] One candidate for a conserved gating interaction is a proposed salt bridge between the residue adjacent to Val46 on loop 2 (αGlu45) and a conserved Arg residue in the preM1 region. Several studies have evaluated its possible role in nAChR function, but it has not been evaluated in other Cys-loop receptors.[16,18,23]

4.3.3 Conclusions

We conclude that, in the nAChR, αVal46 does play a key role in receptor gating by a pin-into-socket mechanism, whereby the pro-S methyl group is nestled into a pocket at the top of the M2 helix. In addition to validating an intriguing feature of the cryo-EM images of this receptor, the present results further illustrate the power of unnatural amino acid mutagenesis to study the complex proteins of neuroscience using the techniques of physical organic chemistry.

4.4 Materials and Methods

4.4.1 Preparation of mRNA and Unnatural Amino Acyl-tRNA

Conventional Mutations and mRNA synthesis: Mutations were incorporated by Quickchange mutagenesis protocol (Stratagene) into the cDNA of the appropriate subunit gene in the pAMV vector. The mRNA coding for the mouse muscle type nAChR

subunits (α, β, γ, and δ) was obtained by linearization of the expression vector (pAMV) with Not1 (Roche), followed by *in vitro* transcription using mMessage mMachine kits (Ambion, Austin, TX).

Preparation of Amino acyl tRNA: 74 nt tRNA was made by runoff transcription using a T7 Megashortscipt kit from Ambion (Austin, TX). 30 μg of 74 nt tRNA is dissolved to 45 μl in 10 mM HEPES. The tRNA/HEPES mixture is placed in boiling water to denature and then cooled to 37˚C in a water bath. 12 μL of 3 mM (in DMSO) dCA-Uaa, 48 μL of 2.5X reaction mix, 7.8 μL water, and 7.2 μL of T4 RNA ligase (New England BioLabs) is added to the tRNA/HEPES mixture. The reaction is incubated for 45 minutes in a 37˚C water bath. The reaction is quenched by addition of 12.5 μl of NaOAc (3.0 M, pH=5.0) and 17.5 μl of water. The ligated tRNA-Uaa is purified by 25:24:1 Phenol:chloroform:isoamyl alcohol (PCI) extraction (150 μl) followed by a back extraction of the PCI layer using 6.3 μl NaOAc (3.0 M, pH=5.0) and 68.7 μl water. The aqueous layers are combined and extracted with 24:1 chloroform:isoamyl alcohol (225 μl). 675 μl of ethanol is added to the aqueous layer and the mixture is left to precipitate overnight at -20˚C. The tRNA-Uaa is pelleted by spinning at 1400 RPM for 20 minutes at 4˚C. The supernatant is removed and the pellet dried in a dessicator for 20 minutes. The pellet is redissolved in 25 μl of 1 mM NaOAc, pH=4.5, checked by MALDI and quantified by UV/Vis.

4.4.2 Electrophysiology and Data Analysis

Two electrode voltage clamp: For conventional mutants, mRNAs of α, β, γ and δ subunits were mixed in the ratio of 2:1:1:1 and microinjected into stage VI oocytes of

Xenopus laevis. Electrophysiology recordings were performed 24-48 hours after injection in two-electrode voltage clamp mode using the OpusXpress 6000A. The clamping voltage was -60 mV and agonist was applied for 15 seconds. Acetylcholine chloride was purchased from Sigma/Aldrich/RBI (St. Louis, MO). All drugs were diluted to the desired concentrations with calcium-free ND96 buffer. Dose-response data were obtained for at least 8 concentrations of agonists and for a minimum of 5 oocytes. Mutants with I_{max} equal to or greater than 400 nA are regarded to be functional. EC_{50} and Hill coefficient were calculated by fitting the dose response relation to the Hill equation (Equation 4.2), where I_{max} is the maximal current, EC_{50} is the effective concentration to elicit a half maximal response, and n is the Hill coefficient. All data are reported as means ± S.E.

$$I = \frac{I_{\max}}{1 + EC_{50}/[A]^n}$$

Equation 4.2

If saturation was not reached at 1000 μM concentrations of acetylcholine, the EC_{50} could not be calculated. For the αV46Thr mutant, a second mutation known to consistently reduce the wild type EC_{50} to 1.2 μM[3] was introduced. The second mutation incorporated a leucine to serine mutation in the β subunit (βL251S). The EC_{50} of the double mutant was then determined as described. The EC_{50} of the single mutant is calculated by multiplying the EC_{50} of the double mutant by by 42 (50/1.2).

Unnatural amino acid suppression: The aminoacyl tRNA was deprotected by photolysis immediately prior to co-injection with mRNA containing an *amber* (TAG) stop codon at the site of interest. The mRNA is mixed in a 10:1:1:1 mixture and co-injected with an equal volume of tRNA-Uaa. Recovery of WT and the conventional

mutation V46I were employed as positive controls. Co-injection of mRNA with 76 nt tRNA (no Uaa) was used to test for re-aminoacylation at this site. This negative control showed no response to 1 mM ACh. An additional negative control of mRNA only (read-through) also showed no response to 1 mM ACh.

Energy Calculations: ΔΔG values for Figure 4.6 were calculated using Equation 4.3. These calculations assume that the mutations affect the gating equilibrium but not the binding equilibrium, as evidenced by other studies at this site.[11]

$$\Delta\Delta G = RT \ln\left(\frac{EC_{50}(\text{mutant})}{EC_{50}(\text{wt})}\right) \qquad \textbf{Equation 4.3}$$

4.4.3 Unnatural Amino Acid Preparation

The amino acids isoleucine, allo-isoleucine, O-methyl threonine, and allo-O-methyl threonine were previously prepared,[3,24] with NVOC protection and cyanomethyl ester activation followed by coupling to dCA as described.[19]

NVOC allo-threonine: 381 mg (3.6 mmol) of Na_2CO_3 and 3.8 mL of water was stirred to make a 10% weight/volume mixture. 115 mg (0.96 mmol) of allo-threonine (Aldrich) was added to this mixture. The entire reaction was then put on ice. NVOC-Cl (278 mg, 1.01 mmol) was added while stirring. The ice was removed and the reaction allowed to warm to room temperature. The reaction was monitored by TLC. After 5 hours the reaction was complete. 50 mL of water was added, turning the reaction cloudy and yellow. 3 x 20 mL of ether was used to wash the aqueous layer. The aqueous layer (clear, yellow) was acidified with 6N HCl to pH<2. The product was extracted into ether (3 x 25 mL), and the organic layer was dried over $MgSO_4$. $MgSO_4$ was removed by filtration and the organic solution was concentrated under reduced pressure to give a

yellow oil (330 mg). MS gives a peak at 380.8 consistent with the mass of NVOC-*a*Thr plus a sodium ion. Proton NMR (300 mHz, Figure 4.7) in CD_3OD gives peaks at 7.75 (s, 1H), 7.21 (s, 1H), 5.48 (q, 2H), 3.97 (s, 3H), 3.91 (s, 3H), 4.14 (t, 1H), 1.23 (d, 3H), and 4.25 (d, 1H). Yield 229 mg (0.64 mmol), 66.5%

Cyanomethyl ester of NVOC-aThr: 229 mg (0.64 mmol) of NVOC-aThr was added to a dry flask that was then purged with argon. 2 mL of dry DMF followed by 2 mL (32 mmol) of chloroacetonitrile, and 0.25 mL (1.92 mmol) of triethylamine were added. The reaction was clear and yellow prior to addition of triethylamine. The reaction was stirred under argon and monitored by TLC. After 3 hours, the solvent was removed (vacuum line, overnight) leaving a yellow/brown solid. The solid was dissolved in methylene chloride and purified on a silica gel column using a gradient of ethyl acetate and methylene chloride. All fractions were spotted on a TLC plate and combined according to their contents. The solvent was removed. The desired product forms a white, needlelike solid that is highly insoluble. Positive ion MS gives peaks at 419.6 and 435.6 consistent with a mass of 396.6 for the product plus the mass of Na and K, respectively. Proton NMR (300 MHz, Figure 4.8) in $CDCl_3$ gives peaks at 7.72 (s, 1H), 6.99 (s, 1H), 5.55 (d of d, 2H), 4.01 (s, 3H), 3.96 (s, 3H), 4.21 (m, 1H), 1.33 (d, 3H), 4.48 (d of d, 1H), 4.82 (d of d, 2H), and 5.76 (d, 1H). Yield 117 mg (0.295 mmol), 46%.

Allo-threonine coupling to dCA: 10 mg (0.025 mmol) of the cyanomethyl ester NVOC-*a*Threonine was dissolved in 0.6 mL of DMF under argon. Once dissolved, 10 mg (0.008 mmol) of dCA and 4.85 mg (0.020 mmol) of tetrabutylammonium chloride were added, and the reaction was stirred under argon, overnight. The reaction was quenched with 1:1 water:acetonitrile, filtered and purified by HPLC. Fractions

containing the dCA-*a*Thr-NVOC (as determined by the ratio of peaks at λ=350 nm and λ=260 nm) were combined. The solvent was removed by lyophilization. The remaining solid was dissolved in 15 mL of 10 mM acetic acid, flash frozen and the solvent was removed by lyophilization. This step was repeated 3 times. The dCA-*a*Thr-NVOC was confirmed by MALDI-TOF (m/z = 975.6).

4.5 Proton NMR Spectra

Figure 4.7 Proton NMR of NVOC-*a*Thr

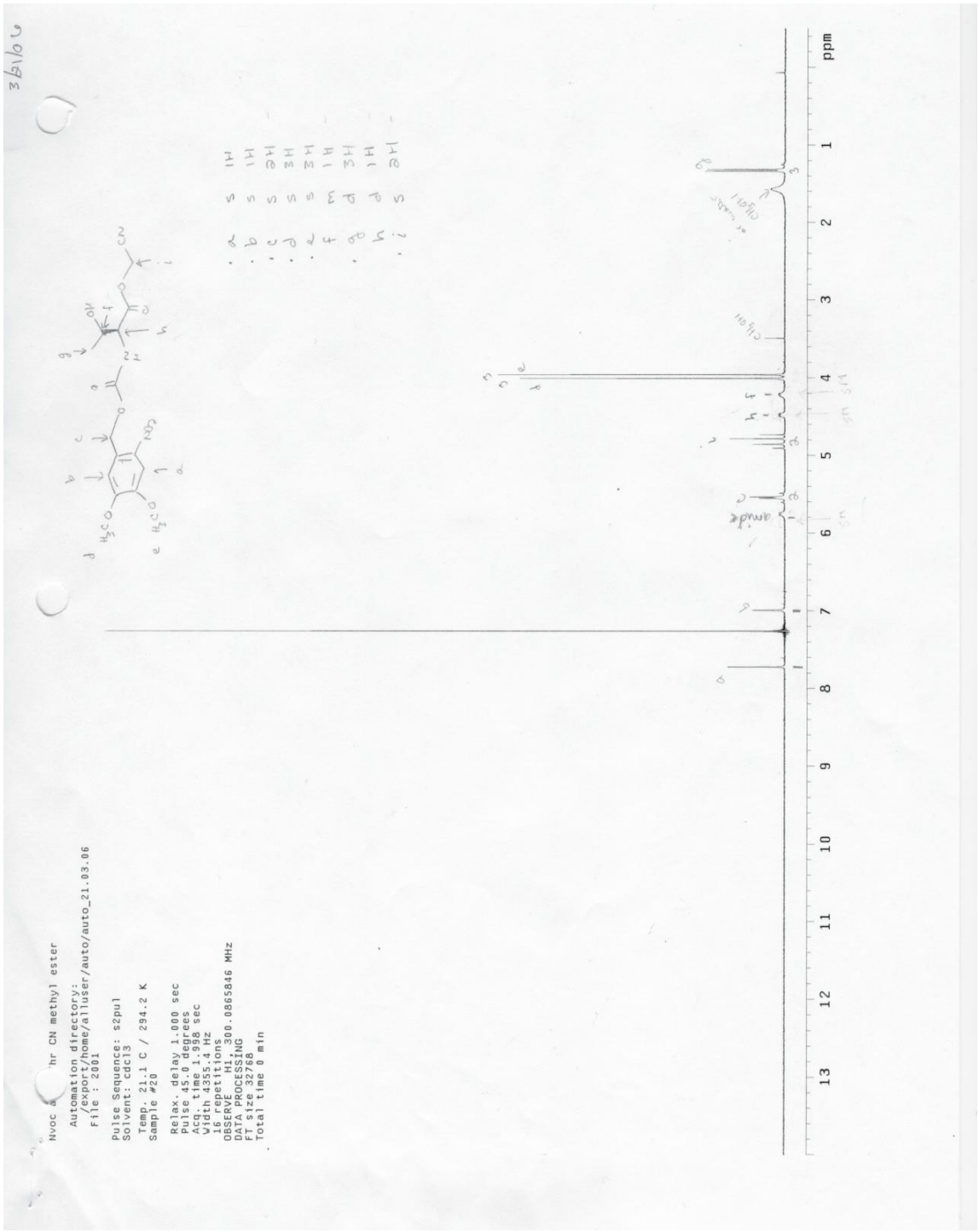

Figure 4.8 Proton NMR of NVOC-*a*Threonine-cyanomethyl ester

4.6 References

(1) Dougherty, D. A. *Chem Rev* **2008**, *108*, 1642-53.
(2) Dougherty, D. A. *J Org Chem* **2008**, *73*, 3667-73.
(3) Kearney, P. C.; Zhang, H.; Zhong, W.; Dougherty, D. A.; Lester, H. A. *Neuron* **1996**, *17*, 1221-9.
(4) Miyazawa, A.; Fujiyoshi, Y.; Stowell, M.; Unwin, N. *J Mol Biol* **1999**, *288*, 765-86.
(5) Miyazawa, A.; Fujiyoshi, Y.; Unwin, N. *Nature* **2003**, *423*, 949-55.
(6) Unwin, N. *Novartis Found Symp* **2002**, *245*, 5-15; discussion 15-21, 165-8.
(7) Unwin, N. *FEBS Lett* **2003**, *555*, 91-5.
(8) Unwin, N. *J Mol Biol* **2005**, *346*, 967-89.
(9) Unwin, N.; Miyazawa, A.; Li, J.; Fujiyoshi, Y. *J Mol Biol* **2002**, *319*, 1165-76.
(10) Bouzat, C.; Gumilar, F.; Spitzmaul, G.; Wang, H. L.; Rayes, D.; Hansen, S. B.; Taylor, P.; Sine, S. M. *Nature* **2004**, *430*, 896-900.
(11) Chakrapani, S.; Bailey, T. D.; Auerbach, A. *J Gen Physiol* **2004**, *123*, 341-56.
(12) Kash, T. L.; Dizon, M. J.; Trudell, J. R.; Harrison, N. L. *J Biol Chem* **2004**, *279*, 4887-93.
(13) Kash, T. L.; Jenkins, A.; Kelley, J. C.; Trudell, J. R.; Harrison, N. L. *Nature* **2003**, *421*, 272-5.
(14) Kash, T. L.; Kim, T.; Trudell, J. R.; Harrison, N. L. *Neurosci Lett* **2004**, *371*, 230-4.
(15) Kash, T. L.; Trudell, J. R.; Harrison, N. L. *Biochem Soc Trans* **2004**, *32*, 540-6.
(16) Lee, W. Y.; Sine, S. M. *Nature* **2005**, *438*, 243-7.
(17) Lummis, S. C.; Beene, D. L.; Lee, L. W.; Lester, H. A.; Broadhurst, R. W.; Dougherty, D. A. *Nature* **2005**, *438*, 248-52.
(18) Xiu, X.; Hanek, A. P.; Wang, J.; Lester, H. A.; Dougherty, D. A. *J Biol Chem* **2005**, *280*, 41655-66.
(19) Nowak, M. W.; Gallivan, J. P.; Silverman, S. K.; Labarca, C. G.; Dougherty, D. A.; Lester, H. A. *Methods Enzymol* **1998**, *293*, 504-29.
(20) Cashin, A. L.; Petersson, E. J.; Lester, H. A.; Dougherty, D. A. *J Am Chem Soc* **2005**, *127*, 350-6.
(21) Cashin, A. L.; Torrice, M. M.; McMenimen, K. A.; Lester, H. A.; Dougherty, D. A. *Biochemistry* **2007**, *46*, 630-9.
(22) Zhong, W.; Gallivan, J. P.; Zhang, Y.; Li, L.; Lester, H. A.; Dougherty, D. A. *Proc Natl Acad Sci U S A* **1998**, *95*, 12088-93.
(23) Jha, A.; Cadugan, D. J.; Purohit, P.; Auerbach, A. *J Gen Physiol* **2007**, *130*, 547-58.
(24) Kearney, P. C.; Nowak, M. W.; Zhong, W.; Silverman, S. K.; Lester, H. A.; Dougherty, D. A. *Mol Pharmacol* **1996**, *50*, 1401-12.

Chapter 5

Cation-π Interactions in the $GABA_A$ and Glycine Receptors Mediate Neurotransmitter Binding

Reproduced in part from:
Claire L. Padgett, A.P. Hanek, H.A. Lester, D.A. Dougherty, and Sarah C.R. Lummis;
J. Neurosci **2007**, 27 (4), 886-892

And
S.A. Pless, K.S. Millen, A.P. Hanek, J.W. Lynch, H.A. Lester, S.C.R. Lummis,
and D.A. Dougherty; *J. Neurosci* **2008** 28 (43), 10937-10942

5.1 Introduction

5.1.1 Cys-loop Neurotransmitter Gated Ion Channels

The γ-amino butyric acid type A ($GABA_A$) and glycine (Gly) receptors are members of the Cys-loop ligand-gated ion channel family, which also includes the nicotinic acetylcholine (nACh), serotonin type 3 ($5\text{-}HT_3$), and γ-amino butyric acid type C ($GABA_C$) receptors. These proteins mediate rapid synaptic transmission in the central and peripheral nervous systems. At rest the receptors are in a closed, non-conducting state. Upon binding of neurotransmitter, the receptor undergoes a conformational change to an open, ion-conducting state, thereby allowing ions to cross the cell membrane, converting a chemical signal (neurotransmitter) to an electrical one.

Each protein has five homologous subunits arranged pseudo-symmetrically around a central ion-conducting pore. Each subunit has a large extraceullular ligand-binding amino-terminal domain principally comprised of two beta sheets, four membrane-spanning helices (M1-M4), a large intracellular loop, and a short extracellular carboxy

tail. The beta strands in the extracellular domain are connected by short, unstructured loops which contribute to ligand binding and to transduction of the conformational change that takes place upon ligand binding.

Agonist binding sites are located at select subunit interfaces. The principle subunit contributes residues located on loops A, B, and C while the complementary subunit contributes loops D, E, and F. Of particular importance are a group of aromatic amino acids associated with loops A-D.[1] These aromatic residues are clustered together in a box-like structure (Figure 5.1) in the crystal structure of the acetylcholine binding protein (AChBP), which is homologous to the extraceullular domain of the $GABA_A$ and Gly receptors.[2] The resulting aromatic box is the location of cation-π interactions between acetylcholine and nicotine in the nAChR,[3,4] serotonin in the $5HT_{3A}R$ and MOD-1 receptor (Cys-loop receptor found in C. *elegans*),[5-7] and GABA in the $GABA_CR$ (Table 5.1).[8]

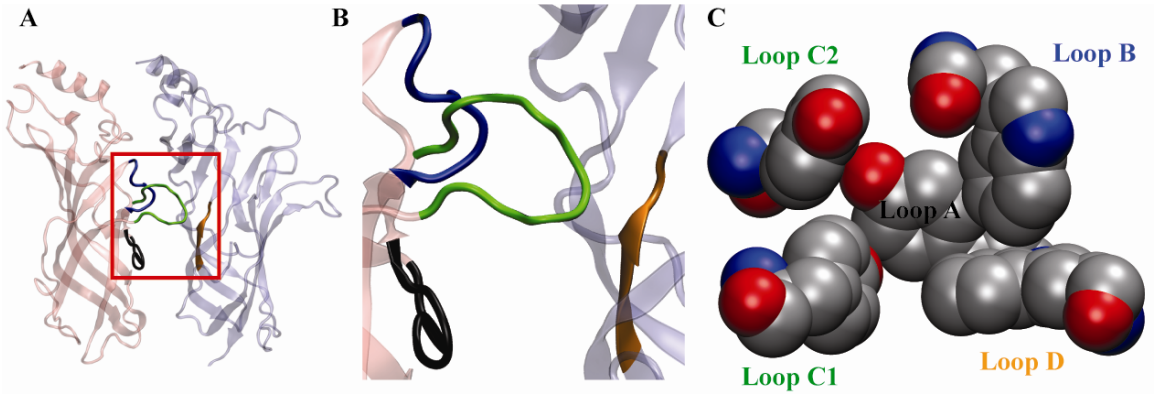

Figure 5.1 The ligand binding site of the nAChR. **A,** The agonist binding site is located at the interface between two subunits; the principle subunit is shown in pink and the complementary in gray. **B,** the area of **A** in the red box highlights the loops A (black), B (blue), and C (green) from the principle subunit and loop D (orange) from the complementary subunit. **C**, The aromatic box from the AChBP structure consists of a Tyr (loop A), Trp (loop B), two Tyr (loop C, residue 1 and 2), and Trp (loop D).

Cation-π interactions have been identified in the binding site of four members of the Cys-loop superfamily: muscle-type nAChR,[4] neuronal $\alpha_4\beta_2$ nAChR,[3] 5-$HT_{3A}R$,[5,6] and

$GABA_cR$.[8] Given the data on these other receptors, the high homology among the Cys-loop superfamily and especially the conservation of the aromatic box (Table 5.1), it seems reasonable that the other predominant mammalian inhibitory Cys-loop receptors, $GABA_AR$ and GlyR, will also bind neurotransmitter agonist through a cation-π interaction.

Table 5.1 The aromatic box is conserved across the Cys-loop family. Residues previously identified as participating in cation-π interactions are shown in red.

Receptor	A	B	C1	C2	D
nACh	Tyr	**Trp**	Tyr	Tyr	Trp
5-HT_3	Glu	**Trp**	Phe	Tyr	Tyr
$GABA_C$	Phe	**Tyr**	Tyr	Tyr	Tyr
$GABA_A$	Tyr	Tyr	Phe	Tyr	Phe
Gly	Phe	Phe	Tyr	Phe	Phe

5.1.2 The Binding Sites

The $\alpha_1\beta_2$ $GABA_AR$ studied has two binding sites, each located at a β/α interface. Given that $GABA_CR$ and $GABA_AR$ both bind GABA (structure, Figure 5.6) and that the aromatic boxes are highly similar (Table 5.1), it seems likely that GABA will bind in a similar manner, making the loop B residue (β_2Tyr157) the most likely candidate for the cation-π interaction. This seems especially likely since the residue is conserved as a Tyr. The other residues in the aromatic box (Figure 5.2) are β_2Tyr97 (loop A), β_2Phe200 (loop C1), β_2Tyr205 (loop C2), and α_1Phe65 (loop D).

The α_1 GlyR is homomeric, thus there are five possible binding sites. Unlike the other Cys-loop receptor binding sites, the predominant aromatic in the GlyR aromatic box is Phe (Figure 5.2, Table 5.1). This is especially intriguing given that no neurotransmitter-Cys-loop receptor cation-π interactions have been found at Phe sites.

Together, α_1Phe99 (loop A), α_1Phe159 (loop B), α_1Tyr202 (loop C1), α_1Phe207 (loop C2), and α_1Phe63 (loop D) comprise the aromatic box.

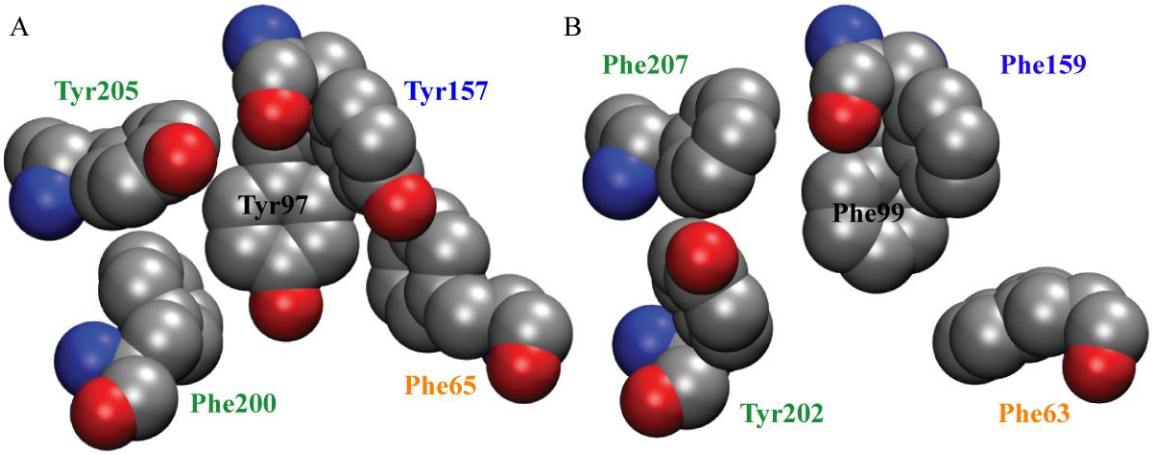

Figure 5.2 The aromatic box of the $GABA_AR$ (**A**) and GlyR (**B**), from homology models based on PDB structure 2BG9.

5.1.3 Probing Cys-loop Receptors for a Cation-π Interaction

Cation-π interactions can be identified by incorporation of fluorinated aromatics at prospective cation-π sites. The cation-π binding affinity of aromatics is strongly influenced by electrostatics, and addition of electron-withdrawing fluorines around the aromatic ring systematically diminishes the negative electrostatic potential on the face of the ring (Figure 5.3), and thus the cation-π binding ability.[9] Thus, a systematic increase in EC_{50} with increasing fluorination provides compelling evidence for a cation-π interaction. The reluctance to participate in H-bonding interactions and small steric size further make fluorine an ideal substituent. Here, we use a series of Phe analogs that contain an increasing number of fluorine atoms on their phenyl rings to probe potential cation-π interactions at the aromatic residues that contribute to the binding sites of the

$\alpha_1\beta_2$ $GABA_A$ and α_1 Gly receptors. These unnatural amino acids were incorporated into receptors expressed in Xenopus oocytes using nonsense suppression.[10,11]

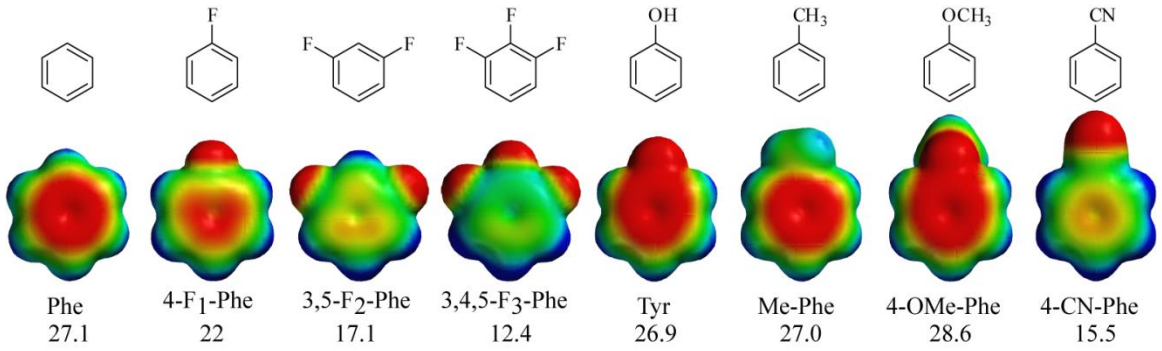

Figure 5.3 Electrostatic potential surfaces of phenylalanine analog side chains. All surfaces are scaled such that red is -40 kcal/mol and blue is +40 kcal/mol. The cation-π binding ability (calculated in the gas phase with a sodium ion using Hartree-Fock 6-31G** methods) is given below in kcal/mol.

5.2 Results

5.2.1 γ-Aminobutyric Acid Receptor

Probing of tryptophan and phenylalanine residues via successive fluorination is straightforward, whereas the 4-position hydroxyl group of tyrosine introduces a complication. Adding electron withdrawing groups to the phenyl ring of Tyr substantially lowers the pK_a of the hydroxyl, such that highly fluorinated tyrosines are expected to be ionized at physiological pH. To avoid complications from the ionization of tyrosines, we first study the Tyr to Phe mutant and then introduce fluorinated phenylalanines. Previous studies have validated this strategy.[8]

Mutation to Phe at $\beta_2$97 was well-tolerated, lowering the EC_{50} to 0.6 μM (Table 5.2). When referenced to the Phe mutation, introduction of a single fluorine increased the EC_{50} 33-fold. Incorporation of 3,5-F_2Phe and then 3,4,5-F_3Phe further increased the EC_{50} 700- and 16,500-fold, respectively, indicating a 22-fold and 24-fold increase for each additional fluorine, respectively. Hill coefficients and macroscopic currents did not

change appreciably. The systematic increase in EC_{50} with the addition of fluorines at position $\beta_2$97 indicates a cation-π interaction is present. The dose-response relationships and a fluorination plot[4] of the cation-π binding energy[9] and the EC_{50} values compared with the parent Phe are shown in Figure 5.4.

Table 5.2 EC_{50} values (μM) for incorporation of fluorinated Phe residues at β_2Tyr97

Amino Acid	EC_{50}	$EC_{50}/EC_{50(WT)}$	$EC_{50}/EC_{50(Phe)}$	n_H	N
$\alpha_1\beta_2$ (WT)	3.5	1	5.8	1.2	4
Phe	0.6	0.17	1	1.4	4
4-F_1Phe	20	5.7	33	1.2	5
3,5-F_2Phe	420	120	700	1.1	4
3,4,5-F_3Phe	9900	2800	16,500	1.9	5

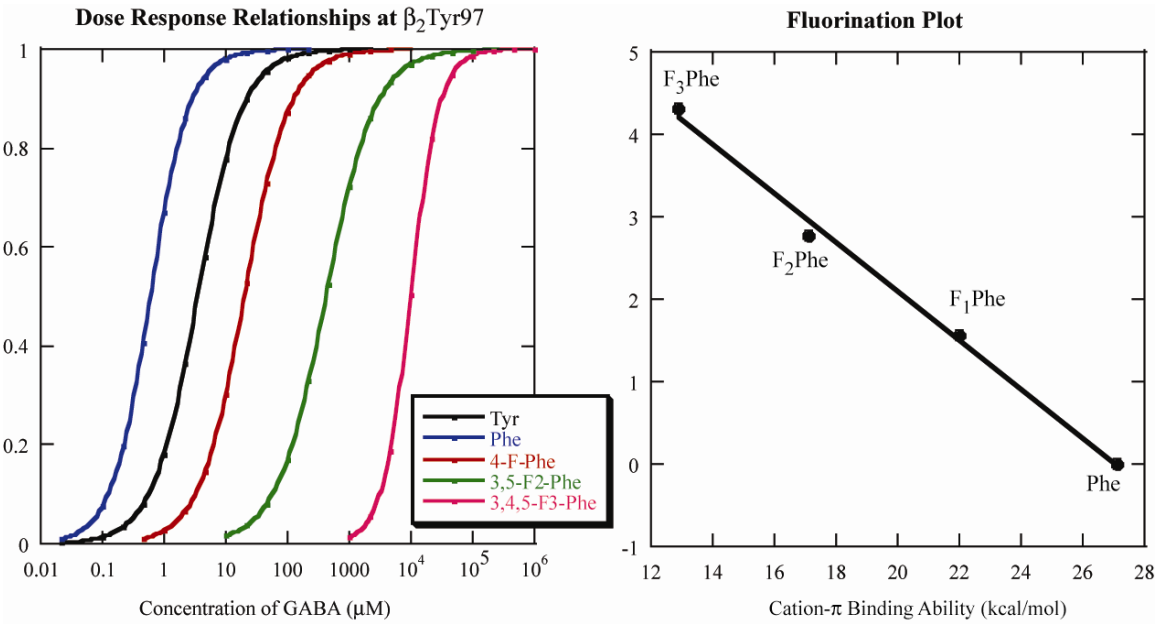

Figure 5.4 The dose response relationship shifts rightward with addition of fluorine residues (left panel). The fluorination plot (right panel) for Phe and Phe analogs at β_2Tyr97 of $GABA_AR$

The β_2Tyr157Phe mutation caused a 400-fold increase in the GABA EC_{50} to 1400 μM (Table 5.3), due to the removal of the 4 position hydroxyl. Incorporation of F_1Phe at the same position restored a wild type like $EC_{50,}$ while incorporation of 3,5-F_2Phe and 3,4,5-F_3Phe increased the EC_{50} but not in a manner consistent with a cation-π interaction.

The sensitivity of the receptor to the Phe mutation but not 4-F_1Phe strongly suggested the hydroxyl of tyrosine was important for channel function. To probe whether or not the OH group filled a steric or hydrogen bonding role, 4-Me-Phe and 4-OMe-Phe were incorporated. The 4-Me-Phe mutant has an EC_{50} 10-fold lower than the Phe mutant but 43-fold higher than wild type. 4-OMe-Phe, however, has an EC_{50} of 5 μM. Partial rescue of the Phe mutant by 4-Me-Phe suggests there is a steric component to the role of the 4 position hydroxyl at β_2Tyr157. Nearly full restoration of the wild type function by 4-OMe-Phe suggests that in addition to a steric role, the hydroxyl of β_2Tyr157 is a hydrogen bond acceptor.

Table 5.3 EC_{50} values for Phe analogues at β_2Tyr157 (loop B), β_2Tyr205 (loop C), and α_1Phe65 (loop D). EC_{50} values are given in μM; n_H is the hill coefficient; and N is the number of oocytes used.

β_2Tyr157	EC_{50}	n_H	N	β_2Tyr205	EC_{50}	n_H	N	α_1Phe65	EC_{50}	n_H	N
Phe	1400	0.9	6	Phe	80	1.4	5	Phe	3.0	1.2	4
F_1Phe	3.0	1.2	6	F_1Phe	1.5	1.9	3	F_1Phe	11	1.4	3
F_2Phe	420	2.0	4	F_2Phe	70	1.9	4				
F_3Phe	110	1.7	4	F_3Phe	90	2.5	4	F_3Phe	11.5	1.5	3
MePhe	5.0	1.2	3								
OMePhe	150	0.8	3								

Substitutions at position β_2Tyr205 (Table 5.3) showed some similarity to those at β_2Tyr157. There was an increase of 24-fold in EC_{50} for the Tyr to Phe mutation, but a wild-type EC_{50} for mutation to 4-F_1Phe. Incorporation of 3,5-F_2- or 3,4,5-F_3-Phe at this position yielded a similar EC_{50} to phenylalanine.

Incorporation of phenylalanine at the loop D residue, α_1Phe65, through nonsense suppression (wild type recovery) reproduced the wild-type GABA EC_{50} (Table 5.3). Addition of a fluorine to the phenyl ring increased EC_{50} to 11 μM. Incorporation of

F_3Phe did not further increase the EC_{50}. There were no significant differences in Hill coefficients for these mutations.

5.2.2 Glycine Results

An alignment of amino acid residues contributing to the aromatic box in Cys-loop receptors reveals that Phe63, Phe99, Phe159, Tyr202, and Phe207 of the α_1 GlyR are all possible candidates to contribute to a cation-π interaction (Table 5.1). A cation-π interaction at Phe99 or Tyr202 was ruled out on the basis of previous studies using conventional mutagenesis.[12,13] Therefore we selected Phe63, Phe159, and Phe 207 for unnatural amino acid incorporation. A recent study using conventional mutagenesis and a computational model[14] implicate Phe159 and Phe207 in a joint cation-π interaction with the glycine amino group (structure, Figure 5.6), making these two residues of particular interest.

Fluorinated Phe residues were incorporated using nonsense suppression. When coinjected with Phe-tRNA, mutant mRNAs encoding Phe63TAG, Phe159TAG, Phe207TAG, and Phe159TAG/Phe207TAG receptors produced functional receptors that responded to the application of glycine. Maximal currents (I_{max}), EC_{50} and n_H values were similar to each other, and to previously published results for wild-type (WT) α_1 homopentameric GlyRs expressed in *Xenopus* oocytes.[15] We thus conclude that the wild-type phenotype is successfully rescued by the nonsense suppression method.

Successive addition of fluorines to Phe159 leads to a progressive decrease in glycine sensitivity (Figure 5.5, Table 5.4), indicating a cation-π interaction at this site. 4-CN-Phe generates an EC_{50} value intermediate between those for 3,5-F_2Phe and 3,4,5-F_3Phe, as predicted by cation-π binding ability.[9] As in previous studies with Trp and Tyr,

the fluorination plot[4] demonstrates a strong linear correlation between the cation-π binding ability and relative log EC_{50} value (scaled to wild type). The magnitude and consistency of the effect show a significant cation-π interaction at Phe159.

Table 5.4 EC_{50} values (μM) for incorporation of fluorinated Phe residues at Phe159. I_{max} is reported in μA

Amino Acid	EC_{50}	$EC_{50}/EC_{50(Phe)}$	n_H	I_{max}	N
Phe	109 ± 2	1	2.8 ± 0.2	7.4 ± 0.6	5
4-F_1Phe	288 ± 6	2.6	3.1 ± 0.2	7 ± 1	4
3,5-F_2Phe	11000 ± 200	100	2.0 ± 0.1	7.7 ± 0.6	6
3,4,5-F_3Phe	103000 ± 3000	940	2.3 ± 0.1	5.6 ± 0.6	7
4-CN-Phe	46000 ± 1000	420	1.9 ± 0.1	9 ± 1	9

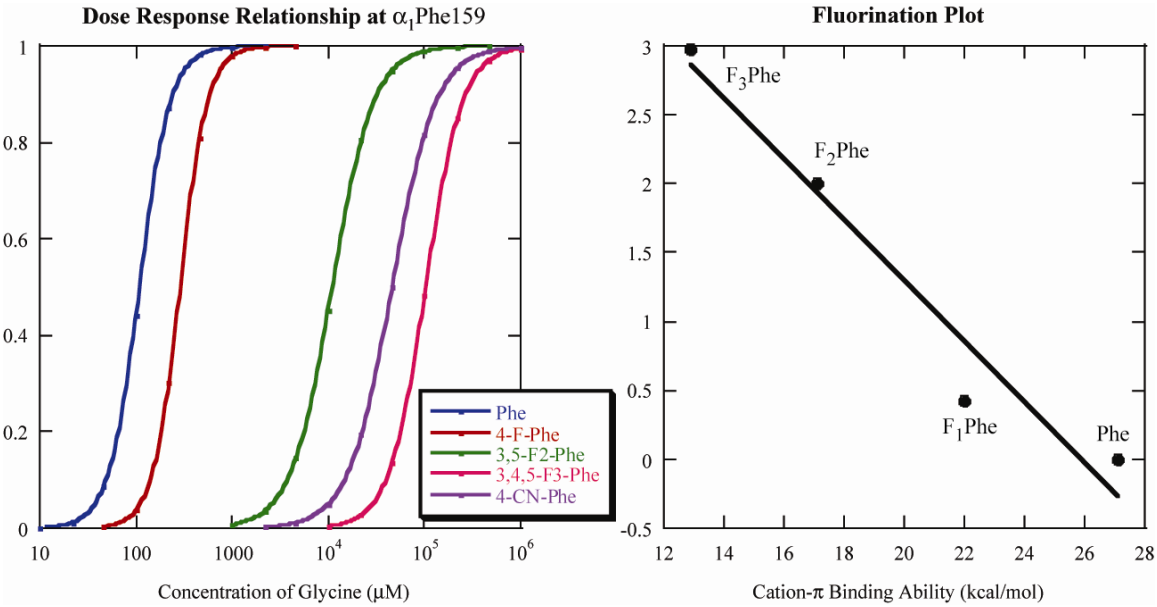

Figure 5.5 The dose response relationship shifts right indicating loss-of-funtion with addition of fluorine residues (left panel). The fluorination plot (right panel) for Phe and Phe analogs at Phe159 in α_1 GlyR

The addition of a single fluorine at Phe207 (F_1Phe) resulted in no change in the glycine EC_{50} value (Table 5.5). However, the addition of larger groups, methyl, methoxy, and cyano, at the 4 position yielded EC_{50} values 10- to 30-fold higher. Incorporation of 3,5-F_2Phe and 3,4,5-F_3Phe increased EC_{50} 500-fold and 100-fold, respectively. These results are not consistent with a cation-π interaction involving Phe207.

Table 5.5 EC_{50} values (μM) for incorporation of fluorinated Phe residues at Phe207 (green, left) and for simultaneous incorporation at Phe159 and Phe207 (red, right). I_{max} is reported in μA.

Amino Acid	EC_{50}	n_H	I_{max}	N	Amino Acid	EC_{50}	n_H	I_{max}	N
Phe	114	2.2	11 ± 1	4	Phe	131	2.7	9 ± 1	18
F_1Phe	151	2.4	10 ± 3	4	F_1Phe	287	2.6	8 ± 2	13
F_2Phe	56700	2.4	8.1 ± 0.2	5	CN-Phe	>400000	1.7	7.4 ± 0.7	4
F_3Phe	13500	2.4	8 ± 1	8					
CN-Phe	3910	2.6	10 ± 1	4					
Me-Phe	1020	2.2	10 ± 3	4					
OMe-Phe	2520	2.2	10 ± 0.4	4					

Additional evidence against a cation-π interaction at Phe 207 stems from results with the Phe159TAG/Phe207TAG double mutant receptor (Table 5.5). If Phe159 and Phe207 both contribute to a cation-π interaction with the glycine amine group, a large increase in EC_{50} would be expected when both interactions are simultaneously weakened. Receptors containing the Phe159TAG/Phe207TAG mutation displayed robust expression and electrophysiological properties similar to those of wild-type receptors when coinjected with Phe-tRNA. Addition of a single fluorine (4-F_1Phe) to both sites produced receptors with only a small decrease in glycine sensitivity (Table 5.5). The Phe159TAG/Phe207TAG double mutant did not produce a functional receptor with 3,5-F_2Phe-tRNA. However, introduction of a cyano group (4-CN-Phe) yielded receptors displaying a greatly reduced glycine sensitivity, with an EC_{50} value in excess of 400 mM.

Table 5.6 EC_{50} values (μM) for incorporation of fluorinated Phe residues at Phe63. I_{max} is reported in μA.

Amino Acid	EC_{50}	n_H	I_{max}	N	Amino Acid	EC_{50}	n_H	I_{max}	N
Phe	113	2.6	9 ± 1	7					
4-F_1Phe	34.5	2.8	8.9 ± 0.7	7	4-CN-Phe	6.5	2.7	8 ± 2	5
3,5-F_2Phe	210	2.1	3 ± 1	3	3,4,5-F_3Phe	348	2.8	4.2 ± 0.7	5

Introduction of a single fluorine in the 4 position at Phe63 decreased the EC_{50} value by a factor of three (Table 5.6). Substitution with 3,5-F_2Phe or 3,4,5-F_3Phe caused relatively small (2- to 3-fold) changes in EC_{50} value that produced no consistent trend when combined with F_1Phe data. We note that 3,5-F_2Phe and 3,4,5-F_3Phe produced significantly lower maximal currents, which may inflate the EC_{50} values slightly.[15] To ensure the lower maximal currents were not causing substantial artifacts in the data, we also incorporated 4-CN-Phe which gave maximal currents similar to both Phe and 4-F_1Phe. Cyano is strongly deactivating in a cation-π interaction (Figure 5.3),[4] and its introduction at a site where a cation-π interaction is present will substantially increase EC_{50}. Mutation to 4-CN-Phe substantially *decreased* EC_{50}, confirming that Phe63 does not participate in a cation-π interaction.

5.3 Discussion

5.3.1 A Cation-π Interaction at Loop A of $GABA_AR$

The $GABA_A$ receptor binding site has been intensively investigated using a range of techniques, including mutagenesis, radioligand binding assays, and photoaffinity labeling.[16-20] These techniques have implicated many amino acids that may be important in the binding site, but they cannot identify the chemical-scale interactions of each amino acid with the neurotransmitter. Here, we used unnatural amino acid mutagenesis combined with functional studies to probe the effects of subtle chemical modifications to aromatic amino acids that form a critical part of this binding site. The results indicate that β_2Tyr97 contributes to a cation-π interaction, the hydroxyl groups of β_2Tyr157 and β_2Tyr205 are critical to receptor function, and that α_1Phe65 is insensitive to subtle chemical changes.

Cysteine accessibility studies previously showed that β_2Tyr97Cys is protected from covalent modification by the presence of GABA or the $GABA_A$ receptor antagonist gabazine (SR95531).[20] indicating this residue lies in the binding pocket of the receptor. Furthermore, mutation to Cys had the same ~100-fold increase on the GABA EC_{50} and on the SR95531 IC_{50}. EC_{50} is an equilibrium measure which incorporates both binding events (the on and off rate of the agonist) and channel activation (the opening and closing rate), thus changes in EC_{50} cannot be directly attributed to changes in the agonist affinity. The antagonist, SR95531, is not able to activate the $GABA_AR$, thus the IC_{50} (concentration of antagonist necessary to achieve half maximal inhibition) is dependent only on binding events. Similar shifts in the EC_{50} of GABA and IC_{50} of SR95531 for the β_2Tyr97Cys mutant strongly indicate that changes in EC_{50} resulting from mutation of β_2Tyr97 are the result of changes in GABA binding.

Our data show a strong correlation between the cation-π binding ability of tyrosine derivatives incorporated at $\beta_2$97 and the EC_{50} (Figure 5.4). The size of this effect and the systematic dependence on the number of fluorines unambiguously establish a cation-π interaction at this site.

The fluorination plot indicates that β_2Tyr97 is involved in a cation-π interaction but does not indicate that the cationic partner is GABA. There are four positively charged amino acids within 10Å of β_2Tyr97 that could perform this role, and without detailed structural information it is difficult to exclude these residues. A homology model of the $GABA_AR$[21] indicates the β_2Lys102 and β_2Lys103 side chains face away from the binding site, suggesting they are unlikely partners for the cation-π interaction.

α_1Arg132 is positioned such that it could interact with β_2Tyr97 but this interaction would restructure the aromatic box such that GABA would not access the binding site. β_2Arg207, the remaining positively charged residue, has previously been proposed to interact with the carboxylate of GABA[22] and would therefore exclude it from contributing to a cation-π interaction at the other end of the molecule. Because all full GABA agonists have a charged amine, it is not possible to use an alternative agonist to provide definitive proof, but given the arguments described above, combined with the precedence of the ligand as the source of the cation in other Cys-loop receptors, we believe that GABA is the source of the cation.

Table 5.7 Sequence Alignment of loop A in the principle subunit of Cys-loop receptor binding sites

Subunit	Alignment	Alternate Alignment
AChBP	SSL**W**V**PD**LAA**Y****N**-AISK	SSL**W**V**PD**LAA**Y****N**-AISK
nACh α_1	ERI**W**R**PD**LVL**Y****N**NADGD	ERI**W**R**PD**LVL**Y****N**NADGD
5-HT_{3A}	DSI**W**V**PD**ILI**N**EFVDVG	DSI**W**V**PD**ILI**N**EFVDVG
Gly α_1	DSI**W**K**PD**L**F**FA**N**EKGAH	DSI**W**K**PD**L--**F**FA**N**EKG
$GABA_C$ ρ_1	KKI**W**V**PD**M**F**FVHSKRSF	KKI**W**V**PD**--M**F**FVHSKR
$GABA_A$ β_2	DQL**W**V**PD**T**Y**FL**N**DKKSF	DQL**W**V**PD**--T**Y**FL**N**DKK

The conserved WxPDxxxxN are shown in bold. The loop A residue of the aromatic box is highlighted.

Thus, the $GABA_A$ receptor becomes the first instance of a Cys-loop receptor that displays a cation-π interaction with a loop A residue. Loop A does contain an aromatic box residue in the nACh receptor, αTyr93, and in the AChBP crystal structures this Tyr aligns with Tyr89, which is clearly located at the "bottom" of the aromatic box. Presumably, $\beta_2$97 of the $GABA_A$ receptor plays the role of αTyr93 and Tyr89, but the alignment is problematic; a gap equivalent to 2 amino acids is required to bring the $\beta_2$97 into alignment with the nACh receptor and AChBP tyrosine residues (Table 5.7). Loop A contains a highly conserved WxPDxxxxN motif, which plays a crucial role in

positioning the rest of the binding site, particularly loop B.[23,24] It is therefore surprising that a gap insertion is necessary in a conserved region with such an important structural role, but the mutagenesis results are compelling.

The location of a cation-π interaction on loop A, contrasting to loop B for other members of the Cys-loop family, supports previous suggestions that a "lock-and-key" metaphor is not appropriate for such receptors.[7] If they required a precise protein–ligand lock-and-key interaction, we would expect related receptors to use cation-π interactions at a conserved location in the three-dimensional structure. This is not the case in the 5-HT-gated 5-HT_3 and MOD-1 receptors, in which the cation-π interactions occur on loop B and loop C, respectively.[5,7] We now find similar variability in the ionotropic GABA receptor family; the cation-π interaction moves from loop B in the $GABA_CR$[8] to loop A in the $GABA_AR$ (the present study). These are very similar receptors, showing 39% sequence identity and 64% homology between $GABA_A(\beta_2)$ and $GABA_C(\rho_1)$ in the extracellular domain. Nevertheless, GABA binds with different orientations in the two receptors. Apparently Cys-loop receptors require only that a ligand occupies the general binding region defined approximately by the aromatic box.

There is no cation-π interaction at $\alpha_1$65: addition of 4-F to the phenyl ring increased GABA EC_{50} slightly, but addition of more fluorines around the ring resulted in no additional increase. This residue has been previously reported to play a role in GABA binding: mutation of α_1Phe64 (α_1Phe65 by human numbering) to Leu increased the GABA EC_{50} from 6 to 1260 μM, with the IC_{50} values of bicuculline and SR95531 increasing by similar amounts.[16] This suggests that the effects of mutations at this position are attributable to disruption of binding rather than gating, and that an aromatic

is preferred here, although our data indicate that α_1Phe65 is tolerant to small chemical changes. A model of the $GABA_AR$[21] indicates that α_1Phe65 is located on the "right-hand" face of the aromatic box (Figure 5.2B), and is partially obscured by β_2Tyr157. Taken together, these data and the model suggest that α_1Phe65 contributes to the general hydrophobicity of the region.

Previous data suggest that β_2Tyr157 and β_2Tyr205 specifically participate in GABA binding: phenylalanine mutations at both these sites significantly increased EC_{50} values, whereas activation of the receptors using pentobarbital, which binds at a location distinct from the GABA binding site, resulted in no change in functional response.[17] Similarly, we observed that removal of the OH (introducing Phe) is highly deleterious at both β_2Tyr157 and β_2Tyr205, resulting in ~400- or 24-fold increases in EC_{50}, respectively. Wild-type behavior can be rescued at β_2Tyr157 by incorporation of 4-F or 4-MeO substituents, whereas 4-Me-Phe or multiply fluorinated phenylalanines increased EC_{50} values 35- to 120-fold. These data suggest that the OH of β_2Tyr157 acts as a hydrogen bond acceptor. The strong penalty for removing the OH and the near wild-type behavior of 4-MeO-Phe support this analysis. In this light, the near wild-type behavior for 4-F-Phe is perhaps surprising. Fluorine is the most electronegative element, and as such it is reluctant to donate a lone pair of electrons to a hydrogen bond donor. As a result, organic fluorine (fluorine bonded to a carbon) hardly ever accepts a hydrogen bond, especially if an alternative, better acceptor can be accessed.[25] Inspection of the region around β_2Tyr157 in a receptor model[21] suggests that there are no alternative hydrogen bond acceptors close to the hydroxyl group within the protein. In such a case, even the very poor acceptor of 4-F-Phe may be better than nothing at all (Phe). The data

for β_2Tyr205 show no clear pattern, although there is an indication that an electronegative atom at position 4 is favored.

5.3.2 A Cation-π Interaction at Loop B of GlyR

A previous model of the GlyR[14] indicated a cation-π interaction involving both Phe159 and Phe207 may exist. In addition to these two residues, there are other aromatic residues in the binding pocket (Phe63, Tyr161, Phe99, Phe100, and Tyr202). We omitted Tyr161 from the present study because the Tyr161Ala was previously shown to function despite a 10-fold loss in glycine sensitivity.[26,27] If this residue was involved in a critical cation-π interaction, it seems unlikely that mutation to Ala would only cause a 10-fold shift in channel function. Phe99 and Phe100 in loop B were omitted for similar reasons, as Ala substitution at these sites results in only small changes to the EC_{50} value.[12] It has been convincingly demonstrated that the hydroxyl group of Tyr202 and not its aromatic character is crucial for agonist binding.[13] Therefore, of the seven residues originally identified, only Phe63, Phe159, and Phe207 were plausible candidates for a cation-π interaction.

The data presented here clearly indicate there is a cation-π interaction with Phe159 and not with Phe207 in the α_1 GlyR. These results are in disagreement with a prior model which proposed a cation-π interaction at both Phe159 and Phe207.[14] We performed experiments with double-mutant receptors (Phe159/Phe207) to confirm there was not a dual cation-π interaction. The measured EC_{50} value of ~300 μM for receptors with 4-F_1Phe at both of these positions is close to the calculated value of ~380 μM that would be expected if the EC_{50} value were simply the product of the two individual

mutations. Substitution with 4-CN-Phe at both sites resulted in functional receptors. Although the glycine EC_{50} value (>400 mM) of the double mutant could not be determined, the data are consistent with the EC_{50} value of ~1.5 M calculated by multiplying the EC_{50} value of the two single mutations. For a dual cation-π interaction we would expect to see an EC_{50} for the double mutant that differed from that predicted by the EC_{50} values of the single mutations. Together, the results from both the Phe207TAG single mutant and the Phe159TAG/Phe207TAG double mutant support the presence of only one cation-π interaction in the GlyR binding site, namely that at position 159.

The data presented here rule out a cation-π interaction at position 207. However, previous studies indicate an aromatic residue at this position is imperative for proper receptor function.[14] Phe207 was highly sensitive to all Phe analogues except 4-F_1Phe, suggesting a sensitivity to the addition of steric bulk, especially at the 3 and 5 positions of the phenyl ring. This result is surprising since a hydrogen to fluorine substitution is usually well tolerated.[3-5,7,8,21,28] Perhaps the higher sensitivity to these mutations in the GlyR is due to the smaller size of the neurotransmitter. Since glycine is a smaller molecule than the ligands that activate other Cys-loop receptors, the GlyR binding site may be more compact than any of the other aromatic boxes examined thus far, thereby making it more sensitive to incorporation of Phe analogues with substituents at the 3 and 5 positions or bulky substituents at the 4 position.

5.3.3 Cys-loop Receptor Cation-π Interactions

A cation-π interaction has been identified in the binding site of all seven cys-loop receptors explicitly tested for the interaction.[3-5,7,8,21,28] Although the location of the interaction varies, the loop B aromatic is involved in five (nAChRs, $5HT_{3A}R$, $GABA_CR$,

and GlyR) of the 7 receptors. The slopes of the fluorination plots are indicative of the strength of the cation-π interaction but (Figure 5.6) vary significantly (3.7-fold) with the $GABA_AR$ having the strongest and the acetylcholine receptors having the weakest. Acetylcholine has a quaternary ammonium group which presents a less focused charge to the aromatic face, thereby decreasing the strength of the cation-π interaction. This may contribute to the shallower slope of the acetylcholine receptors. However, all the other neurotransmitters have primary ammonium moieties, yet there is still a 2.2-fold range in slopes, indicating that the positively charged species alone is not indicative of the strength of the interaction.

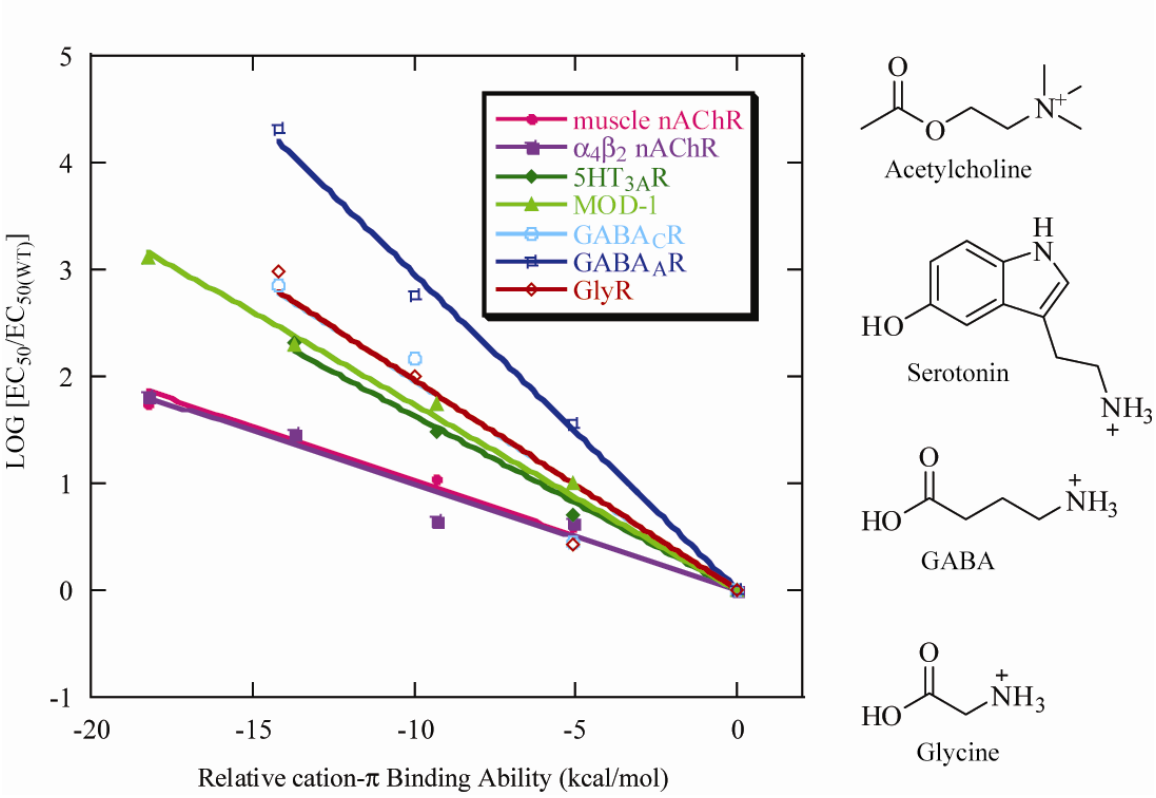

Figure 5.6 Fluorination plot of seven Cys-loop receptors and their neurotransmitter agonists. The $GABA_CR$ (light blue) linear fit is hidden by the GlyR (red).

5.4 Conclusion

In conclusion, cation-π interactions between GABA and a tyrosine on loop A in the $GABA_AR$ and between glycine and a phenylalanine on loop B in the GlyR have been identified by unnatural amino acid mutagenesis. The $GABA_AR$ is the first example of a cation-π interaction with a loop A residue in a Cys-loop receptor, while the cation-π interaction in the GlyR is the first example of such an interaction between a neurotransmitter and phenylalanine residue. The location of the cation-π interaction is not conserved among closely related members of the Cys-loop family, as evidenced by the different locations for the $GABA_A$ (loop A) and $GABA_C$ (loop B) receptors. The results presented here, along with previous studies that identified cation-π interactions in other Cys-loop receptors, emphasize the importance of the cation-π interaction to neurotransmitter binding and thus proper brain function.

5.5 Materials and Methods

Mutagenesis and preparation of mRNA: Mutant $GABA_A$ receptor subunits were developed using pcDNA3.1 (Invitrogen, Abingdon, UK) containing the complete coding sequence for either the human α_1 or human β_2 $GABA_A$ receptor subunit kindly provided by Dr. K. A. Wafford (Merck, Sharp, and Dohme, Harlow, Essex, UK). The codons at positions $\alpha_1$65, $\beta_2$97, $\beta_2$157, and $\beta_2$205 were replaced by a TAG codon as described previously (Beene et al., 2002). Mutagenesis reactions were performed using the method of Kunkel (1985) and confirmed by DNA sequencing. The human GlyR α_1 subunit cDNA was subcloned into pGEMHE to increase expression in oocytes. Site-directed mutagenesis to a TAG codon at positions 63, 159, and 207 was performed with the

QuickChange mutagenesis kit (Stratagene). The mMessage mMachine kit (Ambion) was used to generate capped mRNA for oocyte injection.

Xenopus laevis (Nasco) oocytes were prepared as described below and injected with 5 ng ($GABA_AR$) or 10 ng of mRNA. After injection, oocytes were incubated for 24-48 hours at 18°C prior to electrophysiology recordings.

Xenopus oocyte preparation: Harvested stage V–VI *Xenopus* oocytes were washed in four changes of OR2 buffer (in mM: 82.5 NaCl, 2 KCl, 1 MgCl2, 5 HEPES, pH 7.5), defolliculated in 1 mg/ml collagenase for ~1 hour, washed again in four changes of OR2, and transferred to 70% Leibovitz media (Invitrogen) buffered with 10 mM HEPES, pH 7.5. The following day, they were injected with 5 ng ($GABA_AR$) or 10 ng (GlyR) of mRNA. Electrophysiological measurements were performed 24–72 h after injection.

Synthesis of tRNA and dCA amino acids. This was as described previously (Beene et al., 2004). Briefly, unnatural amino acids were chemically synthesized as nitroveratryloxycarbonyl-protected (NVOC) cyanomethyl esters and coupled to the dinucleotide dCA, which was then enzymatically ligated to 74-mer THG73 $tRNA_{CUA}$ as detailed previously.[10] Immediately before coinjection with mRNA, aminoacyl tRNA was deprotected by photolysis.[29] For the $GABA_AR$ 5 ng of total cRNA was typically injected (1 ng of wild-type α_1 or β_2 subunit and 4 ng of the corresponding α_1 or β_2 mutant subunit) with 25 ng of tRNA-aa in a total volume of 50 nl. For the GlyR, 10 ng of mutant α_1 cRNA and 25 ng of tRNA-aa in a total volume of 50 nl was injected. For a control, cRNA alone and cRNA mixed with dCA-THG_{74} tRNA (no unnatural amino acid

attached) were injected into oocytes. No neurotransmitter-induced currents were detected.

Characterization of mutant receptors: Peak GABA-induced currents were recorded at 22-25°C from individual oocytes using the OpusXpress system (Axon Instruments, Molecular Devices). GABA (Sigma, St. Louis, MO) was stored as 100 mM aliquots at -80°C, diluted in ND96 buffer (in mM: 96 NaCl, 2 KCl, 1 MgCl2, 1.8 CaCl2, 5 HEPES, pH 7.5) and delivered to cells via the automated perfusion system of the OpusXpress. Glass microelectrodes were backfilled with 3 M KCl and had a resistance of 0.5-3.9 MΩ. The holding potential was -60 mV. To determine EC_{50} values, GABA concentration–response data were fitted to the Hill equation (equation 5.1), where I_{max} is the maximal peak current and n is the Hill coefficient.

$$I = \frac{I_{\max}}{1 + EC_{50}/[A]^n} \qquad \textbf{Equation 5.1}$$

5.6 References

(1) Akabas, M. H. *Int Rev Neurobiol* **2004**, *62*, 1-43.
(2) Brejc, K.; van Dijk, W. J.; Klaassen, R. V.; Schuurmans, M.; van Der Oost, J.; Smit, A. B.; Sixma, T. K. *Nature* **2001**, *411*, 269-76.
(3) Xiu, X.; Puskar, N. L.; Shanata, J. A.; Lester, H. A.; Dougherty, D. A. *Nature* **2009**.
(4) Zhong, W.; Gallivan, J. P.; Zhang, Y.; Li, L.; Lester, H. A.; Dougherty, D. A. *Proc Natl Acad Sci U S A* **1998**, *95*, 12088-93.
(5) Beene, D. L.; Brandt, G. S.; Zhong, W.; Zacharias, N. M.; Lester, H. A.; Dougherty, D. A. *Biochemistry* **2002**, *41*, 10262-9.
(6) Beene, D. L.; Price, K. L.; Lester, H. A.; Dougherty, D. A.; Lummis, S. C. *J Neurosci* **2004**, *24*, 9097-104.
(7) Mu, T. W.; Lester, H. A.; Dougherty, D. A. *J Am Chem Soc* **2003**, *125*, 6850-1.
(8) Lummis, S. C.; D, L. B.; Harrison, N. J.; Lester, H. A.; Dougherty, D. A. *Chem Biol* **2005**, *12*, 993-7.
(9) Mecozzi, S.; West, A. P., Jr.; Dougherty, D. A. *Proc Natl Acad Sci U S A* **1996**, *93*, 10566-71.
(10) Nowak, M. W.; Gallivan, J. P.; Silverman, S. K.; Labarca, C. G.; Dougherty, D. A.; Lester, H. A. *Methods Enzymol* **1998**, *293*, 504-29.
(11) Nowak, M. W.; Kearney, P. C.; Sampson, J. R.; Saks, M. E.; Labarca, C. G.; Silverman, S. K.; Zhong, W.; Thorson, J. S.; Abelson, J. N.; Davidson, N.; Schultz, P. G.; Dougherty, D. A.; Lester, H. A. *Science* **1995**, *268*, 439-442.
(12) Vafa, B.; Lewis, T. M.; Cunningham, A. M.; Jacques, P.; Lynch, J. W.; Schofield, P. R. *J Neurochem* **1999**, *73*, 2158-66.
(13) Rajendra, S.; Vandenberg, R. J.; Pierce, K. D.; Cunningham, A. M.; French, P. W.; Barry, P. H.; Schofield, P. R. *EMBO J* **1995**, *14*, 2987-98.
(14) Grudzinska, J.; Schemm, R.; Haeger, S.; Nicke, A.; Schmalzing, G.; Betz, H.; Laube, B. *Neuron* **2005**, *45*, 727-39.
(15) De Saint Jan, D.; David-Watine, B.; Korn, H.; Bregestovski, P. *J Physiol* **2001**, *535*, 741-55.
(16) Sigel, E.; Baur, R.; Kellenberger, S.; Malherbe, P. *EMBO J* **1992**, *11*, 2017-23.
(17) Amin, J.; Weiss, D. S. *Nature* **1993**, *366*, 565-9.
(18) Smith, G. B.; Olsen, R. W. *J Biol Chem* **1994**, *269*, 20380-7.
(19) Boileau, A. J.; Evers, A. R.; Davis, A. F.; Czajkowski, C. *J Neurosci* **1999**, *19*, 4847-54.
(20) Boileau, A. J.; Newell, J. G.; Czajkowski, C. *J Biol Chem* **2002**, *277*, 2931-7.
(21) Padgett, C. L.; Hanek, A. P.; Lester, H. A.; Dougherty, D. A.; Lummis, S. C. *J Neurosci* **2007**, *27*, 886-92.
(22) Wagner, D. A.; Czajkowski, C.; Jones, M. V. *J Neurosci* **2004**, *24*, 2733-41.
(23) Cashin, A. L.; Petersson, E. J.; Lester, H. A.; Dougherty, D. A. *J Am Chem Soc* **2005**, *127*, 350-6.
(24) Lee, W. Y.; Sine, S. M. *J Gen Physiol* **2004**, *124*, 555-67.
(25) Dunitz, J. D. *Chembiochem* **2004**, *5*, 614-21.
(26) Vandenberg, R. J.; French, C. R.; Barry, P. H.; Shine, J.; Schofield, P. R. *Proc Natl Acad Sci U S A* **1992**, *89*, 1765-9.
(27) Yang, Z.; Ney, A.; Cromer, B. A.; Ng, H. L.; Parker, M. W.; Lynch, J. W. *J Neurochem* **2007**, *100*, 758-69.
(28) Pless, S. A.; Millen, K. S.; Hanek, A. P.; Lynch, J. W.; Lester, H. A.; Lummis, S. C.; Dougherty, D. A. *J Neurosci* **2008**, *28*, 10937-42.
(29) Kearney, P. C.; Nowak, M. W.; Zhong, W.; Silverman, S. K.; Lester, H. A.; Dougherty, D. A. *Mol Pharmacol* **1996**, *50*, 1401-12.

Chapter 6

Backbone Cleavage of an Unstructured Region of the $GABA_AR$ Extracellular Domain Prevents GABA but not Pentobarbital Activation

6.1 Introduction

6.1.1 γ-Aminobutyric Acid type A Receptors

The γ-aminobutyric acid type A receptor ($GABA_AR$) is a member of the Cys-loop family of ligand gated ion channels and mediates rapid inhibitory synaptic transmission in the mammalian nervous system. In addition to direct activation by the neurotransmitter GABA, the activity of $GABA_ARs$ can be allosterically modulated by a variety of compounds including benzodiazepines (BZDs), barbitautes, volatile anesthetics, alcohols, and neuroactive steroids.[1] Identifying the mechanisms by which both GABA and these allosteric modulators affect the conformational movements within the $GABA_AR$ are critical for understanding the underlying actions of these pharmaceuticals.

The Cys-loop ligand gated ion channels (LGICs) are a superfamily with a common function and topology. In addition to the $GABA_ARs$, the superfamily contains two other inhibitory members, the $GABA_C$ and glycine (Gly) receptors, as well as two excitatory members, the nicotinic acetylcholine (nACh) and serotonin type 3 ($5\text{-}HT_{3A}$) receptors. At rest these receptors are in a closed, non-conducting state. Binding of the appropriate neurotransmitter initiates a conformational change to an open, ion-conducting state. The conformational change from closed to open is called activation and the residues involved in the transition are part of the activation pathway.

Cys-loop LGICs are pentameric proteins with the five homologous subunits arranged pseudo-symmetrically around the central ion-conducting pore (Figure 6.1). In addition to numerous biochemical studies, structural information of these receptors has been aided by the crystal structure of the acetylcholine binding protein (AChBP)[2] and the cryo-EM structure of the *Torpedo californica* nicotinic acetylcholine receptor.[3] The primary sequence of each has a large amino-terminal extracellular domain followed by four membrane-spanning helices and a short extracellular carboxy-terminus. The extracellular domain consists primarily of two beta sheets with the beta strands connected by unstructured loops which contribute to the ligand binding site[2,4] and to the activation pathway.[5-8] The second transmembrane helix of each subunit lines the channel pore and contains the channel gate, some 50-60 Å from the neurotransmitter binding site.

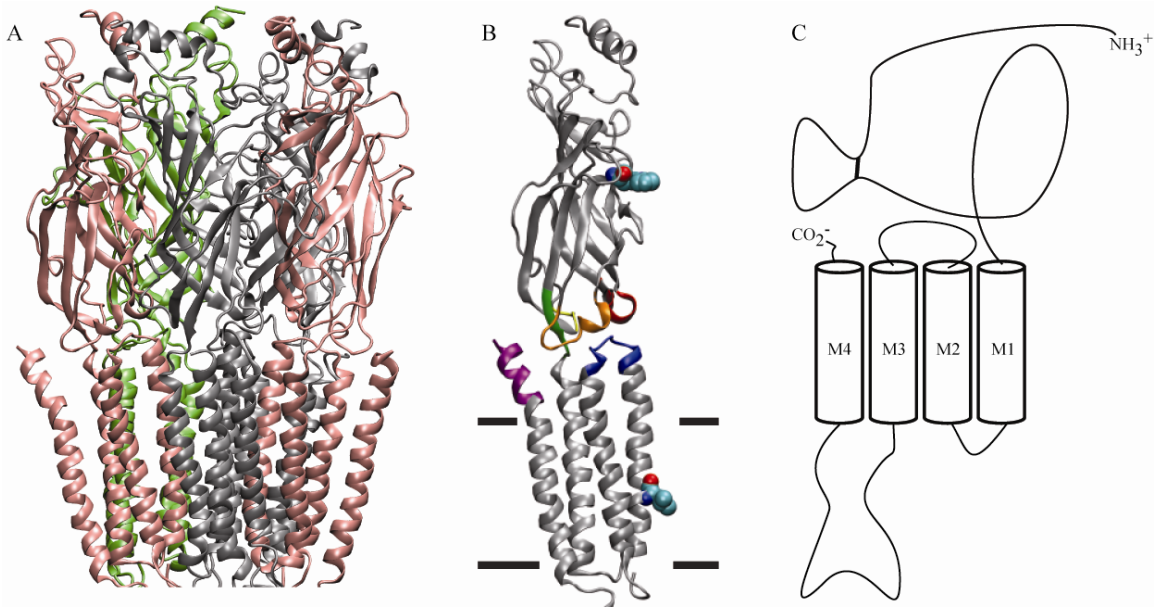

Figure 6.1 General topology of $GABA_AR$. **A**, homology model of the $GABA_AR$ (built from Protein Data Bank 2BG9) with the α subunits in pink, β subunits in gray, and the γ subunit in green. **B**, An individual subunit from A with the ligand binding site and channel gate highlighted as VDW and the edges of the membrane bilayer marked with black boxes. **C,** Schematic cartoon of each subunit. Each subunit has a predominantly beta sheet, N-terminal extracellular domain, four membrane-spanning helices, and a short extracellular carboxy terminus. The large intracellular loop between M3 and M4 has been omitted from **A** and **B**.

There are 19 identified $GABA_AR$ subunits designated α_1-α_6, β_1-β_3, γ_1-γ_3, δ, ε, π, and θ, however not all combinations of subunits form functional receptors. In the mammalian brain, all $GABA_ARs$ contain two α and two β subunits.[9] The GABA binding site is located at the β/α interface. The β subunit is considered the primary subunit of the binding site as it contributes four of the five residues in the aromatic box.[10] The α subunit contributes the fifth residue to the binding site and is the complementary subunit. The fifth subunit of $GABA_ARs$ is most commonly a γ_2 subunit. Together $\alpha_1\beta_2\gamma_2$, $\alpha_2\beta_3\gamma_2$, and $\alpha_1\beta_2\gamma_2$ make up over two-thirds of $GABA_ARs$ in the mammalian brain, with $\alpha_1\beta_2\gamma_2$ comprising ~40% of all $GABA_ARs$.[11] Receptors containing α_1-α_3, or α_5 and γ_2 subunits are sensitive to clinically prescribed benzodiazepines (BZDs).[12,13] The BZD binding site is located at the α/γ interface. Site-directed mutagenesis and substituted cysteine scanning methods (SCAM) have identified a histidine residue in loop A of the α subunit (His101 in α_1 numbering) as critical to BZD action (Figure 6.2).[14-16]

Residues outside but near the aromatic box of Cys-loop receptors have been implicated in neurotransmitter binding and activation.[17-23] Mutagenesis and SCAM studies have identified residues α_1N115, α_1L117, α_1R119, α_1I120, α_1T129, and α_1R131 (Figure 6.2) that contribute to GABA binding.[24,25] The primary sequence of the α_1 subunit connects His101 to these residues through an unstructured (as indicated in the AChBP and cryo-EM structures) linker. Allosteric modulators of $GABA_ARs$ bind at sites distinct from the GABA binding site and are believed to initiate an allosteric transition in the protein that indirectly modifies the conformation of the binding site.[26] Furthermore, numerous binding studies have shown that GABA and BZD binding is cooperative,[25,27]

providing additional evidence that the binding sites exert an effect on each other. Based on this evidence, we reasoned that the linker between His101 and N115 was critical to allosteric modulation and that cleavage of the backbone peptide in this region of the α_1 subunit would disrupt BZD potentiation of the GABA current. Herein, we use nonsense suppression[28,29] to site-specifically incorporate a photoactive unnatural amino acid to cleave the $GABA_AR$ backbone.

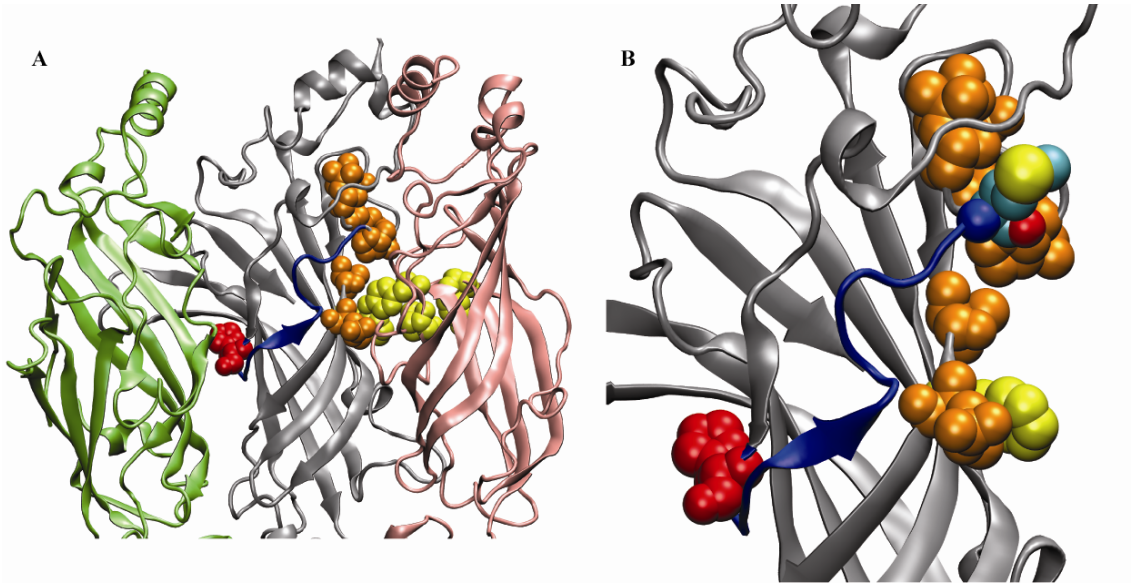

Figure 6.2 An unstructured linker connects the GABA binding site and BZD binding site. **A**, the linker (blue) in the α subunit (gray) stretches from the β/α interface (β in pink) to the α/γ interface (γ in green). His101 (loop A residue) is shown in red. Yellow residues denote the aromatic box for GABA. Orange residues have been shown to be involved in GABA binding but are not part of the aromatic box. **B**, Magnification of the linker region. M113 is added (cyan) to mark the site where Npg will be incorporated.

6.1.2 Proteolytic Cleavage by Photolysis

The design of nitrophenylglycine (Npg) was based on the photochemistry of 2-nitrobenzyl derivatives. Compounds of this type, including Npg, have been used as protecting groups in organic synthesis to produce caged neurotransmitters, ions, and second messengers that can be liberated photochemically.[30-40] When Npg is incorporated into a protein (Scheme 6.1), photolysis induces a series of rearrangements shown in Scheme 6.1, ultimately cleaving the peptide backbone.

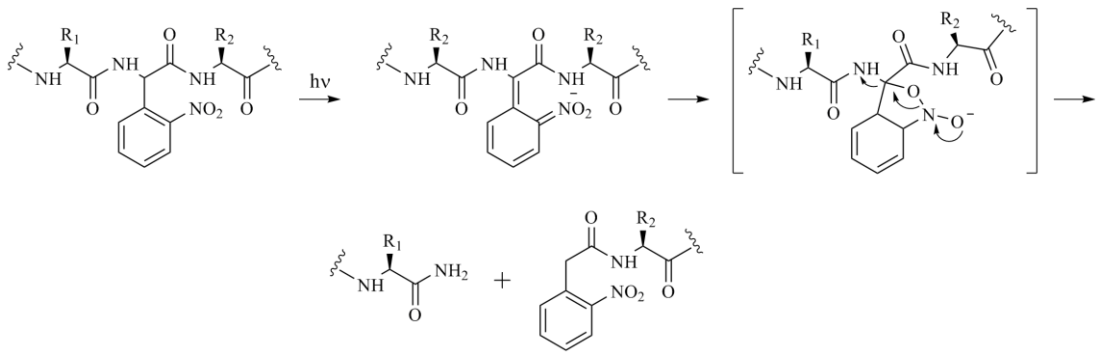

Scheme 6.1

6.2 Results

6.2.1 Heterologous Expression of GABA$_A$R

Expression of $\alpha_1\beta_2\gamma_2$ GABA$_A$Rs in heterologous expression systems such as *Xenopus* oocytes can result in a mixed population of $\alpha_1\beta_2\gamma_2$ and $\alpha_1\beta_2$ receptors.[41] When mRNA is injected in a 1:1:1 ratio, a mixed population results. $\alpha_1\beta_2$ GABA$_A$Rs are not modulated by BZDs, whereas $\alpha_1\beta_2\gamma_2$ GABA$_A$Rs are. Thus for a mixed population of receptors, we expect to see potentiation levels in between zero (expected for pure $\alpha_1\beta_2$) and that of pure $\alpha_1\beta_2\gamma_2$ populations (~2.5 for the benzodiazepine flurazepam). For wild type receptors, the relative amount of γ_2 mRNA is increased until maximum potentiation is reached, and this ratio is used for additional experiments with conventional mutants.

When using the nonsense suppression methodology, expression depends on the batch of oocytes, relative expression levels of the mRNA, the quality of the tRNA-Uaa, and the oocyte's ability to incorporate the unnatural amino acid. Group observations[2] have indicated less consistency using the nonsense suppression methodology than seen with conventional mutagenesis. Specifically, we have found that expression levels vary considerably from one unnatural amino acid to another and from one batch of oocytes to

[2] Group observation from the labs of Dennis Dougherty, Division of Chemistry and Chemical Engineering, California Institute of Technology, Pasadena, CA 91125

the next. Therefore, we expected that an mRNA ratio for wild type recovery (incorporation of the wild type amino acid using the nonsense suppression methodology) would not necessarily work for our unnatural amino acids. Furthermore, the BZD potentiation test cannot be used since we expect our mutations to disrupt BZD potentiation. Due to these concerns, we decided to first conduct our experiments in the $\alpha_1\beta_2$ $GABA_AR$ to determine if they should be carried over to the more complicated system of the $\alpha_1\beta_2\gamma_2$ $GABA_AR$.

Oocyes were injected with wild type α_1, β_{2S}, or γ_{2L} mRNAs individually. These oocytes did not respond to 10 mM GABA, indicating that the individual subunits were not sufficient to form functional $GABA_ARs$. As expected, oocytes injected with α_1/β_{2S} mRNA gave functional $GABA_ARs$ with an EC_{50} of 1-3 μM and a Hill coefficient between 1.2 and 1.8 for individual oocytes. Injection of α_1/γ_{2L} or β_{2S}/γ_{2L} mRNA was not expected to produce receptors that respond to GABA. As anticipated, α_1/γ_{2L} injected oocytes did not respond to GABA. However, the β_{2S}/γ_{2L} injected oocytes responded to GABA in a concentration-dependent manner. The EC_{50} of the individual oocytes ranged from 70-200 μM. All oocytes had Hill coefficients less than 1, providing a defining characteristic of this $GABA_AR$ subtype. GABA-induced responses in β_{2S}/γ_{2L} injected oocytes further complicate suppression experiments in the α_1 subunit of $\alpha_1\beta_{2S}\gamma_{2L}$ $GABA_ARs$, providing another reason to first do experiments with $\alpha_1\beta_{2S}$ $GABA_ARs$.

6.2.2 Site-Selection for Npg Incorporation

The goal of structure-function studies is to elucidate the role of a particular residue in the wild type receptor. When using Npg and UV light we are effectively

making two mutations, the first is incorporation of Npg and the second is cleavage of the backbone. Differences in channel function before and after proteolysis provide information about the mutant Npg-containing receptor. However, we can still gain insight into the wild type receptor by selecting a site for Npg incorporation such that the mutant receptor has a similar pharmacology to the wild type receptor; thus candidate sites for Npg incorporation must be tolerant of side chain mutations.

While sites highly tolerant to side chain mutations are ideal for the analysis of Npg incorporation, these same sites can be problematic when using the nonsense suppression methodology. The complication arises from the orthogonality of the suppressor tRNA. In a nonsense suppression experiment, suppressor tRNA is charged with an unnatural amino acid (Uaa-tRNA). Once the unnatural amino acid is incorporated into the nascent protein, the uncharged suppressor tRNA (dCA-tRNA) is released back into the ooctye cytoplasm. If the suppressor tRNA is completely orthogonal, the amino-acyl transferases within the oocyte do not recognize dCA-tRNA as a tRNA molecule and thus will not charge the dCA-tRNA with a naturally occurring amino acid. However, if the dCA-tRNA is not completely orthogonal, it can be charged with an amino acid (re-aminoacylated) which can then compete for incorporation in place of the Uaa at the site containing the stop codon. Recent studies have shown that for THG73 (the suppressor tRNA used here), glutamine is most often the amino acid incorporated.[42]

One advantage to using electrophysiology to evaluate protein function is that our assays only detect functional receptors. Therefore, we use the control experiments explained below to identify candidate sites for Npg incorporation. For re-aminoacylation

control experiments, oocytes are injected with a mixture of uncharged dCA-tRNA and mRNA and tested for response to GABA. To control for read-through, oocytes are injected with only the mRNA and tested for response to GABA to ensure the ribosome does not read-through the stop codon. Finally, the wild type recovery control is conducted to ensure that suppression at the site of interest using the wild type residue reproduces wild type receptors. Ideally suppression sites with little or no response to GABA during the re-aminoacylation and read-through control experiments but high expression and wild type behavior during the recovery control will be identified.

Table 6.1 Results of wild type recovery experiments at four sites in the αβ $GABA_AR$

Site	Wild Type Recovery				Read-through	Re-amino acylation
	EC_{50} (μM)	n_H	I_{max} (μA)	N		
αβ (WT)	2.33 ± 0.04	1.4	-3.3 ± 0.7	9	N/A	N/A
αV107	3.4 ± 0.1	1.3	-4 ± 1	9	-0.08	-0.88
αM111	2.9 ± 0.2	1.3	-0.6 ± 0.4	10	-0.08	-0.03
αM113	2.3 ± 0.1	1.3	-2.3 ± 0.6	14	-0.06	-0.15
αP114	1.8 ± 0.1	1.7	-3.5 ± 0.5	5	-0.14	-0.08

I_{max} values (μA) were determined from the same oocytes used to determine the EC_{50} and Hill coefficients (n_H). N is the number of oocytes used to determine the EC_{50}, n_H, and I_{max}. Read-through and re-aminoacylation values are the average of the maximal current of two oocytes with the highest level of expression.

Npg is a beta-branched, hydrophobic amino acid, thus we reasoned it would be least likely to alter protein pharmacology at a site with hydrophobic and bulky side chains within the linker region. Therefore we selected V107, M111, M113, and P114 as candidate sites. Wild type recovery experiments at all four sites gave EC_{50} values and Hill coefficients (n_H) similar to the wild type αβ $GABA_AR$. There was no appreciable difference in the shape of the dose response relationships (Figure 6.3, A). Oocytes injected with only the mRNA (read-through, Table 6.1) produced little current when tested with 10 mM GABA. When the mRNA was coinjected with dCA-tRNA, only the

αV107Tagβ showed significant current (I_{max}>300 nA), such that the EC_{50} (6.5 ± 0.3 μM) and Hill coefficient (1.0) could be determined.

Table 6.2 Wild type recovery experiments at four sites in the αβγ $GABA_AR$

	EC_{50} (μM)	**n_H**	**I_{max} (μA)**	**N**
αβγ (WT)	55 ± 2	1.5	-6 ± 2	7
αV107Tagβγ + Val	26 ± 1	1.6	-10 ± 1	13
αM111Tagβγ + Met	49 ± 2	1.6	-2.0 ± 0.6	11
αM113Tagβγ + Met	39 ± 1	1.5	-6 ± 1	9
αP114Tagβγ + Pro	44 ± 1	1.5	-6 ± 1	12

Table 6.3 Results of read-through and re-aminoacylation experiments for nonsense suppression at four sites in the αβγ $GABA_AR$

	Read-through				Re-aminoacylation			
Site	**EC_{50} (μM)**	**n_H**	**I_{max} (μA)**	**N**	**EC_{50} (μM)**	**n_H**	**I_{max} (μA)**	**N**
V107	330 ± 70	0.67	-1.5 ± 0.2	8	46 ± 2	1.19	-5 ± 1	5
M111	340 ± 40	0.72	-1.0 ± 0.2	6	1300 ± 200	0.73	-3.4 ± 0.9	5
M113	530 ± 90	0.64	-1.3 ± 0.1	5	1400 ± 500	0.60	-3.7 ± 0.8	4
P114	250 ± 40	0.73	-1.2 ± 0.3	8	38 ± 3	1.12	-4.8 ± 0.6	3

Wild type recovery experiments in the αβγ $GABA_AR$ gave EC_{50} and Hill coefficients similar to that of wild type at three of the four sites (Table 6.2, Figure 6.3, B). At V107, the EC_{50} was approximately half that of the wild type receptor. I_{max} values were similar to wild type for M113 and P114, but significantly lower for M111. Read-through and re-aminoacylation controls gave whole cell currents large enough to determine the dose response relationships (Figure 6.3, C and D). All four sites had similar I_{max}, EC_{50}, and n_H values in the read-through experiments (Table 6.3). Re-aminoacylation of the tRNA and subsequent incorporation of the amino acid at V107 and P114 produced higher I_{max} values than at M111 or M113 and EC_{50} values similar to wild type receptors.

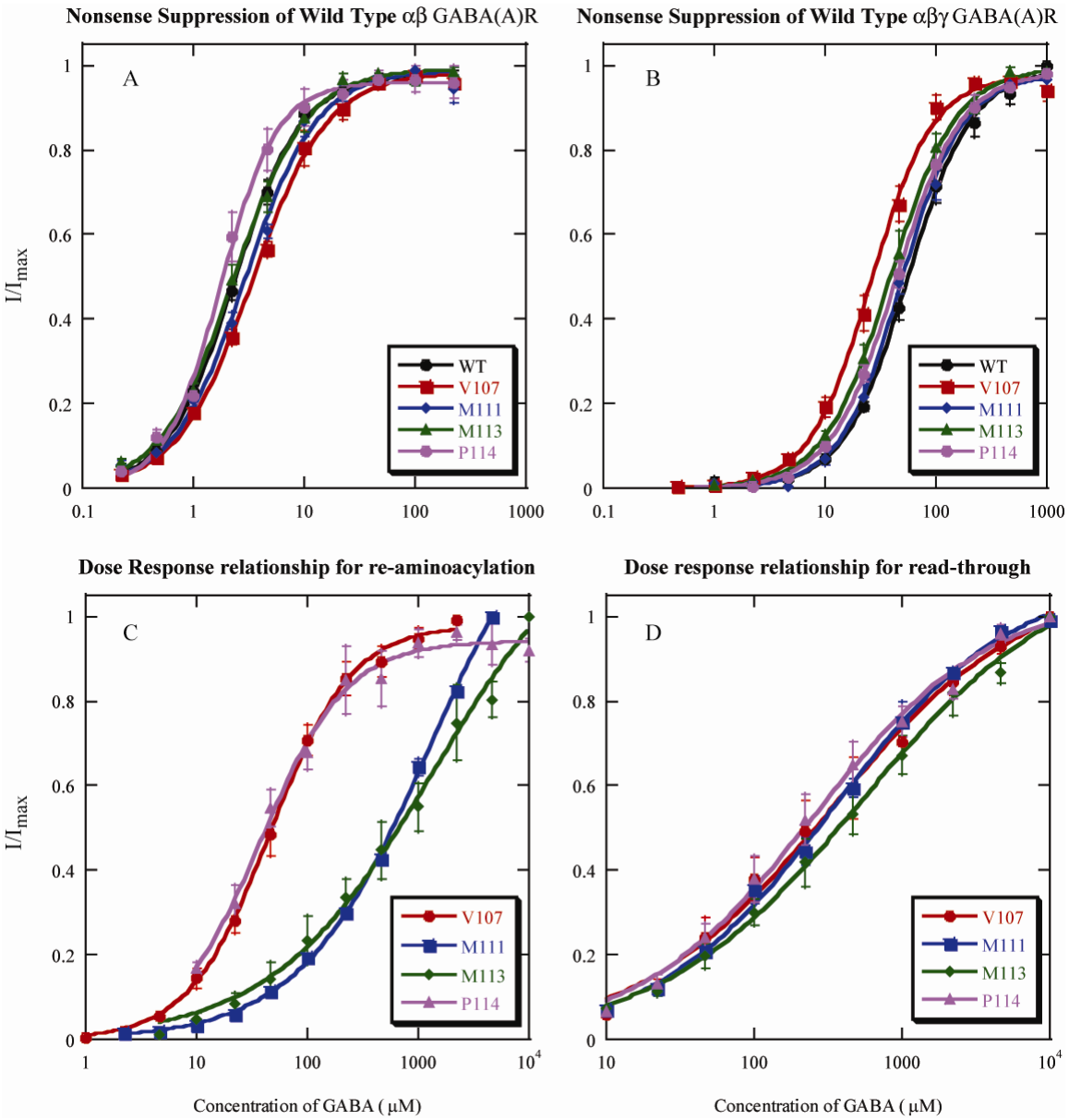

Figure 6.3 Dose response relationships for control experiments using the nonsense suppression methodology at four sites (V107, M111, M113, and P114) in the α subunit of the $GABA_AR$. Wild type recovery in αβ $GABA_AR$ (**A**) αβγ $GABA_AR$ (**B**). The GABA dose response relationship for re-aminoacylation of dCA-tRNA (**C**) and read-through (**D**)

Taken together, these results indicate that V107 and P114 would be poor sites for incorporation of Npg. V107 shows re-aminoacylation current in the αβ receptor. Furthermore, for both V107 and P114, re-aminoacylation and subsequent incorporation of the amino acid gave receptors with EC_{50} values similar to wild type, suggesting it will be difficult to tell the difference between the pharmacology of the receptors containing

the unnatural amino acid and those resulting from re-aminoacylation. Both M111 and M113 gave receptors resulting from re-aminoacylation that are pharmacologically different from the wild type receptor. Of these two sites, M113 has higher I_{max} values for wild type recovery in both the αβ and αβγ receptors, suggesting M113 is the best site for Npg incorporation.

6.2.3 Incorporation of Npg at M113 of the αβ $GABA_AR$

The αM113Npgβ mutant $GABA_AR$ functioned normally with a slight decrease in EC_{50} (Table 6.4). There was no significant difference in dose-response relationships, Hill coefficients, or macroscopic currents for wild type, wild type recovery (αM113Metβ), and mutant receptors (Figure 6.4). αM113Npgβ receptors had lower I_{max} values than wild type recovery, suggesting lower surface expression. We attribute the lower expression of the mutant receptor to using racemic Npg, as D-amino acids are unlikely to pass through the oocyte ribosome. Additionally, Npg is a β-branched amino acid, a structural type which is sometimes more difficult to incorporate using the nonsense suppression methodology.

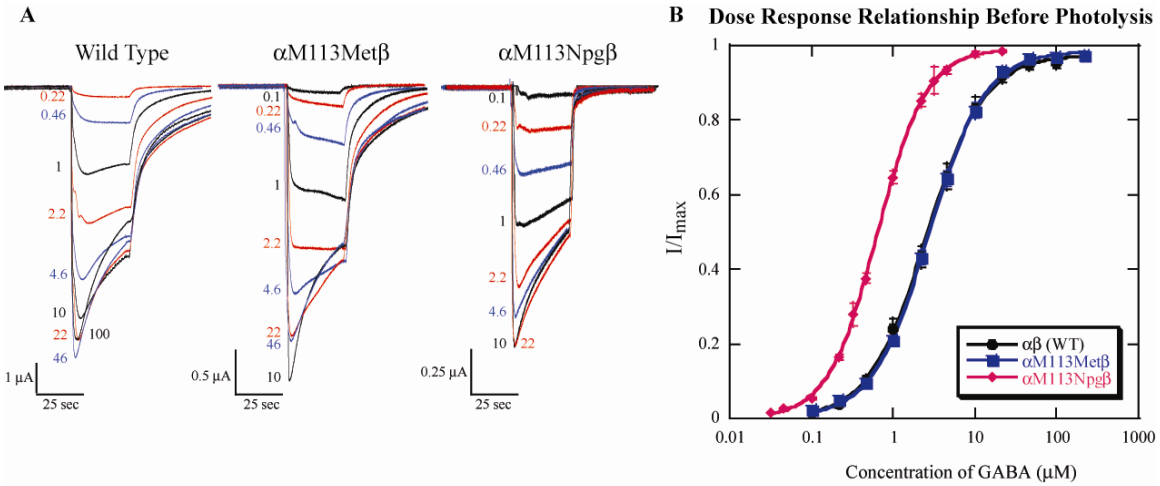

Figure 6.4 Incorporation of Met and Npg at αM113 gives similar macroscopic currents (**A**) and similarly shaped GABA dose response relationships (**B**) to the wild type receptor

Table 6.4 EC_{50} values for wild type recovery and Npg at αM113

Receptor	EC_{50} (μM)	n_H	I_{max}	N
αβ (WT)	2.57 ± 0.05	1.25 ± 0.03	-4.2 ± 0.7	18
αM113Metβ	2.72 ± 0.05	1.26 ± 0.03	-2.7 ± 0.4	32
αM113Npgβ	0.57 ± 0.04	1.6 ± 0.2	-1.3 ± 0.1	25

6.2.4 Proteolytic Cleavage of the αβ $GABA_AR$ in Linker Region

The unnatural amino acid Npg was used to proteolytically cleave the fully folded $GABA_AR$. The nitrophenyl group can absorb a photon of UV light and undergo a rearrangement that ultimately results in backbone cleavage of the peptide (Figure 6.1). Oocytes expressing αM113Npgβ $GABA_ARs$ were placed under a UV light source. Exposure time was monitored closely. Increasing the exposure of the αM113Npgβ expressing oocytes led to a substantial decrease in the macroscopic current, an increase in EC_{50}, and decrease in Hill coefficient (Table 6.5). After 8 hours of exposure to UV light whole cell currents of αM113Npgβ expressing oocytes had decreased such that the EC_{50} could be accurately determined. These whole cell currents are similar to those of the re-aminoacylation controls (Table 6.1). These data suggest photolysis is complete after 8 hours, and the remaining current is due to re-aminoacylation product.

To ensure these changes in current size, EC_{50}, and Hill coefficients of αM113Npgβ $GABA_AR$ expressing oocytes were due to cleavage of the backbone and not merely an artifact of exposure to light, control experiments with wild type $GABA_ARs$ and αM113Metβ $GABA_ARs$ were conducted. Wild type $GABA_ARs$, expressed by injection of the wild type gene or by nonsense suppression, showed no trends in the magnitude of the whole-cell current, EC_{50}, or Hill coefficient with increased exposure to UV light

(Table 6.5). These results suggest the decrease in macroscopic current is due to cleavage of the backbone by Npg rather than simply from exposing the oocytes to UV light.

Table 6.5 Increased exposure to UV light decreases the whole cell current of oocytes expressing αM113Npgβ but not wild type $GABA_A$Rs.

	αM113Npgβ				**αM113Metβ**				**αβ**	
Time	EC_{50}	n_H	I_{max}	N	EC_{50}	n_H	I_{max}	N	I_{max}	N
0 hours	0.57	1.6	-2.3 ± 0.3	8	4.2	1.3	-2.1 ± 0.7	7	-9.8 ± 2.2	4
2 hours	1.1	1.2	-0.6 ± 0.1	6	3.8	1.3	-2.6 ± 1.2	6	-6.6 ± 1.8	4
4 hours	1.1	1.2	-0.32 ± 0.07	8	2.6	1.5	-1.22 ± 0.09	6	-8.9 ± 0.9	4
6 hours	11	0.6	-0.20 ± 0.04	7	2.1	1.3	-1.3 ± 0.4	6	-8.4 ± 3.2	4
8 hours			-0.11 ± 0.05	7			-2.3 ± 0.9	4	-3.9 ± 0.9	4

Note: All these data were collected on the same day using oocytes from the same frog, injected at the same time. This extra measure was taken to control for differences in expression level due to any differences resulting from variability in batches of oocytes.

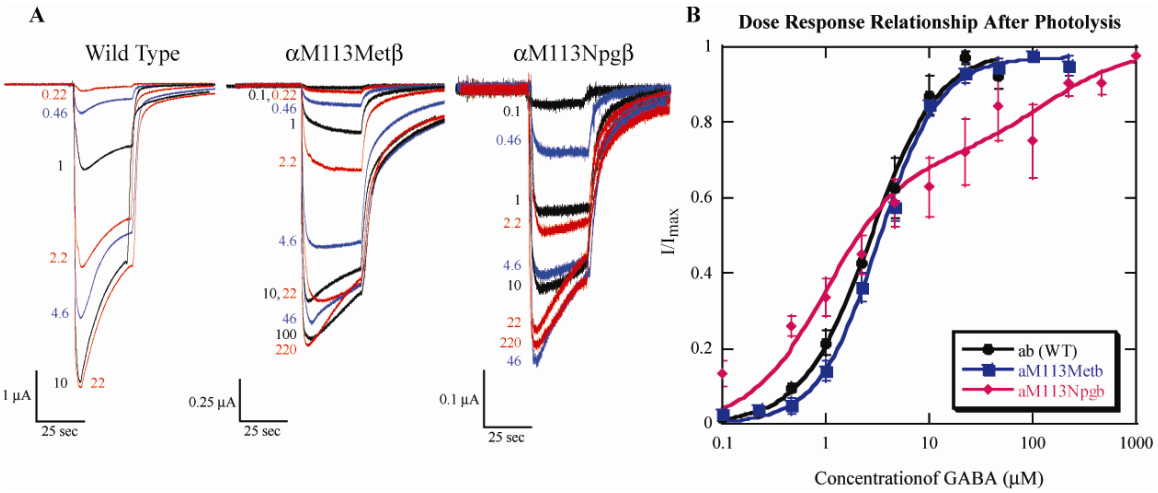

Figure 6.5 8 hours of exposure to UV light does not alter the macroscopic kinetics (**A**), or GABA dose response relationship (**B**) of wild type $GABA_A$Rs. There is a decrease in the magnitude of the macroscopic currents of oocytes expressing αM113Npgβ $GABA_A$Rs after exposure to UV light, however, the overall shape of the trace remains the same (**A**). The GABA dose response relationship for $GABA_A$Rs for wild type, wild type recovery, and αM113Npgβ $GABA_A$R after 8 hour exposure to UV light (**B**). Receptors cleaved at αM113 are biphasic. For comparison to non-photolyzed oocytes, see Figure 6.4.

Once an eight hour exposure was determined to be sufficient for complete photolysis of Npg, these results were repeated on several batches of oocytes on different days to ensure these results were not due to anomalies occurring from the oocytes used (Table 6.6). On average, the EC_{50} of the proteolyzed $GABA_A$Rs increased 5.4-fold while the whole cell current decreased 89%. Despite the decrease in current size, the

macroscopic currents of the αM113Npgβ $GABA_AR$ expressing oocytes exposed to UV light (Figure 6.5) have similar macroscopic kinetics to those that were not exposed to UV light (Figure 6.4) Wild type and αM113Metβ $GABA_ARs$ remained unchanged by exposure to UV light (Figure 6.5, Table 6.6).

Table 6.6 Cumulative results of 8 hours of UV exposure

	Before UV exposure					After 8 hours UV exposure				
	EC_{50}	n_H	N	I_{max}	N	EC_{50}	n_H	N	I_{max}	N
WT	2.57 ± 0.05	1.3	18	9 ± 1	8	2.3 ± 0.3	1.6	5	5 ± 1	7
αM113Met	2.72 ± 0.05	1.3	32	1.9 ± 0.5	9	3.2 ± 0.2	1.5	7	2.5 ± 0.7	5
αM113Npg	0.57 ± 0.04	1.6	25	1.5 ± 0.2	23	3.1 ± 0.8	0.52	6	0.17 ± 0.03	24

Note: Higher expression of the wild type receptor caused greater scatter in the I_{max} values. Although the I_{max} value after exposure to UV light is ~55% of the before UV light value, we believe this difference is meaningless due to the high level of current seen in both cases.

6.2.5 Pentobarbital Activation of the αβ $GABA_AR$

Decreases in macroscopic current upon photolysis can be explained by having fewer surface expressed receptors, a decrease in the single-channel conductance, or a decrease in GABA activation. To determine which of these factors come into play, we studied $GABA_AR$ activation by the barbiturate pentobarbital. Pentobarbital (PB) binds to a completely different site from GABA, likely in the transmembrane region of the β subunits.[43-45] The single-channel conductance of PB activated $GABA_ARs$ resembles those of GABA activated receptors, suggesting the open states of the ion channel are similar.[46,47] At low concentrations (<100 μM), PB modulates GABA induced currents, while at higher concentrations PB directly activates $GABA_ARs$ and at still higher concentrations blocks the receptors. Studies using the surface cysteine accessibility method with simultaneous fluorescence and electrophysiological recordings have established that PB activation of the $GABA_AR$ elicits conformational changes in the $GABA_AR$ that are different from those of GABA activation.[48,49]

If cleavage of the backbone by Npg leads to receptor endocytosis or a change in the single channel conductance, the maximal currents elicited by PB should decrease with photolysis. However, if proteolysis at αM113 prevents activation of the receptor by GABA, we anticipate that PB currents should remain the same before and after photolysis. The dose response relationships of wild type and αM113Npgβ $GABA_AR$s were determined both before and after photolysis (Figure 6.6). To reach saturation, concentrations of PB that block the receptor were used. In these cases the peak of the tail current was used as the measurement (Figure 6.6B).

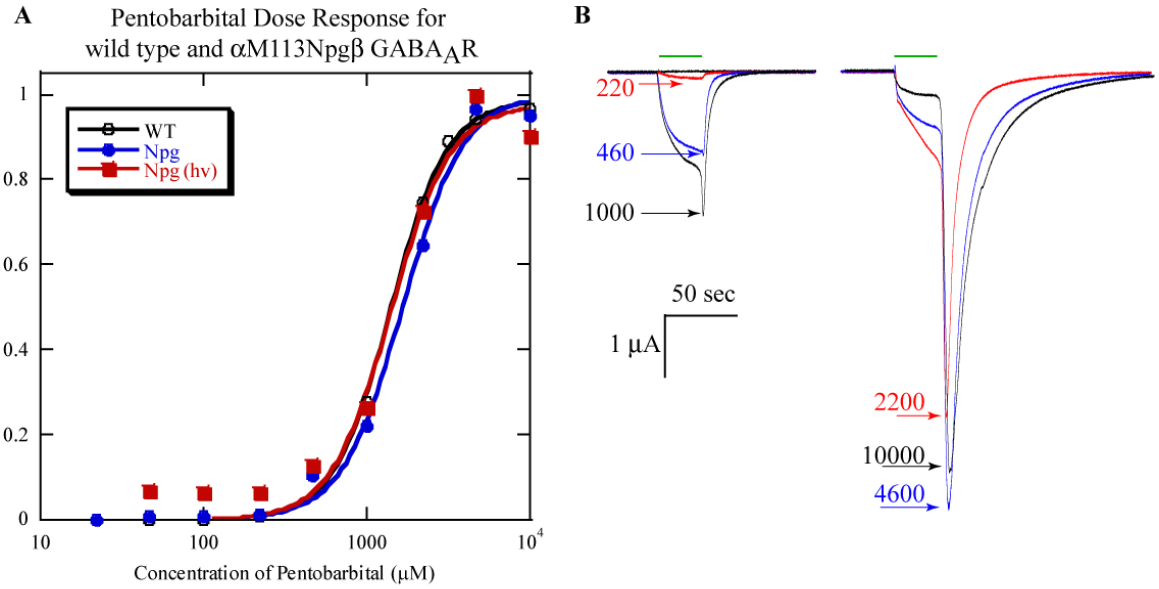

Figure 6.6 Pentobarbital dose response relationships for wild type and αM113Npgβ (before and after photolysis) $GABA_AR$ (**A**). PB induced currents of wild type $GABA_AR$ (**B**). Concentrations are in μM.

The PB dose response relationship for the αM113Npgβ mutant before and after irradiation was not appreciably different from that of wild type (Figure 6.6). The EC_{50} values were similar for wild type, αM113Npgβ, and αM113Npgβ after photolysis (1400, 1700, and 1400 μM, respectively) as were the Hill coefficients (2.5, 2.3, and 2.4,

respectively). The dose response relationships indicate that in all three cases, 10 mM PB is sufficient to saturate the whole-cell current.

Table 6.7 Macroscopic currents induced by exposure to Pentobarbital remain constant despite 8 hours of UV irradiation. Currents are reported in μA.

	Before UV exposure			After UV exposure		
	I_{GABA}	I_{PB}	N	I_{GABA}	I_{PB}	N
αM113Metβ	4 ± 2	4 ± 1	6	3.7 ± 0.4	4.1 ± 0.5	6
αM113Npgβ	0.61 ± 0.07	1.4 ± 0.3	12	0.27 ± 0.04	1.4 ± 0.3	12

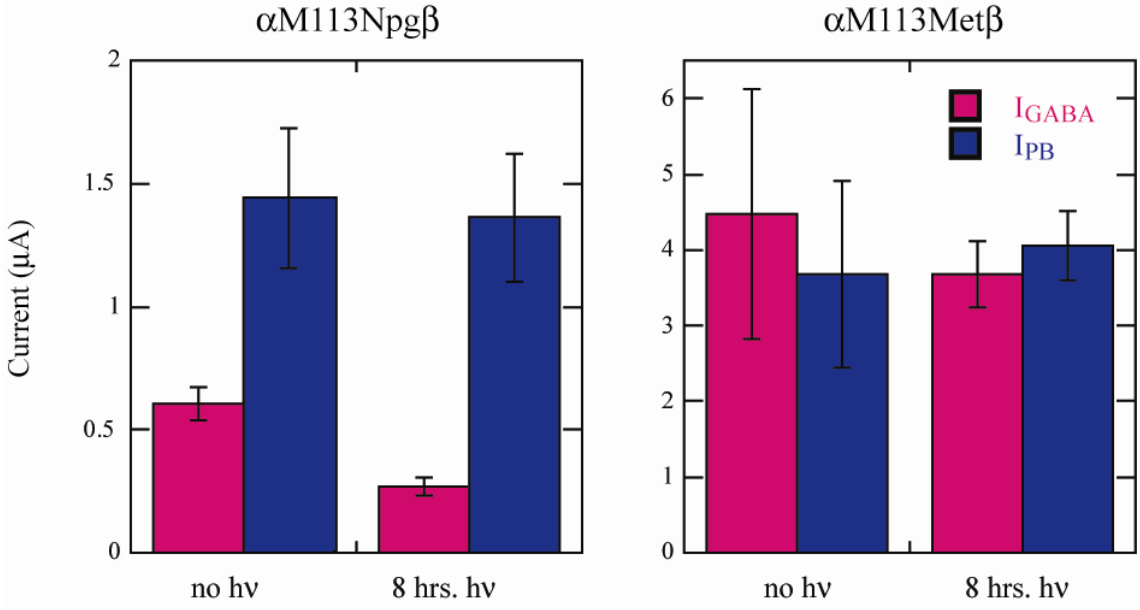

Figure 6.7 Macroscopic whole-cell currents induced by saturating doses of GABA (pink) or pentobarbital (blue). *Left*: PB induced currents are unchanged by proteolytic cleavage of the αM113Npgβ mutant. *Right*: Control experiments with the wild type receptor

Macroscopic currents for wild type $GABA_A$Rs were similar in size for both agonists (Figure 6.7, Table 6.7) before and after UV exposure. These data indicate PB is a full agonist for the wild type receptor and, as expected, exposure of the wild type channel to UV irradiation does not alter channel function. The αM113Npgβ mutant shows larger macroscopic currents for pentobarbital than for GABA, indicating that the mutation lowers GABA but not PB efficacy. Proteolytic cleavage at αM113 had no

effect on PB induced currents (Figure 6.7, Table 6.7), suggesting the decrease in GABA induced currents is not due to endocytosis of the receptors or to a change in the single-channel conductance.

6.3 Discussion

The data indicate that proteolytic cleavage of the $GABA_AR$ backbone at αM113 is sufficient to prevent GABA activation of the receptor. There are at least two possible causes of decreased activation. One possibility is that backbone cleavage alters the GABA binding site such that the receptor is unable to bind GABA. The second possibility is that proteolytic cleavage has disrupted the activation pathway for GABA. We have not explicitly investigated these two possibilities. However, αM113 is well removed from the aromatic residues that form the GABA binding site.[10] Thus it seems unlikely that proteolytic cleavage at this site prevents GABA binding. Given the location of cleavage, the results from the pentobarbital studies, and work by others[25,27] implicating the linker region in the activation pathway of $GABA_AR$, it seems unlikely that the backbone cleavage at αM113 impedes binding of GABA to the receptor.

Given that disruption of GABA binding is unlikely, the reduction of macroscopic currents following proteolytic cleavage strongly suggests the linker connecting loops A and E of the complementary subunit of the $GABA_AR$ is a critical part of the activation pathway for GABA. Additionally, these data support the available structural information indicating that in the closed-state this region of the receptor is lacking a defined secondary structure.[2,3] If αM113 was part of a β-sheet or α-helix, the stabilizing backbone H-bond network might be expected to retain the overall structure following

proteolytic cleavage. Thus we would not expect the dramatic change in GABA activation seen here.

Although we hoped to study the role of the linker region in benzodiazepine modulation of $GABA_AR$s, we have restricted our studies to the BZD-insensitive $\alpha_1\beta_2$ $GABA_AR$. Extending these studies to the $\alpha_1\beta_2\gamma_2$ $GABA_AR$ is unlikely to provide additional information about GABA or BZD activation pathways for the following reasons. The GABA binding sites of $\alpha_1\beta_2$ and $\alpha_1\beta_2\gamma_2$ $GABA_AR$s are essentially identical. Thus the conformational changes occurring in the α subunit during GABA-induced activation are likely to be the same for both $GABA_AR$ subtypes. Therefore, we expect that proteolytic cleavage in the $\alpha_1\beta_2\gamma_2$ $GABA_AR$ will be sufficient to prevent GABA activation of the receptor. BZDs modulate GABA-induced changes in the $GABA_AR$, and without GABA activation we will not be able to detect the affects of BZD application. This reasoning, combined with the difficulty of nonsense suppression experiments in the α subunit of the $\alpha\beta\gamma$ receptor establish that incorporation of Npg and subsequent photo-induced cleavage of the linker backbone in the $\alpha\beta\gamma$ $GABA_AR$ were not likely to provide additional insight into $GABA_AR$ function at present.

In conclusion, we find that proteolytic cleavage of the complementary α_1 subunit between loops E and A of the $GABA_AR$ is sufficient to prevent GABA activation, but not PB activation. These data indicate that the linker region is critical to normal receptor function and provide additional evidence that pentobarbital and GABA utilize different activation pathways within the same receptor.

6.4 Materials and Methods

6.4.1 Electrophysiology

Mutagenesis and preparation of mRNA: Human α_1, β_{2S}, and γ_{2L} $GABA_AR$ genes in pGEMHE were obtained from S.C.R. Lummis (Department of Biochemistry, University of Cambridge, Cambridge, United Kingdom). Quickchange PCR was used to make α_1V107Tag, α_1M111Tag, α_1M113Tag, and α_1P114Tag mutants and mutation was confirmed by sequencing (Laragen Sequencing). The cDNA was linearized using Nhe1 (Roche) for the α_1 and γ_{2L} subunits and either Spe1 (Roche) or Sph1 (Roche) for the β_{2S} subunit. The mMessage mMachine kit (Ambion) was used to generate capped mRNA for oocyte injection.

Oocyte Injection: Wild type $\alpha_1\beta_{2S}$ mRNA was mixed in a 1:1 ratio and diluted to a final concentration of 100 ng/μl. Each oocyte was injected with 50 nL of mRNA mix, or 5 ng of mRNA mix.

For suppression experiments, a 5:1 mix of the mRNA of the mutated α_1 gene and β_{2S} at a final concentration of 1 μg/μl was used. For wild type recovery experiments, this mRNA mix was mixed in a 1:1 (by volume) ratio with the deprotected aa-tRNA. Each oocyte was injected with a total volume of 50 nL of RNA mix; 25 ng mRNA and 15-50 ng of aa-tRNA . The aa-tRNA was stored with the amino group protected by an NVOC group. Prior to mixing the aa-tRNA with the mRNA mix, the aa-tRNA was deprotected by photolysis.

For Npg-tRNA, the amino group of Npg was protected by a 4-PO group. To deprotect Npg, a 1:1 mixture of Npg-tRNA and saturated aqueous iodide was made and allowed to sit at room temperature for 10 minutes. One equivalent of mRNA mix was

added and 50 nL of the mRNA/Npg-tRNA/$I_{2(aq)}$ mixture was injected into each oocyte. This yielded a total of 16.7 ng each of mRNA and Npg-tRNA per oocyte.

Val- and Pro-tRNA were prepared as described previously.[28,29,50] Briefly, the amino acids were protected using a nitroveratryloxycarbonyl group and the carboxylic acid was activated as the cyanomethyl ester. The activated compound was coupled to the dinucleotide dCA, which was then enzymatically ligated to 74-mer THG73 $tRNA_{CUA}$ as detailed previously.

After injection, oocytes were incubated for 24-48 hours at 18°C prior to electrophysiology recordings. For a control, cRNA alone and cRNA mixed with dCA-THG (no unnatural amino acid attached) were injected into oocytes.

Characterization of mutant receptors: Peak GABA-induced currents were recorded at 22-25°C from individual oocytes using the OpusXpress system (Axon Instruments, Molecular Devices). A stock solution of 10 mM GABA (Sigma, St. Louis, MO) in ND96 buffer (in mM: 96 NaCl, 2 KCl, 1 MgCl2, 1.8 CaCl2, 5 HEPES, pH 7.5) was made fresh for each day's recording. Drug solutions were made from the stock by dilution in ND96 buffer. Drug was delivered to cells via the automated perfusion system of the OpusXpress. Glass microelectrodes were backfilled with 3 M KCl and had a resistance of 0.5-3.0 MΩ. The holding potential was -60 mV. To determine EC_{50} values, GABA concentration-response data were fitted to the Hill equation (Equation 6.1), where I_{max} is the maximal peak current and n is the Hill coefficient.

$$I = \frac{I_{\max}}{1 + EC_{50}/[A]^n} \qquad \textbf{Equation 6.1}$$

The dose-response relationship for pentobarbital (purchased as pentobarbital chloride from Aldrich) was determined in the same manner as GABA. For concentrations of pentobarbital that caused channel block, the tail current was used to determine I_{max}. For determination of I_{max} values from both GABA and PB, a high dose of GABA was applied, followed by a saturating does of GABA (I_{GABA}) and then a saturating dose of PB (I_{PB}). PB solutions were stored at room temperature to minimize crystallization.

Oocyte Irradiation: Oocytes in ND96 containing theophylline and gentamicin as well as 4% horse serum were irradiated at 4°C in sterile 12 well polystyrene plates (Greiner bio-one Cellstar) with the lid in place. The irradiation source was a 288 W Hg lamp (BLAK-RAY Longwave Ultraviolet Lamp, Ultraviolet Products, San Gabriel, CA) equipped with a 360 nm band pass filter at a distance of 15-30 cm for a total of 8 hours, unless otherwise indicated. The proximity of the oocytes to the irradiation source caused significant warming of the bath solution, thus the oocyte bath solution ($ND96^+$ with 4% horse serum) was replaced every 1.5-2 hours to avoid excessive heating. Non-irradiated oocytes were maintained at 18°C. Prior to electrophysiology measurements, irradiated oocytes were placed in fresh $ND96^+$ with 4% horse serum at room temperature for at least 30 minutes. This improved the resting potentials and leak currents of the oocytes, but did not affect the dose response relationship or I_{max} values.

6.4.2 Nitrophenyl Glycine Synthesis (Scheme 6.2)

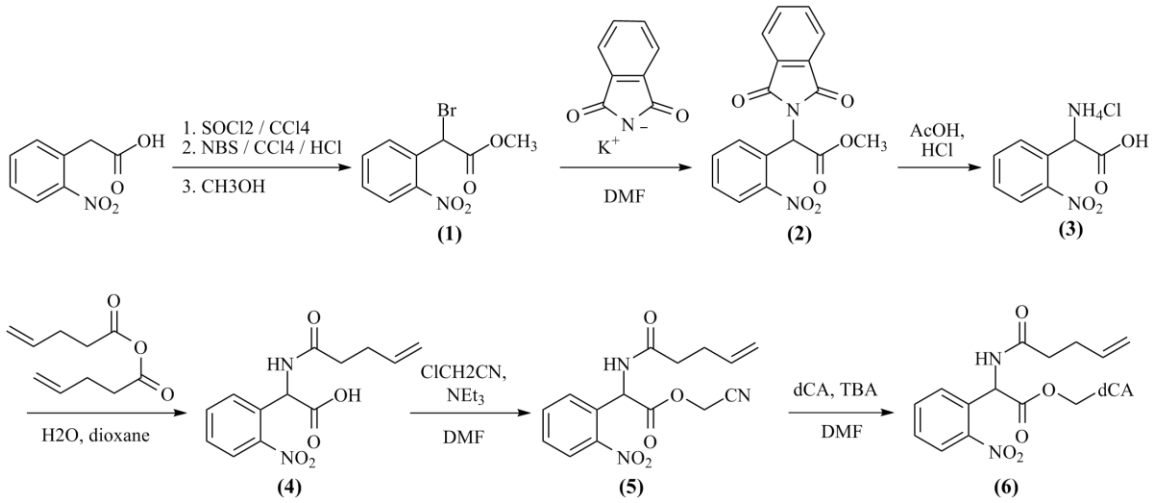

Scheme 6.2

Methyl-α-Bromo-o-nitrophenylacetate (**1**) was prepared as described previously.[50,51] 2-Nitrophenyl acetic acid (3.0 g, 16.6 mmol), 10 mL of carbon tetracholoride were added to a 250 mL round bottom flask containing a stir bar. Addition of 10 mL (137 mmol) of thionyl chloride caused the reaction to turn orange/pink. A reflux condenser was attached and the reaction was heated to 55-60°C for 30 minutes. 3.61 g (20.3 mmol) of N-Bromosuccinimide in 25 mL of carbon tetrachloride and 10 drops of 6N HCl were added. The heat was adjusted to 65°C to bring the reaction to reflux. After 45 minutes black chunks were floating in the reaction mixture. After 3 hours, the reaction was cooled in an ice bath. While in the ice bath, 15 mL of MeOH was slowly added to the reaction mixture, followed by 50 mL of saturated aqueous sodium carbonate, turning the reaction mixture to a uniform brown-red liquid. The reaction mixture was extracted with 100 mL methylene chloride. The organic layer (red-brown, clear) was saved. The aqueous layer (brown, cloudy) was extracted with methylene chloride until the organic layer was pale yellow and clear (5 x 70 mL). All methylene

chloride layers were combined (clear, red liquid) and dried over magnesium sulfate. The magnesium sulfate was removed by filtration and the filtrate was run through a plug of alumina. The alumina was washed with another 300 mL of methylene chloride. The methylene chloride solution was concentrated and the various productes were separated by silica gel column chromatography. The initial moving phase was 1:1 CH_2Cl_2:Hexane. The polarity of the moving phase was increased on a gradient to 5:3 CH_2Cl_2:Hexane then pure CH_2Cl_2. Pure EtOAc was used to remove all compounds form the column. Like fractions were combined and concentrated. Title compound was a pale, yellow solid. ^{1}H NMR (300 MHz, Figure 6.8) in $CDCl_3$: δ7.92 (m, 2H), δ7.64 (m, 1H), δ7.46 (m, 1H), δ6.03 (s, 1H), and δ3.72 (s, 3H). Yield is 1.356 g (4.6 mmol, 28%).

Methyl α-phthalimido-o-nitrophenyl acetate (**2**): 1.14 g (4.16 mmol) of **1** and 0.779 g (4.20 mmol) of potassium phthalimide (Aldrich) were placed in a 25 mL round bottom flask. 15.5 mL of DMF was added and the liquid immediately turned deep purple giving a cloudy, purple mixture. After 2 hours stirring at room temperature, the reaction was orange-yellow and cloudy. The precipitate (KBr) was removed by filtration giving a clear, orange/yellow filtrate. Addition of 20 mL chloroform and 50 mL water was used to separate the organic (cloudy, orange.yellow) and aqueous (cloudy, colorless) layers. After extraction of the aqueous layer (2 x 20 mL) with additional chloroform, the organic layers were combined, and dried over anhydrous sodium sulfate (Aldrich). Removal of the sodium sulfate by filtration yielded a clear, orange/yellow solution. After concentration and removal of DMF, a dark orange oil (1.444 g) remains. Hot ethanol was added, and a white powder precipitated out. The powder was isolated by filtration and washed with water to give the title compound. Proton NMR (300 MHz, Figure 6.9) in

$CDCl_3$: δ8.15 (d, 1H), δ7.9 (m, 2H), δ7.8 (m, 2H), δ7.55 (m, 2H), δ7.4 (d, 1H), δ6.95 (s, 1H), δ3.75 (s, 3H). Yield 0.89 g (2.62 mmol, 63%).

o-Nitrophenylglycine chloride salt (**3**): 2.6 mmol (0.89 g) of **2**, 6 mL of concentrated HCl and 4 mL of glacial acetic acid were combined in a 25 mL round bottom flask containing a stir bar. The reaction was slowly heated to 120°C and allowed to reflux. At reflux the solid dissolves giving a clear, yellow/orange solution. After 6.5 hours at reflux, the flask was cooled to room temperature overnight, then cooled to 5°C in an ice bath. Acidified (to pH=3.0 using HCl) water was added and the reaction was washed with ethyl acetate. The aqueous layer was concentrated yielding the title compound as a white solid. Proton NMR (300 MHz, Figure 6.10) in D_2O: δ8.15 (d, 1H), δ7.75 (t, 1H), δ7.6 (t, 1H), δ7.55 (d, 1H), δ5.37 (s, 1H). Yield: 0.363 g (1.56 mmol, 60%).

4-PO-Nitrophenylglycine (**4**): 1.56 mmol (0.363 g) of **3** was dissolved in 4 mL of water and 2.5 mL of dioxane. Sodium carbonate (0.498 g, 4.7 mmol) was added. Pent-4-enoic anhydride (0.314 g, 1.72 mmol) and 1.5 mL of dioxane were added. After stirring at room temperature for 3 hours, the reaction was poured into 25 mL of saturated $NaHSO_4$ then washed with methylene chloride (3 x 25 mL). The aqueous layer was acidified with HCl to pH=2.5 (aqueous layer gets cloudy), then extracted with methylene chloride (3 x 25 mL). The methylene chloride layers were combined and concentrated to yield the title compound as a pale yellow solid. ^1H NMR (300 MHz, Figure 6.11) in CD_3OD: δ8.06 (d, 1H), δ7.7 (m, 1H), δ7.62-7.53 (m, 2H), δ6.21 (s, 1H), δ5.8 (m, 1H), δ5.04-4.97 (m, 3H), δ2.42-2.28 (m, 4H). Yield is 0.142 g (0.52 mmol, 33%).

Cyanomethyl ester of 4-PO-Nitrophenylglycine (**5**): 0.101 g (0.363 mmol) of **4** was added to a 5 mL round bottom flask containing a stir bar. After purging the flask with argon, 1 mL of chloroacetonitrile (15.8 mmol) and 150 μl (1.07 mmol) of triethylamine were added. The reaction was stirred under argon overnight. Diethylether was used to dilute the reaction and then extracted against water. The organic layer was removed and dried over $MgSO_4$. The solvent was removed with reduced pressure leaving a yellow oil that still contained chloroacetonitrile. The excess chloroacetonitrile was removed by vacuum. The product was isolated by column chromatography (silica gel) starting with a solvent of 2:1 hexane:ethyl acetate, followed by 1:1, 1:2, and 1:4. A small yellow band still remained at the base of the column. MeOH was added to remove this band. Fractions were combined according to contents and the solvent was removed. The second isolated compound was the desired product (white powder). Proton NMR (300 MHz, Figure 6.12) in $CDCl_3$: δ8.18 (d, 1H), δ7.74-7.65 (m, 2H), δ7.58 (m, 1H), δ6.84 (d, 1H), δ6.17 (d, 1H), δ5.76 (m, 1H), δ5.0-4.97 (m, 2H), δ4.75 (d of d, 2H), 2.45-2.25 (m, 4H). Yield is 20 mg (0.063 mmol, 17.4%).

6.4.3 Protection and Activation of Methionine (Scheme 6.3)

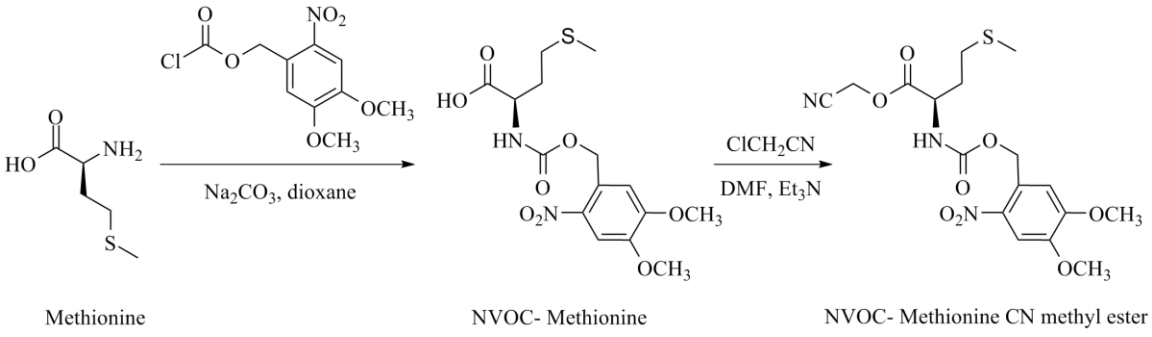

Scheme 6.3

NVOC-Methionine: In a 50 mL round bottom flask, sodium carbonate (0.832 g, 7.85 mmol) was dissolved in 8.25 mL of water to make a 10% weight/volume solution. While stirring, 0.300 g (2.01 mmol) L-methionine, then 5.75 mL of 1,4-dioxane were added. The flask was placed in an ice bath and 0.597 g (2.16 mmol) 4,5-dimethoxy-2-nitorbenzyl chloroformate (NVOC-Cl) was slowly added. Reaction became orange and cloudy. While stirring, the reaction was allowed to come to room temperature and turned yellow and cloudy. After 6 hours, the reaction contents were poured into 100 mL deionized water and washed with ether (3 x 45 mL). The organic layer was discarded. 6N HCl was added to the aqueous layer ($pH \leq 2.0$) and a white precipitate crashed out of solution. The precipitate (pale yellow solid) was removed by filtration to give the title compound. Proton NMR (300 MHz, Figure 6.13) in $CDCl_3$: δ7.75 (s, 1H), δ7.0 (s, 1H), δ5.55 (m, 2H), δ4.55 (m, 1H), δ4.0 (s, 3H), δ3.95 (s, 3H), δ2.6 (t, 2H), δ2.15 (d of m, 2H), and δ2.1 (s, 3H). Yield is 0.635 g (1.63 mmol, 81.3%).

NVOC-Methionine cyanomethyl ester: 0.384 g (0.989 mmol) NVOC-methionine was added to a 25 mL oven dried round bottom flask containing a stir bar. The flask was purged with argon and 3.2 mL dry DMF was slowly added. The solid dissolved to give a clear, yellow solution. 3.2 mL (50.6 mmol) chloroacetonitrile and 0.4 mL (2.87 mmol) triethylamine were added and the reaction was stirred under argon for 3 hours. The reaction as concentrated overnight by high vacuum leaving a yellow, sticky solid. Column chromatography (silica gel) was used to separate product from unreacted starting material. Initially the moving phase was 1:3 EtOAc:CH_2Cl_2 and was used to collect a yellow band. A yellow-orange band remained at the top of the column and was removed using 100% methanol. The first band contains the title compound. Fractions were

combined and concentrated to give a yellow solid. Proton NMR (300 MHz, Figure 6.14) in $CDCl_3$: δ7.72 (s, 1H), δ7.0 (s, 1H) δ5.62-5.47 (m, 2H), δ4.55 (m, 1H), δ4.01 (s, 3H), δ3.98 (s, 3H), δ2.61 (t, 2H), δ2.25-2.05 (d of m, 2H), δ2.11 (s, 3H). Yield is 0.188 g (0.435 mmol, 44%)

6.5 NMR Spectra

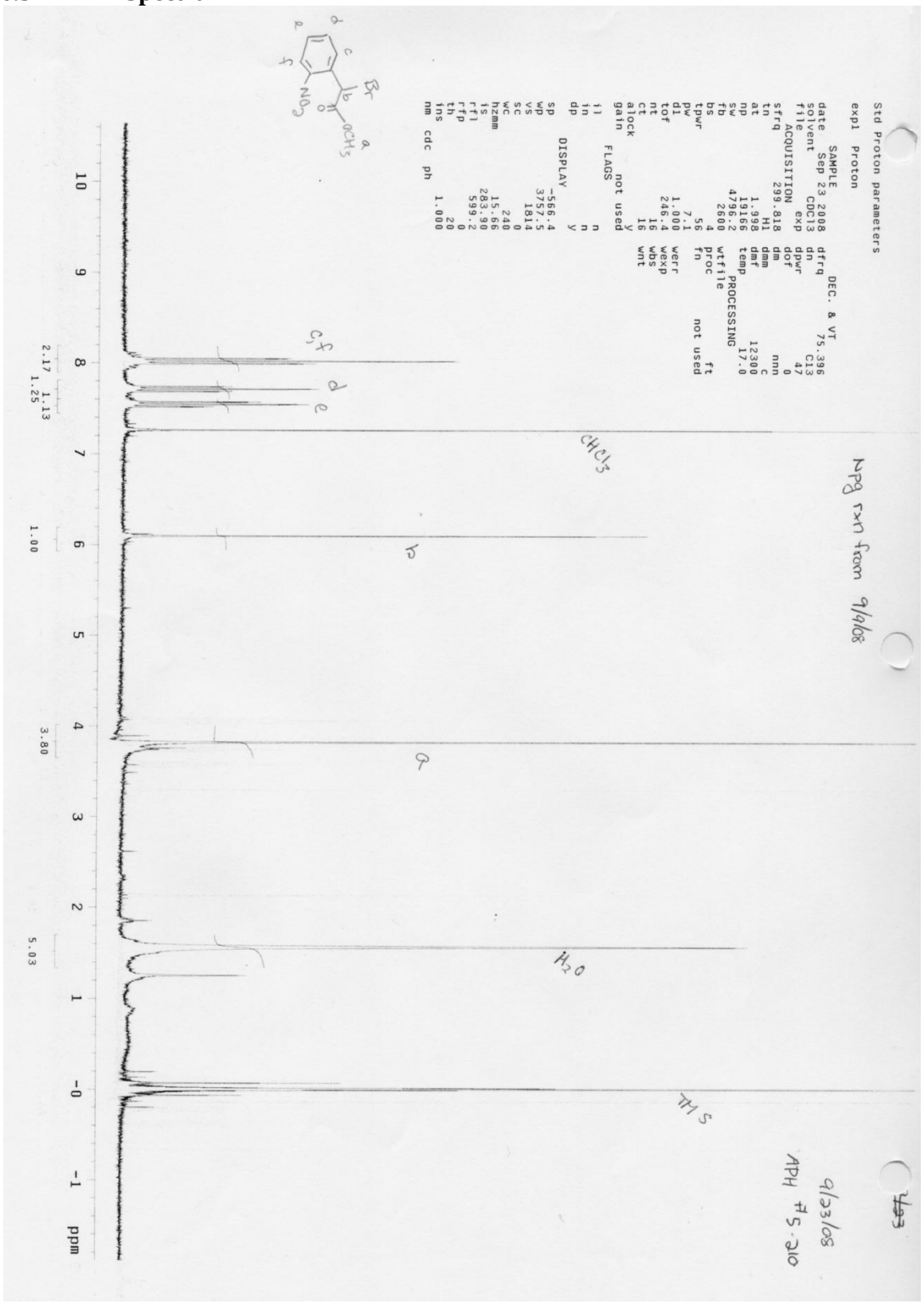

Figure 6.8 Proton NMR spectra of Methyl-α-Bromo-o-nitrophenylacetate (**1**)

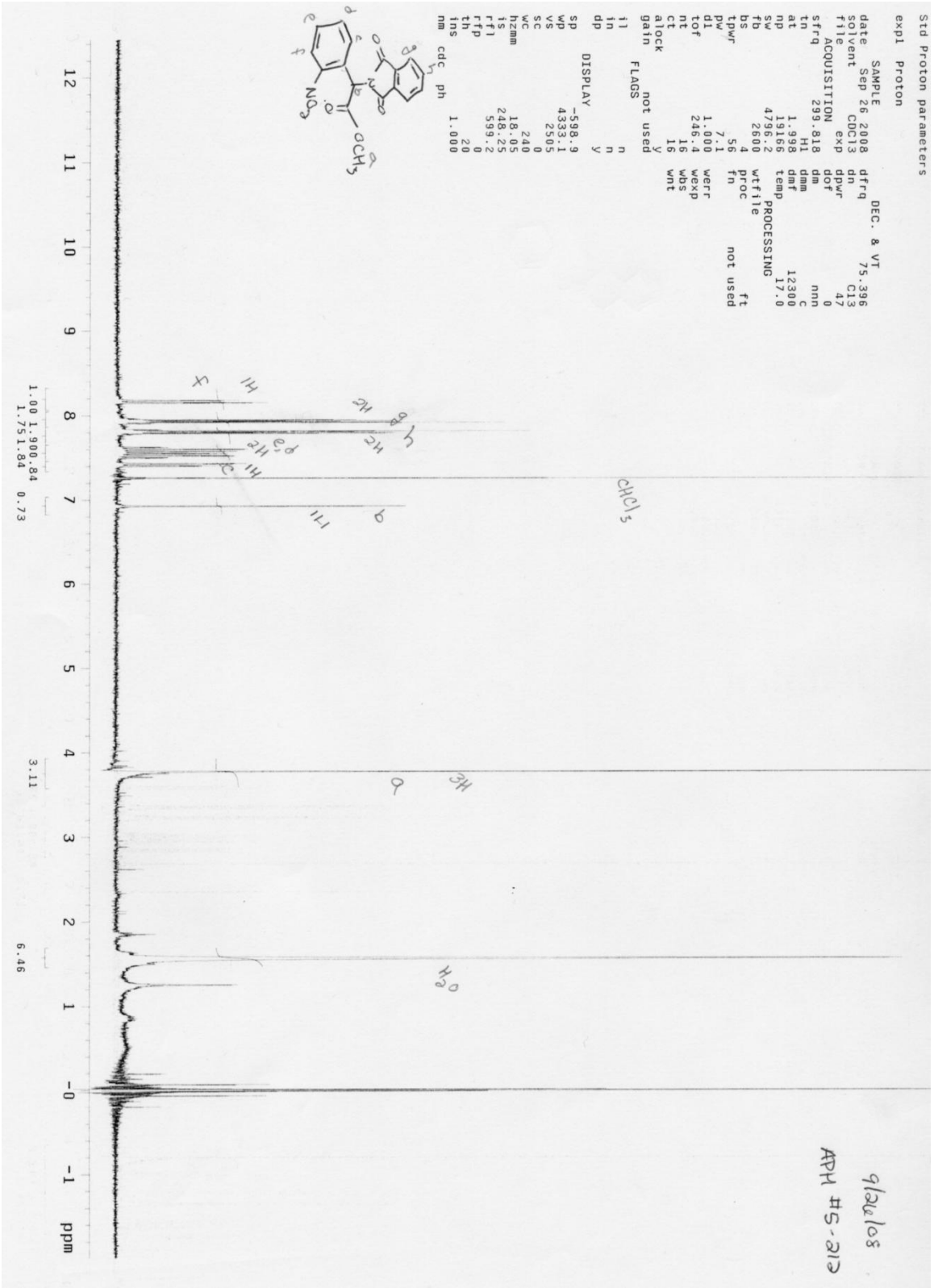

Figure 6.9 Proton NMR spectra of Methyl α-phthalimido-o-nitorphenyl acetate (**2**)

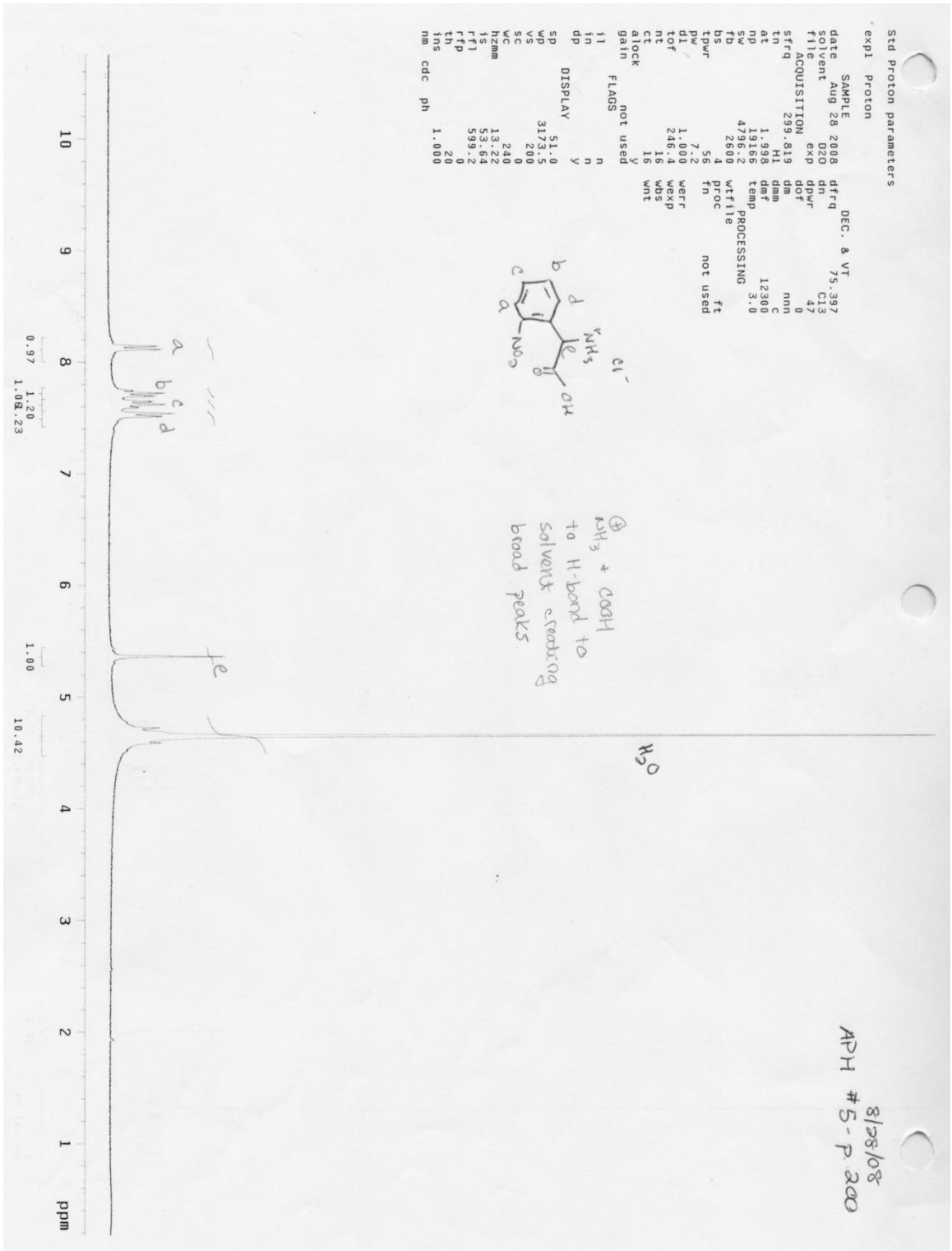

Figure 6.10 Proton NMR spectra of *o*-Nitrophenylglycine chloride salt (**3**)

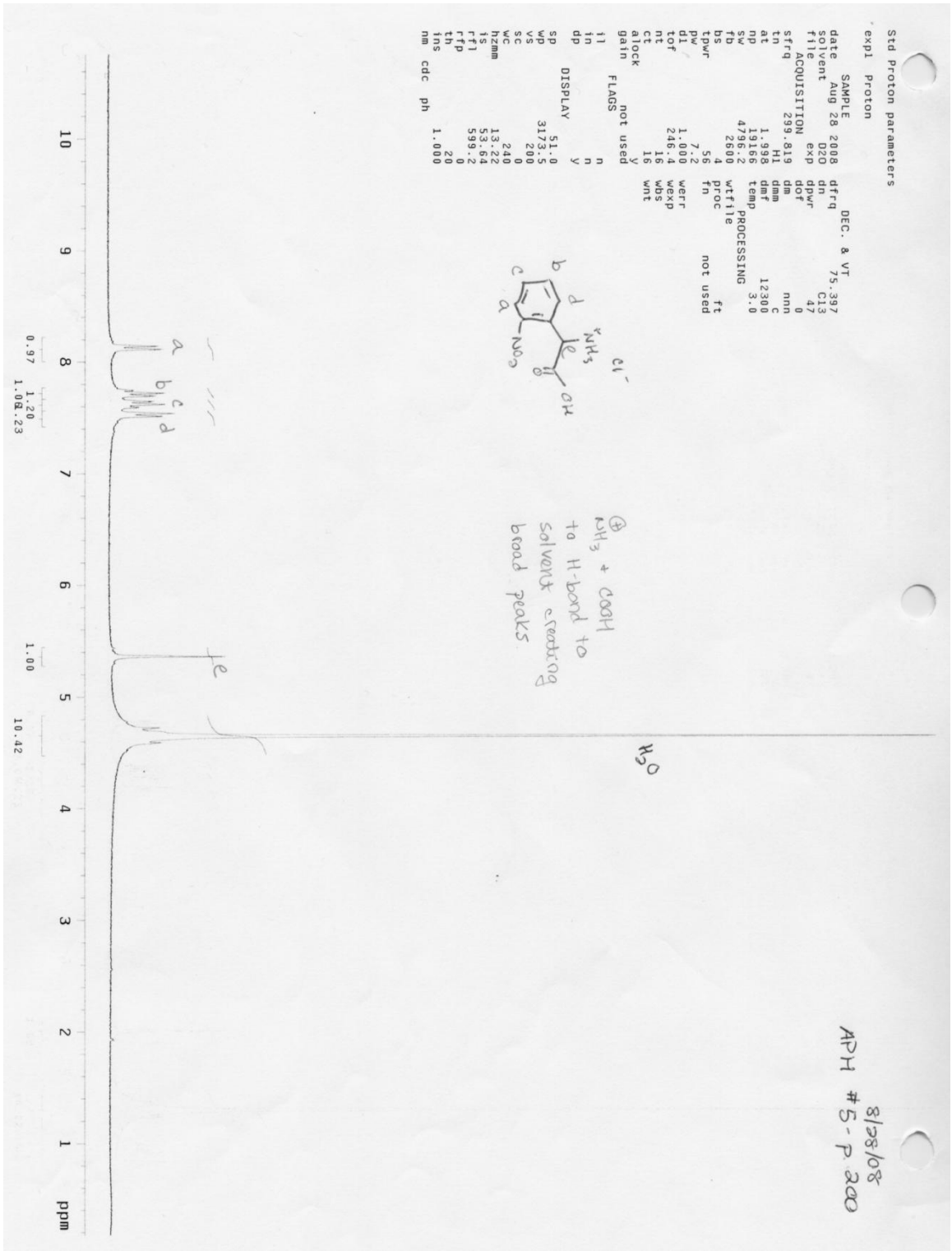

Figure 6.11 Proton NMR spectra of 4-PO-Nitrophenylglycine (**4**)

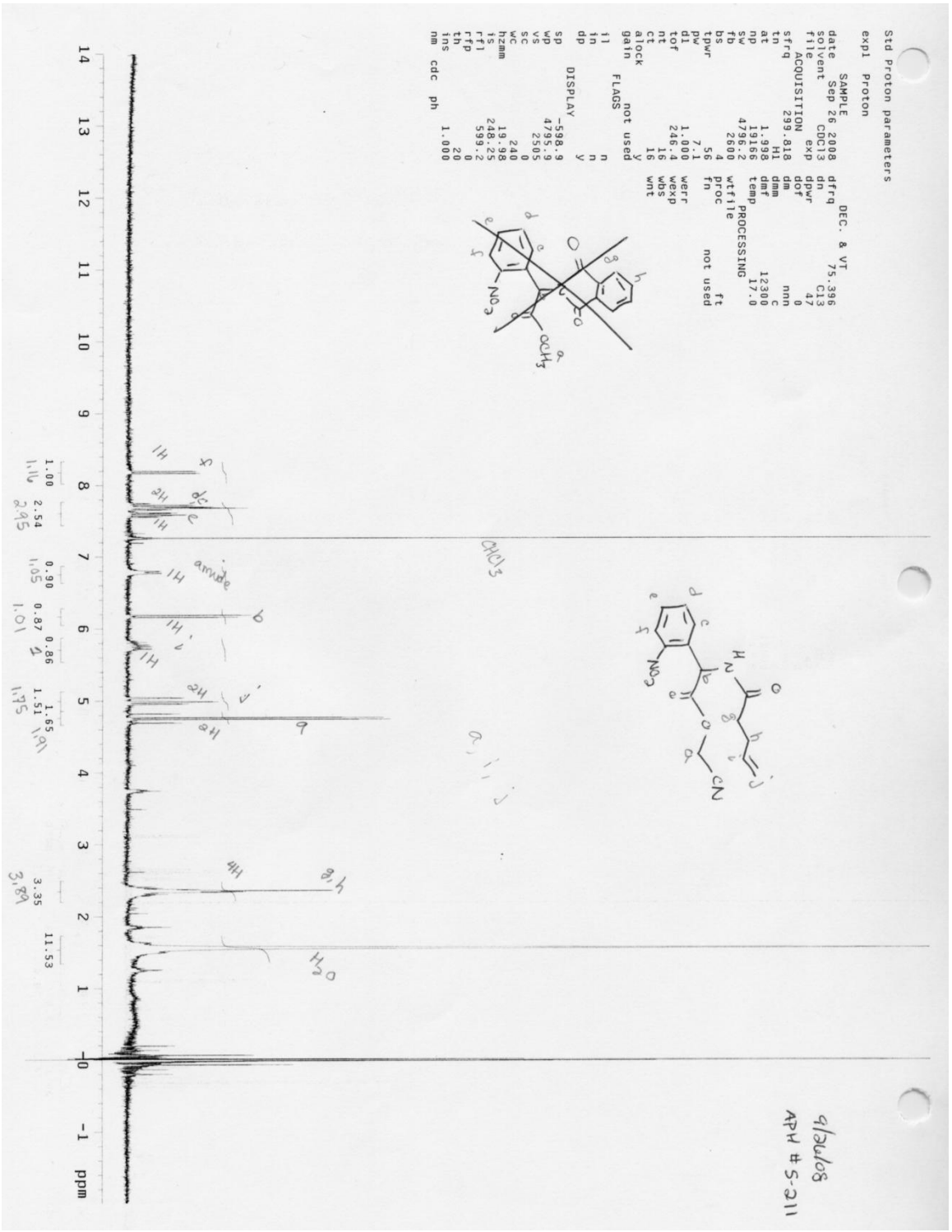

Figure 6.12 Proton NMR spectra of Cyano methyl ester of 4-PO-Nitrophenylglycine (**5**)

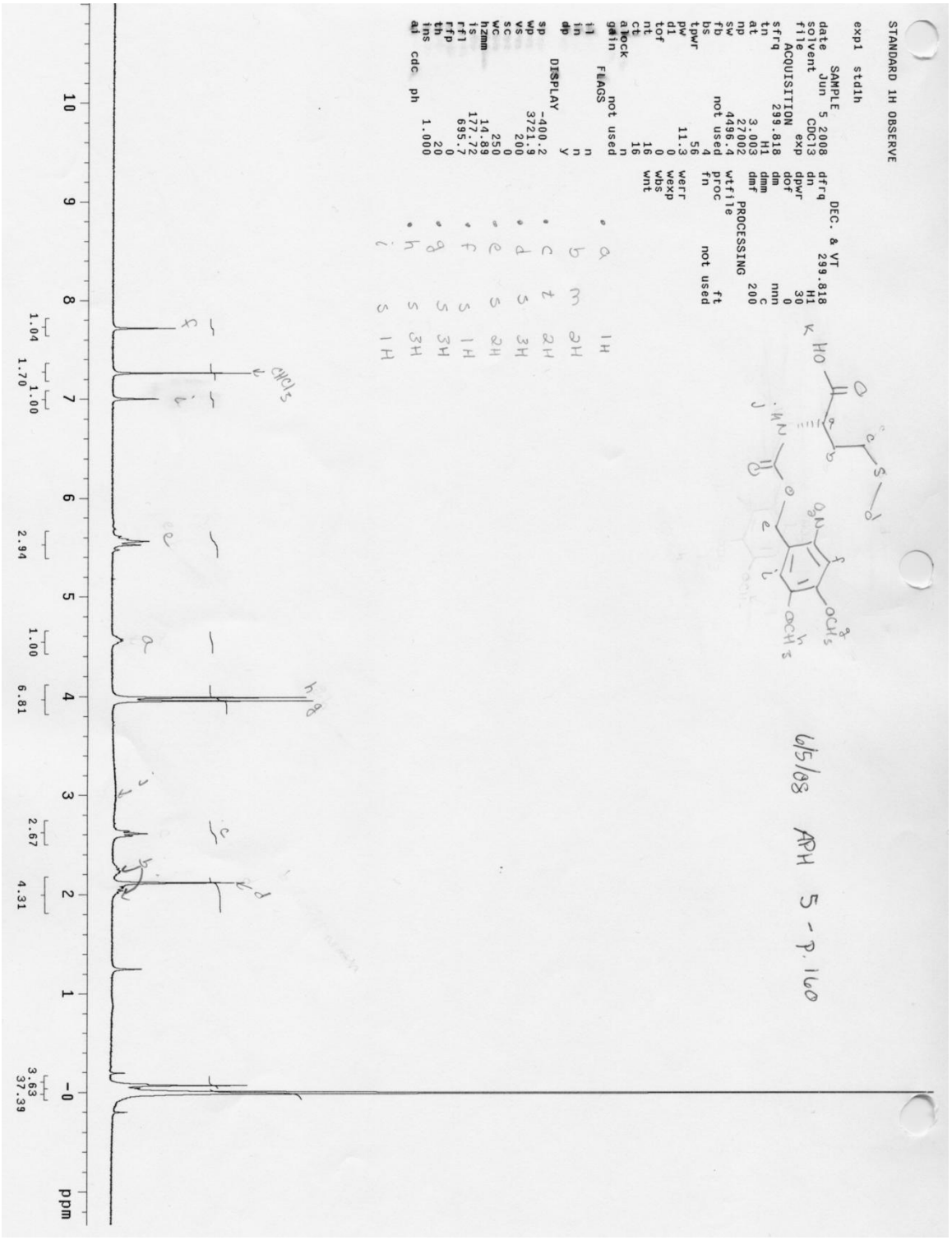

Figure 6.13 Proton NMR spectra of NVOC-Methionine

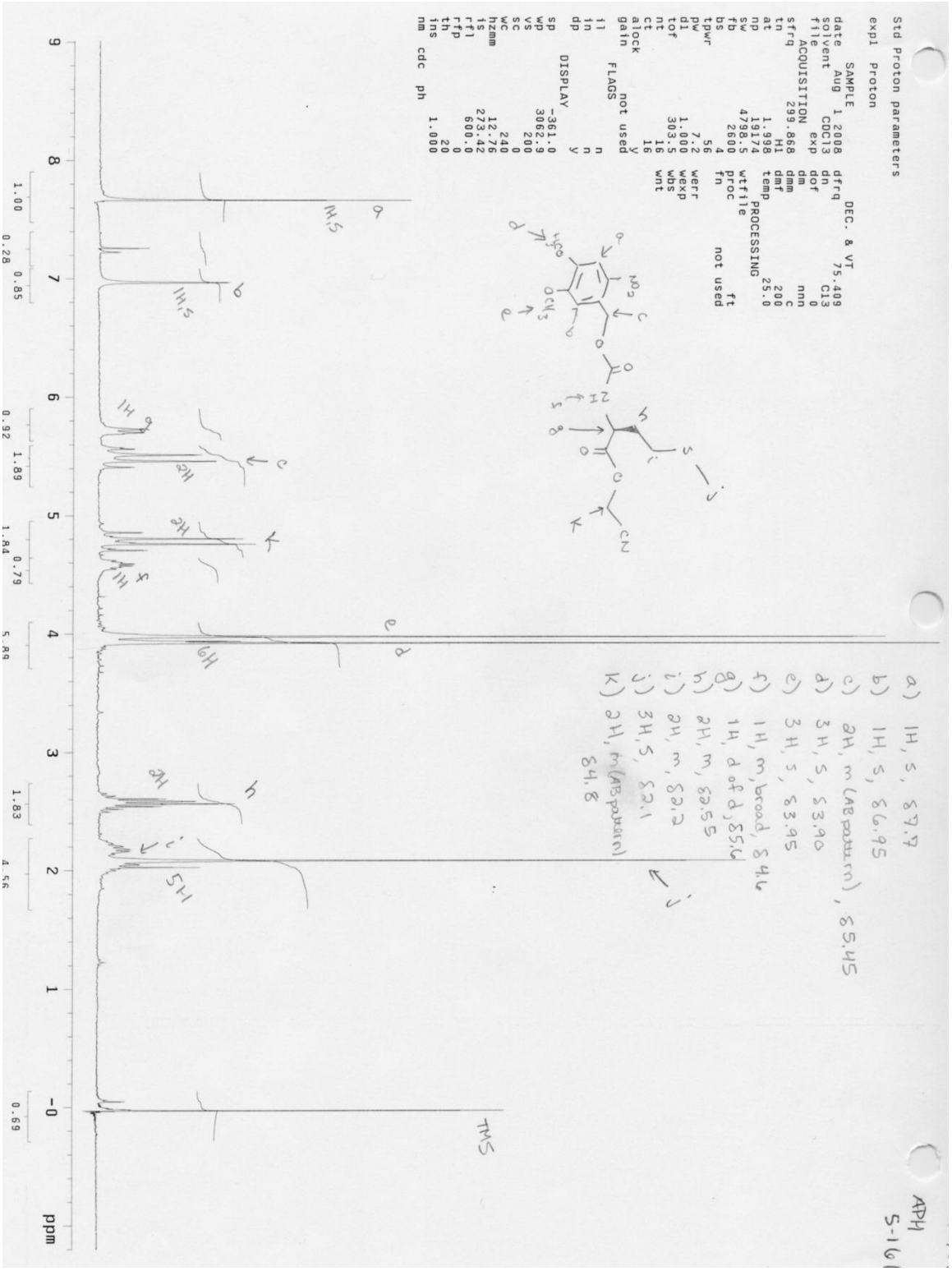

Figure 6.14 Proton NMR spectra of NVOC-Methionine CN methyl ester

6.6 References

(1) Akabas, M. H. *Int Rev Neurobiol* **2004**, *62*, 1-43.
(2) Brejc, K.; van Dijk, W. J.; Klaassen, R. V.; Schuurmans, M.; van Der Oost, J.; Smit, A. B.; Sixma, T. K. *Nature* **2001**, *411*, 269-76.
(3) Unwin, N. *J Mol Biol* **2005**, *346*, 967-89.
(4) Corringer, P. J.; Le Novere, N.; Changeux, J. P. *Annu Rev Pharmacol Toxicol* **2000**, *40*, 431-58.
(5) Bouzat, C.; Gumilar, F.; Spitzmaul, G.; Wang, H. L.; Rayes, D.; Hansen, S. B.; Taylor, P.; Sine, S. M. *Nature* **2004**, *430*, 896-900.
(6) Chakrapani, S.; Bailey, T. D.; Auerbach, A. *J Gen Physiol* **2004**, *123*, 341-56.
(7) Hanek, A. P.; Lester, H. A.; Dougherty, D. A. *J Am Chem Soc* **2008**, *130*, 13216-8.
(8) Xiu, X.; Hanek, A. P.; Wang, J.; Lester, H. A.; Dougherty, D. A. *J Biol Chem* **2005**, *280*, 41655-66.
(9) Wafford, K. A. *Curr Opin Pharmacol* **2005**, *5*, 47-52.
(10) Padgett, C. L.; Hanek, A. P.; Lester, H. A.; Dougherty, D. A.; Lummis, S. C. *J Neurosci* **2007**, *27*, 886-92.
(11) Whiting, P. J. *Drug Discov Today* **2003**, *8*, 445-50.
(12) McKernan, R. M.; Rosahl, T. W.; Reynolds, D. S.; Sur, C.; Wafford, K. A.; Atack, J. R.; Farrar, S.; Myers, J.; Cook, G.; Ferris, P.; Garrett, L.; Bristow, L.; Marshall, G.; Macaulay, A.; Brown, N.; Howell, O.; Moore, K. W.; Carling, R. W.; Street, L. J.; Castro, J. L.; Ragan, C. I.; Dawson, G. R.; Whiting, P. J. *Nat Neurosci* **2000**, *3*, 587-92.
(13) Rudolph, U.; Crestani, F.; Benke, D.; Brunig, I.; Benson, J. A.; Fritschy, J. M.; Martin, J. R.; Bluethmann, H.; Mohler, H. *Nature* **1999**, *401*, 796-800.
(14) Berezhnoy, D.; Nyfeler, Y.; Gonthier, A.; Schwob, H.; Goeldner, M.; Sigel, E. *J Biol Chem* **2004**, *279*, 3160-8.
(15) Buhr, A.; Baur, R.; Malherbe, P.; Sigel, E. *Mol Pharmacol* **1996**, *49*, 1080-4.
(16) Kucken, A. M.; Teissere, J. A.; Seffinga-Clark, J.; Wagner, D. A.; Czajkowski, C. *Mol Pharmacol* **2003**, *63*, 289-96.
(17) Cashin, A. L.; Torrice, M. M.; McMenimen, K. A.; Lester, H. A.; Dougherty, D. A. *Biochemistry* **2007**, *46*, 630-9.
(18) Gleitsman, K. R.; Kedrowski, S. M.; Lester, H. A.; Dougherty, D. A. *J Biol Chem* **2008**, *283*, 35638-43.
(19) Lee, W. Y.; Sine, S. M. *J Gen Physiol* **2004**, *124*, 555-67.
(20) Petersson, E. J.; Choi, A.; Dahan, D. S.; Lester, H. A.; Dougherty, D. A. *J Am Chem Soc* **2002**, *124*, 12662-3.
(21) Price, K. L.; Bower, K. S.; Thompson, A. J.; Lester, H. A.; Dougherty, D. A.; Lummis, S. C. *Biochemistry* **2008**, *47*, 6370-7.
(22) Wagner, D. A.; Czajkowski, C.; Jones, M. V. *J Neurosci* **2004**, *24*, 2733-41.
(23) Xiu, X.; Puskar, N. L.; Shanata, J. A.; Lester, H. A.; Dougherty, D. A. *Nature* **2009**.
(24) Cromer, B. A.; Morton, C. J.; Parker, M. W. *Trends Biochem Sci* **2002**, *27*, 280-7.
(25) Kloda, J. H.; Czajkowski, C. *Mol Pharmacol* **2007**, *71*, 483-93.
(26) Changeux, J. P.; Edelstein, S. J. *Neuron* **1998**, *21*, 959-80.
(27) Olsen, R. W. *Annu Rev Pharmacol Toxicol* **1982**, *22*, 245-77.
(28) Nowak, M. W.; Gallivan, J. P.; Silverman, S. K.; Labarca, C. G.; Dougherty, D. A.; Lester, H. A. *Methods Enzymol* **1998**, *293*, 504-29.
(29) Nowak, M. W.; Kearney, P. C.; Sampson, J. R.; Saks, M. E.; Labarca, C. G.; Silverman, S. K.; Zhong, W.; Thorson, J. S.; Abelson, J. N.; Davidson, N.; Schultz, P. G.; Dougherty, D. A.; Lester, H. A. *Science* **1995**, *268*, 439-442.
(30) Adams, S. R.; Tsien, R. Y. *Annu Rev Physiol* **1993**, *55*, 755-84.
(31) Gurney, A. M.; Lester, H. A. *Physiol Rev* **1987**, *67*, 583-617.
(32) Kaplan, J. H.; Somlyo, A. P. *Trends Neurosci* **1989**, *12*, 54-9.
(33) McCray, J. A.; Trentham, D. R. *Annu Rev Biophys Biophys Chem* **1989**, *18*, 239-70.
(34) Mendel, D.; Ellman, J. A.; Schultz, P. G. *Journal of the American Chemical Society* **1991**, *113*, 2758-2760.

(35) Milburn, T.; Matsubara, N.; Billington, A. P.; Udgaonkar, J. B.; Walker, J. W.; Carpenter, B. K.; Webb, W. W.; Marque, J.; Denk, W.; McCray, J. A.; et al. *Biochemistry* **1989**, *28*, 49-55.
(36) Miller, J. C.; Silverman, S. K.; England, P. M.; Dougherty, D. A.; Lester, H. A. *Neuron* **1998**, *20*, 619-24.
(37) Philipson, K. D.; Gallivan, J. P.; Brandt, G. S.; Dougherty, D. A.; Lester, H. A. *Am J Physiol Cell Physiol* **2001**, *281*, C195-206.
(38) Ramesh, D.; Wieboldt, R.; Billington, A. P.; Carpenter, B. K.; Hess, G. P. *Journal of Organic Chemistry* **1993**, *58*, 4599-4605.
(39) Wieboldt, R.; Gee, K. R.; Niu, L.; Ramesh, D.; Carpenter, B. K.; Hess, G. P. *Proc Natl Acad Sci U S A* **1994**, *91*, 8752-6.
(40) Wieboldt, R.; Ramesh, D.; Carpenter, B. K.; Hess, G. P. *Biochemistry* **1994**, *33*, 1526-33.
(41) Boileau, A. J.; Baur, R.; Sharkey, L. M.; Sigel, E.; Czajkowski, C. *Neuropharmacology* **2002**, *43*, 695-700.
(42) Rodriguez, E. A.; Lester, H. A.; Dougherty, D. A. *RNA* **2007**, *13*, 1703-14.
(43) Amin, J. *Mol Pharmacol* **1999**, *55*, 411-23.
(44) Amin, J.; Weiss, D. S. *Nature* **1993**, *366*, 565-9.
(45) Serafini, R.; Bracamontes, J.; Steinbach, J. H. *J Physiol* **2000**, *524 Pt 3*, 649-76.
(46) Jackson, M. B.; Lecar, H.; Mathers, D. A.; Barker, J. L. *J Neurosci* **1982**, *2*, 889-94.
(47) Rho, J. M.; Donevan, S. D.; Rogawski, M. A. *J Physiol* **1996**, *497 (Pt 2)*, 509-22.
(48) Mercado, J.; Czajkowski, C. *J Biol Chem* **2008**, *283*, 15250-7.
(49) Muroi, Y.; Theusch, C. M.; Czajkowski, C.; Jackson, M. B. *Biophys J* **2009**, *96*, 499-509.
(50) England, P. M.; Lester, H. A.; Davidson, N.; Dougherty, D. A. *Proc Natl Acad Sci U S A* **1997**, *94*, 11025-30.
(51) Muralidharan, S.; Nerbonne, J. M. *Journal of Photochemistry and Photobiology B-Biology* **1995**, *27*, 123-137.

Chapter 7

Side Chain and Backbone Mutations Between Loops A and E of the $GABA_AR$ α_1 Subunit Alter Benzodiazepine Potentiation and GABA Activation

7.1 Introduction

γ-Aminobutyric acid type A ($GABA_A$) receptors are members of the Cys-loop family of ligand gated ion channels which mediate rapid synaptic transmission in the mammalian central nervous system. At rest the receptors are in a closed, non-conducting state. Upon binding of their cognate neurotransmitter agonist, the receptors undergo a conformational change, termed activation, to an open, ion-conducting state. Biochemical studies of these receptors has been guided by the X-ray crystal structure of the acetylcholine binding protein (AChBP)[1] and cryo-EM images of the *torpedo Californica* nicotinic acetylcholine receptor (nAChR).[2] Both these structures are highly homologous to nAChRs, another member of the Cys-loop family of receptors, and to a lesser extent other members of the superfamily. Homology models of the $GABA_AR$ based on both the AChBP and cryo-EM structures suggest the primary sequence linking loops A and E of the α_1 subunit of the $GABA_AR$ is highly unstructured (Figure 7.1).

In the preceding chapter, we identified this region of the receptor as a key element in the GABA activation pathway. Using photo-activated proteolytic cleavage of the $GABA_AR$ backbone (Chapter 6) we have shown that this linker must be intact for GABA activation and that the linker does not have a defined secondary structure in the closed state of the receptor. Proteolytic cleavage of the backbone introduces more flexibility to this region of the receptor and prevented GABA activation and therefore our ability to study the role of this region for benzodiazepine (BZD) potentiation. The added flexibility

in the primary structure may impact GABA activation directly or by displacing key amino acid side chains. In the present work we investigate these two affects separately.

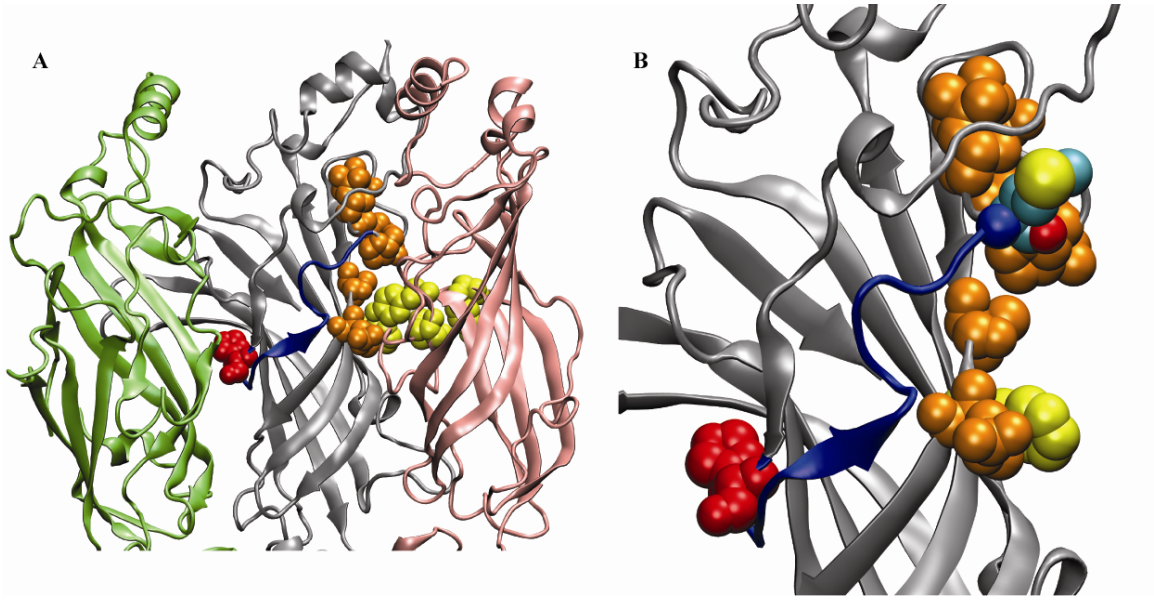

Figure 7.1 An unstructured linker connects loops A and E of the $GABA_AR$ α_1 subunit. **A,** the extracellular domain of three subunits, γ (lime), α (gray), and β (pink) as viewed from the channel pore. The loop A residue (red) and loop E residues (orange) of the α subunit are shown as Van der Waals residues. The GABA binding site is identified by yellow residues. **B,** The α subunit with the linker region (blue) highlighted. M113, the subject of the previous chapter, is shown in CPK coloring.

BZDs are allosteric modulators of the $GABA_AR$, and as such bind to the receptor at a site distinct from the GABA binding site. α_1His101, a loop A residue of the α_1 subunit, has been identified as contributing to the putative BZD binding site.[3-5] BZDs act in several ways including as inverse agonists inhibiting the GABA induced current,[6,7] positive modulators that potentiate the GABA current,[8] and antagonists that competitively bind at the BZD binding site but have no effect on GABA current.[9] The more common BZDs, flurazepam and diazepam, act by potentiating the GABA current, therefore application of these BZDs and GABA result in larger macroscopic current than application of GABA alone. Potentiation (P) is defined according to Equation 7.1

$$P=\frac{I_{FLZM}}{I_{GABA}}-1 \qquad \textbf{Equation 7.1}$$

Given that the structural information[1,2] and available biochemical studies[10,3] indicate the region between loops A and E does not have a defined secondary structure, it is surprising that the primary sequences are highly conserved (Table 7.1). We noted no conserved differences in this region between the BZD sensitive (1-3, 5) and insensitive (4, 6) α subunits. We selected G103, K104, K105, M111, M113, and P114 for conventional mutagenesis. We reasoned that G103 and P114 present unique structural elements that may be crucial to receptor function. Conserved positive charges at K104 and K105 suggested a possible role for electrostatic interactions. M111 was selected because it is conserved as a hydrophobic residue but is only a Met in the α subunits. Finally, M113 was selected both due to less conservation and because it was previously used for Npg incorporation.

Table 7.1 Sequence Alignment of $GABA_AR$ subunits

GABA α_1	**P**	**D**	T	F	F	H	**N**	G	K	K	S	V	A	H	N	M	T	M	P	N	K	L	L	R	I
GABA α_2	**P**	**D**	T	F	F	H	**N**	G	K	K	S	V	A	H	N	M	T	M	P	N	K	L	L	R	I
GABA α_3	**P**	**D**	T	F	F	H	**N**	G	K	K	S	V	A	H	N	M	T	T	P	N	K	L	L	R	L
GABA α_4	**P**	**D**	T	F	F	R	**N**	G	K	K	S	V	S	H	N	M	T	A	P	N	K	L	F	R	I
GABA α_5	**P**	**D**	T	F	F	H	**N**	G	K	K	S	I	A	H	N	M	T	T	P	N	K	L	L	R	L
GABA α_6	**P**	**D**	T	F	F	R	**N**	G	K	K	S	I	A	H	N	M	T	T	P	N	K	L	F	R	I
GABA β_1	**P**	**D**	T	Y	F	L	**N**	D	K	K	S	F	V	H	G	V	T	V	K	N	R	M	I	R	L
GABA β_2	**P**	**D**	T	Y	F	L	**N**	D	K	K	S	F	V	H	G	V	T	V	K	N	R	M	I	R	L
GABA γ_1	**P**	**D**	T	F	F	R	**N**	S	R	K	S	D	A	H	W	I	T	T	P	N	R	L	L	R	I
GABA γ_2	**P**	**D**	T	F	F	R	**N**	S	K	K	A	D	A	H	W	I	T	T	P	N	R	M	L	R	I
GABA γ_3	**P**	**D**	T	I	F	R	**N**	S	K	T	A	E	A	H	W	I	T	T	P	N	Q	L	L	R	I
GABA γ_4	**P**	**D**	T	F	F	R	**N**	S	K	R	T	H	E	H	E	I	T	M	P	N	Q	M	V	R	I
						101												114							

The superfamily has a conserved WxPDxxxxN domain, the P, D, and N residues are shown in bold. Loop A residues are highlighted with red and loop E residues with yellow. G103, K104, K105, M111, M113, and P114 are colored as hydrophobic (red), polar (green), or cationic (blue).

[3] Chapter 6

Both glycine and proline are structurally unique when compared to the rest of the naturally occurring amino acids. Glycine (Figure 7.2) has a hydrogen atom as its side chain and therefore is not chiral. Its small size leads to fewer conformational restrictions and as such glycine residues are often found in hinge regions of proteins giving them a structural role in protein function.[11] Proline is the only naturally occurring cyclic amino acid and as such cannot make hydrogen bonds, as it lacks an N-H for hydrogen bonding. Additionally, proline can form *cis* amide bonds at a much higher frequency (~5%) than the other naturally occurring amino acids (<0.1%)[12] thus proline can also adopt unique conformations and often plays a structural role. For both glycine and proline residues, mutation to another naturally occurring amino acid often disrupts protein function,[13] and as such these residues seemed likely to play a role in activation.

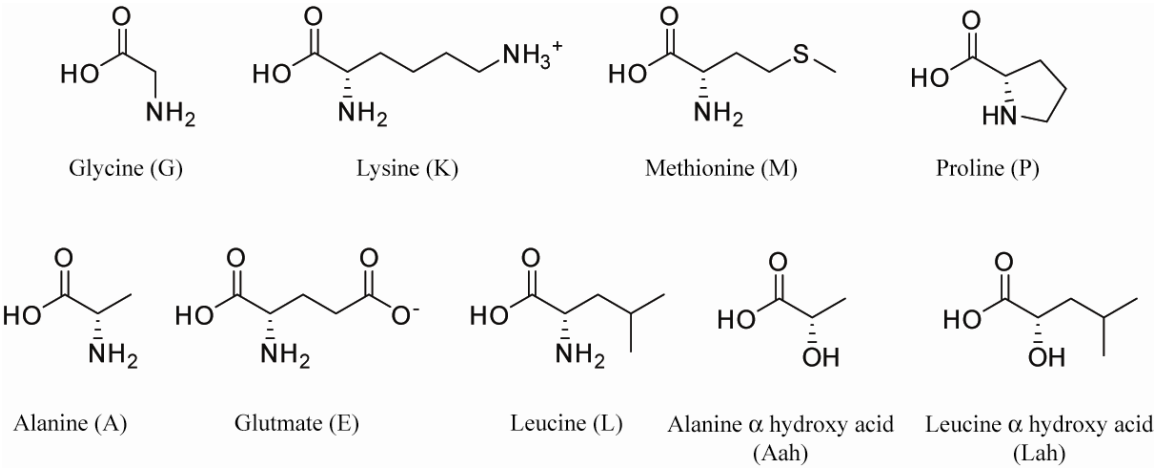

Figure 7.2 Chemical structures for wild type (top row) amino acids, conventional mutants (bottom row, left), and α-hydroxy acids (bottom, right)

7.2 Results

7.2.1 Conventional Mutagenesis – Side Chain Mutations

No electrical signal was detected for αG103Aβ $GABA_A$Rs even when the total mRNA was increased to 50 ng. The same mutation in the αβγ $GABA_A$R responded to

GABA in a concentration dependent manner. However, the amount of mRNA required was 100x greater than for wild type or other conventional mutants and I_{max} values were still lower than for most other mutations (Table 7.2). Despite lower current sizes, the GABA EC_{50} and Hill coefficient (n_H), as well as flurazepam (FLZM) potentiation (P) for αG103Aβγ $GABA_A$Rs were similar to wild type receptors. P114A mutant $GABA_A$Rs also behaved similarly to wild type receptors (Table 7.2). I_{max} values for the αP114Aβ $GABA_A$R were significantly lower than for wild type, but αP114Aβγ $GABA_A$R I_{max} values were similar to wild type. These data suggest that mutations in the αβ $GABA_A$R may affect surface expression to a greater extent than in the αβγ $GABA_A$R.

Table 7.2 Conventional mutagenesis in the linker region has little impact on EC_{50} (μM)

	$\alpha_1\beta_{2S}$ $GABA_A$R			**$\alpha_1\beta_{2S}\gamma_{2L}$ $GABA_A$R**			
Mutant	EC_{50}	n_H	I_{max}	EC_{50}	n_H	I_{max}	P
Wild type	1.8 ± 0.1	1.4	7 ± 1	44 ± 1	1.3	4.9 ± 0.6	2.6 ± 0.2
αG103A	NR			49 ± 4	1.4	1.4 ± 0.3	2.4 ± 0.8
αK104A	2.4 ± 0.2	1.1	3.6 ± 0.9	42 ± 3	1.1	2.4 ± 0.5	0.9 ± 0.1*
αK104E	5.9 ± 0.4	1.1	3.3 ± 0.6	64 ± 4	0.96	1.4 ± 0.2	2.2 ± 0.3
αK105A	8.4 ± 0.6	1.0	7 ± 1	87 ± 4	1.2	3.9 ± 0.9	1.5 ± 0.1*
αK105E	4.2 ± 0.1	1.2	5 ± 1	38 ± 2	1.5	11 ± 2	2.2 ± 0.2
αM111A	9.4 ± 0.7	0.93	3.7 ± 0.7	75 ± 3	1.0	2.4 ± 0.4	2.0 ± 0.2
αM111L	7.5 ± 0.4	1.1	4 ± 1	124 ± 6	1.1	2.1 ± 0.5	2.0 ± 0.2
αM113A	1.6 ± 0.1	1.4	7 ± 1	23 ± 1	1.3	9 ± 2	1.6 ± 0.2*
αM113L	4.7 ± 0.2	1.2	1.6 ± 0.2	73 ± 2	1.2	2.4 ± 0.6	1.2 ± 0.1*
αP114A	3.0 ± 0.1	1.2	2.3 ± 0.5	37 ± 2	1.3	3.5 ± 0.5	2.1 ± 0.3

NR denotes there was no response to 10 mM GABA. EC_{50} is reported in μM of GABA and I_{max} is reported in μA. All EC_{50} values are calculated from an average of at least 5 oocytes. Potentiation values are averaged from at least 8 oocytes, except for the G103A mutant which uses 4 oocytes. * indicates the potentiation is significantly different from wild type (two-tail unpaired t-test, $p<0.01$).

Amino acids at the positions analogous to K104 and K105 are conserved as positively charged amino acids in all the GABA α and β subunits. Given the proximity to the channel pore it seems reasonable that these side chains may stick into the channel pore and therefore may not interact with other side chains, rendering them insensitive to

mutation. However, these residues are conserved in the α_1, β_2, and γ_2 subunits, suggesting a positive ring of charge in this region of the receptor may be important. Surprisingly, removal of the side chain at αK104 (αK104A) had little effect on the EC_{50} of the αβ and αβγ $GABA_AR$ (Table 7.2), but a large effect on FLZM potentiation. The FLZM potentiation dropped to 0.9 (Figure 7.3) compared to 2.6 for the wild type receptor. The same mutation at position 105 (αK105A) increased EC_{50} for both αβ and αβγ receptors and decreased potentiation, though to a lesser extent than the αK104A mutation. Both alanine mutations had lower Hill coefficients than the wild type receptors, which may indicate a loss of cooperativity between subunits.

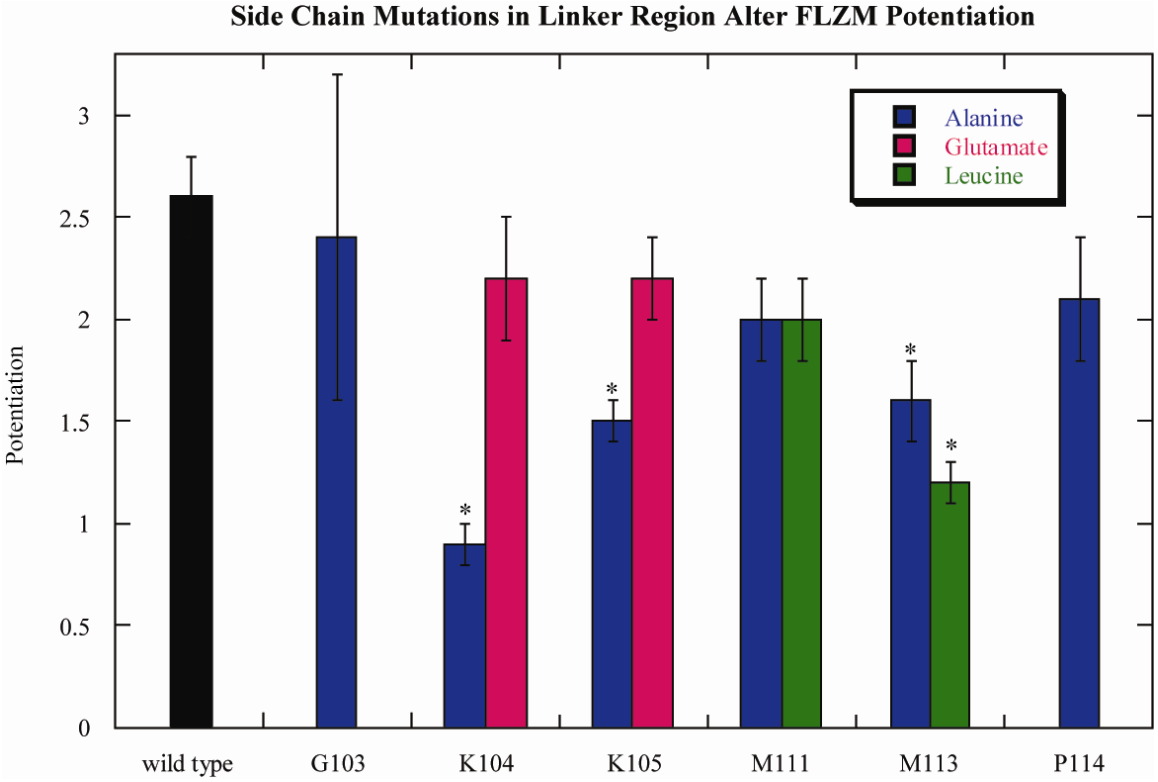

Figure 7.3 Conventional mutations in linker region alter FLZM potentiation. Four mutations, K104A, K105A, M113A, and M113L reduce FLZM potentiation. * indicates the value is significantly different from wild type (unpaired, two-tail t-test, $p<0.01$)

Charge reversal at positions 104 (αK104E) and 105 (αK105E) gave $GABA_A$Rs that functioned similarly to wild type receptors. The GABA EC_{50} of the αβ receptor increased ~3- and 2-fold, respectively. These mutations had a smaller impact on the GABA EC_{50} of the of the αβγ receptor such that values were not appreciably different form the wild type receptor. FLZM potentiation was not significantly different from wild type. Interestingly, the αK104E mutation lowered the Hill coefficient of both the αβ and αβγ receptors, indicating this residue may play a role in subunit cooperativity.

The methionine residues at positions 111 and 113 were mutated to alanine and leucine. αM111A and αM111L mutations increased the GABA EC_{50} 5.2- and 4.2-fold, respectively, in the αβ $GABA_A$R and 1.7- and 2.8-fold in the αβγ $GABA_A$R. Despite the shifts in GABA EC_{50}, neither mutation at αM111 altered FLZM potentiation. The opposite scenario occurred at αM113. For αM113 mutants, the GABA EC_{50} was not altered but FLZM potentiation decreased significantly. The αM113Aβ $GABA_A$R was nearly identical to the wild type receptor in terms of EC_{50}, Hill coefficient, and I_{max} values. In the αβγ receptor, this mutation was gain-of-function, lowering the EC_{50} ~2-fold. FLZM potentiation, however, was reduced to 1.6. The αM113L mutant, a more subtle mutation, increased EC_{50} slightly for both the αβ and αβγ $GABA_A$Rs yet decreased FLZM potentiation to only 1.2.

FLZM potentiation is dependent on the concentration of GABA and FLZM used. Potentiation is larger at lower concentrations of GABA (EC_{5-10}) thus we conducted all potentiation experiments within this range of GABA (Table 7.3). The FLZM concentration was held constant at 1 μM, which we initially assumed to be EC_{80-90} for all

mutations. To ensure this was the case, we determined the FLZM dose response relationship for the four mutations that altered FLZM potenitation as well as the M111A mutation (Table 7.3, Figure 7.4). The data indicate that 1 μM FLZM is between EC_{70-90} for all mutations and EC_{64} for the wild type receptor.

Table 7.3 The EC_{50} of potentiation ($EC_{50,P}$) and Hill coefficients for the FLZM dose response relationships

	$EC_{50,P}$ (nM)	n_H	$EC_{X,FLZM}$	N	[GABA]	$EC_{X,GABA}$
αβγ (WT)	500 ± 100	0.8 ± 0.1	64	12	5 μM	5.70
αK104Aβγ	220 ± 30	1.1 ± 0.1	84	5	5 μM	8.95
αK105Aβγ	300 ± 70	0.8 ± 0.1	72	4	10 μM	6.80
αM111Aβγ	300 ± 20	1.05 ± 0.06	78	5	5 μM	5.79
αM113Aβγ	400 ± 80	1.0 ± 0.1	71	5	3 μM	6.87
αM113Lβγ	230 ± 30	1.3 ± 0.2	87	4	10 μM	8.13

1 μM FLZM corresponds to EC_{64} for wild type and EC_{70-90} for all mutations. The concentration of GABA used for the potentiation and for determination of the FLZM dose response relationship was between EC_{5-10} for all mutations.

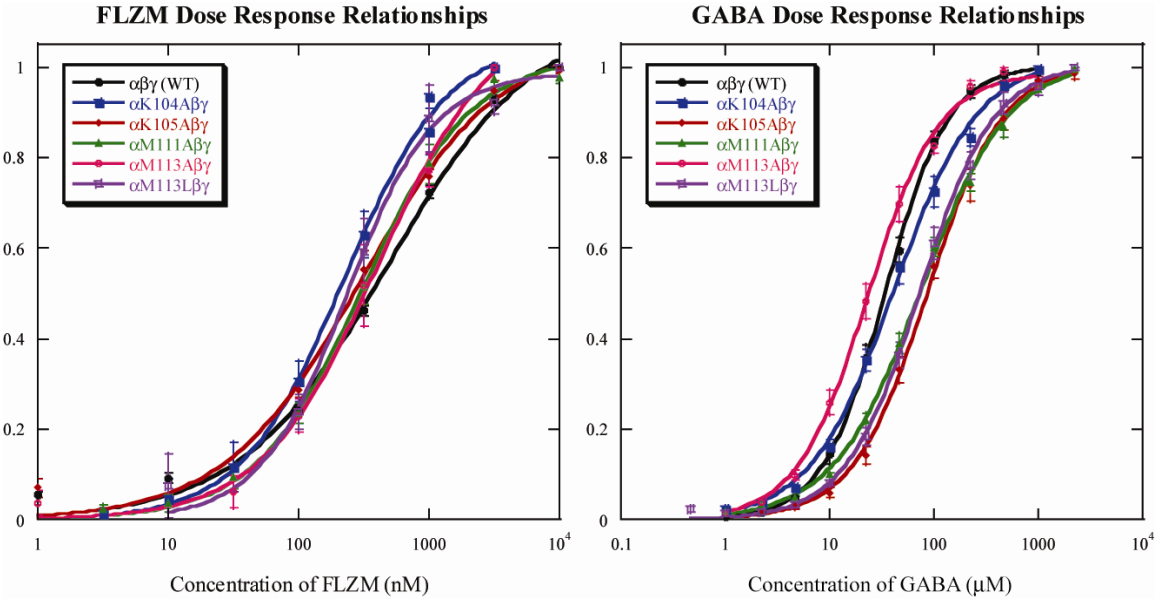

Figure 7.4 FLZM and GABA dose response relationships for wild type and selected conventional mutants. *Left*: Conventional mutations do not shift the FLZM dose response relationship significantly. *Right*: For comparison, the GABA dose response relationships are shown for the same mutations. There is more scatter in the GABA plot than the FLZM plot.

7.2.2 Incorporation of α-Hydroxy Acids

Side chain mutations at αM113 impacted FLZM potentiation while those at αM111 did not. Given the sensitivity of the region to proteolytic cleavage (Chapter 6), we reasoned that increasing the flexibility of the backbone, achieved by incorporation of an α-hydroxy acid, would either decrease potentiation with the αM111 mutations or rescue FLZM potentiation at αM113.

Table 7.4 Incorporation of α-hydroxy acids at αM111 increases GABA EC_{50} and decreases FLZM potentiation

Receptor	EC_{50} (μM)	n_H	I_{max} (μA)	P	ah/aa shift*
αM111Metβ	2.3 ± 0.1	1.3 ± 0.1	0.8 ± 0.2		
αM111Aahβ	120 ± 7	0.99 ± 0.05	1.0 ± 0.2		12.8
αM111Lahβ	31 ± 1	0.87 ± 0.02	2 ± 1		4.1
αM111(dCA)β			0.12 ± 0.05		
αM111Metβγ	41 ± 1	1.36 ± 0.05	3.5 ± 0.8	2.3 ± 0.2	
αM111Aahβγ	800 ± 40	0.97 ± 0.03	2.8 ± 0.4	0.54 ± 0.06	10.7
αM111Lahβγ	440 ± 30	0.90 ± 0.03	2.1 ± 0.2	1.3 ± 0.1	3.6
αM111(dCA)βγ	900 ± 100	0.81 ± 0.04	1.2 ± 0.1	0.67 ± 0.06	

*The final column gives the fold shift in GABA EC_{50} for the alpha hydroxy acid relative to the amino acid.

Incorporation of methionine by nonsense suppression at αM111 reproduced the GABA and FLZM behavior of the wild type αβ and αβγ wild type receptors (Table 7.4). Re-aminoacylation control (described in Chapter 6 and designated here as dCA) experiments gave maximal currents less than 150 nA in the αβ $GABA_AR$. The same experiments in the αβγ $GABA_AR$ gave significant current such that the GABA EC_{50} and Hill coefficient, as well as the FLZM potentiation, could be determined. Receptors resulting from re-aminoacylation of the suppressor tRNA and subsequent incorporation into the protein gave receptors with a pharmacology distinct from the wild type receptors. Incorporation of alanine-α-hydroxy acid (Aah, Figure 7.2) substantially increased the

EC_{50} (Table 7.4) of the αβ $GABA_AR$, as did leucine-α-hydroxy acid (Lah). Similar increases in GABA EC_{50} occurred for the αβγ $GABA_AR$ along with a decrease in FLZM potentiation. The GABA EC_{50} and Hill coefficient, as well as the FLZM potentiation for αM111Aahβγ $GABA_ARs$ is not pharmacologically different from the re-aminoacylation controls.

Wild type recovery (incorporation of methionine by nonsense suppression) experiments at αM113 yielded $GABA_ARs$ nearly identical to the wild type receptors for both the αβ and αβγ subtypes (Table 7.5). Re-aminoacylation control experiments gave enough current to determine the GABA EC_{50} and Hill coefficients in both subtypes as well as the FLZM potentiation in the αβγ receptor. These receptors were pharmacologically distinct from wild type. Aah increased the GABA EC_{50} slightly for both the αβ and αβγ receptors (Table 7.5). FLZM potentiation of the mutant receptor was similar to wild type. Incorporation of Lah substantially increased the EC_{50} of the αβ $GABA_AR$. The GABA EC_{50} of αM113Lahβγ $GABA_ARs$ is indistinguishable from that of the re-aminoacylation controls.

Table 7.5 Incorporation of α-hydroxy acids at αM113 increases GABA EC_{50} and decreases FLZM potentiation

Receptor	EC_{50} (μM)	n_H	I_{max} (μA)	P	ah/aa shift*
αM113Metβ	2.2 ± 0.1	1.5 ± 0.1	3.5 ± 1.1		
αM113Aahβ	3.7 ± 0.2	1.12 ± 0.07	0.9 ± 0.2		2.3
αM113Lahβ	26 ± 1	1.09 ± 0.04	1.5 ± 0.4		5.5
αM113(dCA)β	6.4 ± 0.8	0.77 ± 0.07	0.22 ± 0.07		
αM113Metβγ	43 ± 1	1.23 ± 0.04	4.5 ± 0.9	2.5 ± 0.2	
αM113Aahβγ	160 ± 20	0.84 ± 0.05	6 ± 2	2.8 ± 0.4	6.9
αM113Lahβγ	290 ± 20	1.05 ± 0.04	2.9 ± 0.5	1.45 ± 0.05	3.6
αM113(dCA)βγ	290 ± 40	0.92 ± 0.09	1.7 ± 0.4	0.81 ± 0.4	4.0

*The final column gives the fold shift in GABA EC_{50} for the alpha hydroxy acid relative to the amino acid.

7.3 Discussion

7.3.1 Side Chain Mutations: Affects on GABA EC_{50}

Conventional mutagenesis of the linker region had similar effects on GABA EC_{50} in both the αβ and αβγ $GABA_A$Rs, suggesting this region undergoes similar conformational changes during GABA activation in both receptor subtypes. The GABA EC_{50} shifts were generally larger in the αβ receptor, thus we restrict further discussion about the GABA EC_{50} to this subtype, unless otherwise specified. In the αβ $GABA_A$R, shifts in GABA EC_{50} for the alanine mutants ranged from 0.9 to 5.2-fold. Given the drastic nature of the alanine mutation, these shifts are relatively small, suggesting GABA activation is not highly dependent on side chain interactions with these residues. For the proposed structural residues, G103 and P114, we anticipated a much larger shift in the GABA EC_{50}, thus the data indicate that these two residues are not critical to the GABA activation pathway.

No electrical signal was detected for αG103Aβ mutant $GABA_A$Rs, suggesting the receptors could be non-functional or are not surface expressed. An inability for GABA to bind or disruption of the GABA activation pathway would both lead to non-functional receptors. αG103 is well removed from the GABA binding site, thus it seems unlikely that this mutation affects GABA binding. αG103Aβγ $GABA_A$Rs were surface expressed in sufficient quantity to determine the EC_{50} only when the amount of mRNA was increased 100-fold compared to the other conventional mutations. Given that increased mRNA amounts resulted in functional receptors with pharmacology similar to wild type and the location of αG103 near the subunit interface, it is most likely that αG103 plays a role in $GABA_A$R assembly and/or trafficking and thus that insufficient surface expression

of αG103Aβ $GABA_AR$ rather than nonfunctional receptors results in no detectable signal.

Charge reversal mutations at αK104 and αK105 are well tolerated. If these residues are involved in critical electrostatic interactions, we would expect mutation to alanine or glutamate to disrupt the interaction and severely impair channel function. Instead we see small shifts in EC_{50} (<5-fold), suggesting the residues are not involved in electrostatic interactions. Additionally, at αK105, charge reversal partially rescues the alanine mutation, suggesting an ionized species at this position aids channel function. At αK104, however, mutation to glutamate increased EC_{50} while alanine was similar to wild type. Taken together, the different results at these two positively charged, adjacent residues suggest the side chains are in distinct environments.

αM111 was most sensitive to side chain mutation. The alanine mutation produced the largest increase in EC_{50} (5.2-fold) of all the conventional mutations, indicating the methionine side chain may be important to receptor function. Interestingly, the more subtle mutation to leucine also increased EC_{50}. Like methionine, the leucine side chain is hydrophobic and relatively bulky (Figure 7.2). Chief structural differences between the two residues include a sulfur atom, one methylene difference in length, and branching in the leucine side chain. In contrast, αM113 was most tolerant of side chain mutations with mutation to alanine giving an EC_{50} nearly identical to wild type. Surprisingly, mutation to leucine, increased the EC_{50} (2.6-fold) slightly. This increase is only significant since alanine did not affect EC_{50}. At both methionine sites, mutation to leucine gives a larger increase in EC_{50} than expected for the subtlety of the mutation, especially given the data for the alanine mutations. These data strongly suggest the

GABA activation pathway is sensitive to the steric dimensions of the methionine side chains, such that introducing a γ-branched amino acid is sufficient to disrupt normal channel function.

7.3.2 Side Chain Mutations: Affects on FLZM Potentiation

Recent work by Kloda et al.[10] demonstrated that residues on loop E of the α subunit move when FLZM is applied to oocytes expressing mutant αβγ $GABA_AR$. The primary sequence of the α subunit links the BZD binding site (loop A) to loop E, thus it seems likely that residues in the linker would affect FLZM potentiation. Given that the linker is unstructured, we anticipated that side chain mutations would be unlikely to alter BZD potentiation. Initial experiments at two structural residues, G103 and P114, met our expectations, as the alanine mutants responded to FLZM similarly to wild type receptors. SCAM studies of these residues indicate that GABA and FLZM binding and activation are not affected by introduction of a larger MTSEA-Biotin group at G103[14] and P114.[10] The data from our studies corroborate the SCAM studies indicating the side chains of G103 and P114 are not integral to the mechanism of BZD potentiation.

At both αK104 and αK105, mutation to alanine decreased FLZM potentiation, clearly indicating the presence of a side chain is important to the potentiation mechanism. However, mutation to glutamate (present study) did not alter FLZM potentiation and mutation to cysteine did not alter FLZM EC_{50}.[14] Clearly, both cysteine and glutamate mutations are able to rescue the deleterious affect of mutation to alanine. SCAM studies of the cysteine mutation[14] indicate the side chain is either not accessible to MTSEA-biotin modification or that the modification does not affect GABA currents or FLZM

potentiation. Given that mutation to alanine caused decreased potentiation, but that cysteine, glutamate, and possibly MTSEA-biotin are able to function at these locations, it seems most likely that the size of both the K104 and K105 side chains is critical to FLZM potentiation.

Both αM113Aβγ and αM113Lβγ $GABA_A$Rs showed reduced FLZM potentiation, clearly indicating the side chain at this site is important to the potentiation mechanism. SCAM studies at this site indicate mutation to cysteine has a small effect on GABA EC_{50} and that MTSEA-biotin modification of the cysteine has a relatively small affect (~30% decrease) on GABA currents,[10] indicating the residue does not contribute to GABA binding and that side chain modifications do not prevent GABA activation. The SCAM study did not address FLZM induced changes at αM113. Our results, combined with the SCAM evidence showing αM113 modification does not impact GABA events, suggest that the side chain mutations affect only BZD potentiation. Interestingly, the same mutations at αM111 did not affect BZD potentiation, indicating the result is specific to αM113.

FLZM potentiation from application of 1 μM FLZM would be altered by changes to the potentiation pathway or by shifting the FLZM dose response curve. To ensure the dose response relationship was not altered, the potentiation dose response relationship was determined for representative mutations at each of K104, K105, M111, and M113. The data indicate that 1 μM FLZM is higher on the dose response curve for the mutant $GABA_A$Rs than for the wild type receptors; therefore if the FLZM potentiation pathway is unaffected by the mutations, we would expect wild type or higher potentiation values

in response to 1 μM FLZM. Thus, we can attribute the changes in FLZM potentiation from the conventional mutants to alterations of the potentiation mechanism.

It is interesting to note that, in several instances, mutations with small changes in GABA EC_{50} affected FLZM potentiation, while mutations with larger changes in GABA EC_{50} did not. αK104A $GABA_A$Rs had a smaller affect on GABA EC_{50} than αK104E $GABA_A$Rs, yet only the αK104A mutation affected FLZM potentiation. Similarly, mutations to αM111 had a larger impact on GABA EC_{50} than mutations to αM113, but FLZM potentiation was unaffected by αM111 mutant receptors and affected greatly by αM113 mutants. The trend is not perfect, as αG103A and αP114A receptors had small shifts in GABA EC_{50} and FLZM potentiation was unaffected, while at αK105 the alanine mutation had a larger effect on GABA EC_{50} and FLZM potentiation than the glutamate mutation. Still, if GABA activation and FLZM potentiation act through the same pathway, we would expect mutations to adversely impact both GABA EC_{50} and FLZM potentiation, which is clearly not always the case. The data presented herein indicate that while mechanisms of GABA activation and FLZM potentiation may be complementary[10,15,16] they clearly are not identical in terms of the involvement of amino acid side chains.

7.3.3 Backbone Mutations: Affects on $GABA_AR$ Activation

While we anticipated that α-hydroxy acid incorporation would alter receptor function, we were unsure if it would impact GABA EC_{50}, FLZM potentiation, or both, as well as whether the alteration would be a gain-of-function or loss-of-function. Additionally the α-hydroxy acids available were Aah and Lah, thus we wanted to be able to compare the affects of these mutations to that of the conventional mutant. Affects on

GABA EC_{50} and FLZM potentiation were similar for the alanine and leucine mutations at both αM111 and αM113, thus each of these sites already had an established pattern for the side chain mutations. Furthermore the established patterns for FLZM potentiation were opposite at the two sites, providing a means of detecting both gain-of-function or loss-of-function for the α-hydroxy acids.

The nonsense suppression methodology[17,18] is not perfect. In two cases presented here (αM111Aahβγ and αM113Lahβγ), we are unable to distinguish the data from α-hydroxy acid incorporation from that of the re-aminoacylation control experiment. We do note that in both cases the α-hydroxy acid experiments had approximately twice the current size of the controls and that the anticipated EC_{50} was similar to the measured EC_{50}. However, these results are not sufficient to definitively characterize the mutant receptor as distinct from the control experiments. Therefore, the remainder of the discussion and all conclusions drawn will not take into consideration the results from these two mutant receptors.

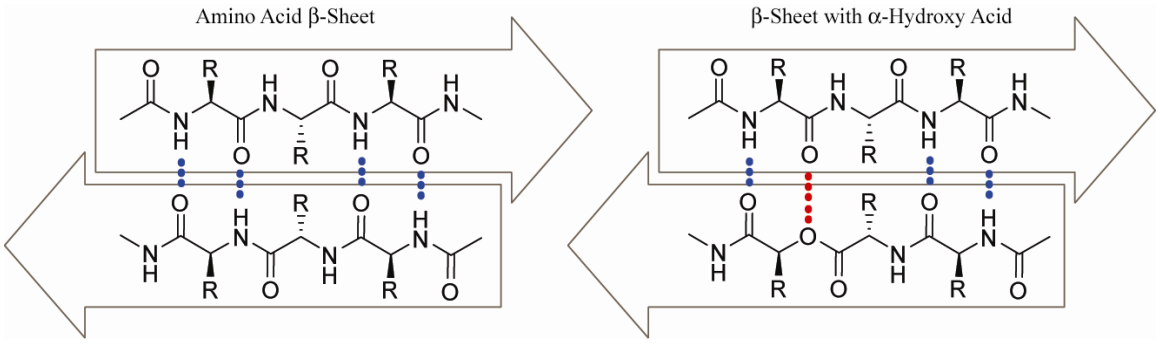

Figure 7.5 Hydroxy acids destabilize β-sheet structure. Typical β-sheets (left) have stabilizing (blue) hydrogen bond interactions between β-strands. When a α-hydroxy acid is incorporated (right) the attractive, stabilizing hydrogen bond interaction is replaced by a repulsive (red) O-O interaction, thereby destabilizing the secondary structure.

Incorporation of α-hydroxy acids at both positions increased the GABA EC_{50}. The changes were larger for αM111. Interestingly, Lah incorporation at both sites resulted in similar GABA EC_{50} values. These data clearly indicate that replacement of the amide bond with an ester bond impairs channel function, suggesting the region may adopt a defined secondary structure upon GABA activation. An increase in EC_{50} can be attributed to impaired GABA binding, stabilization of the closed state, destabilization of the open state or a combination of these factors. Given the location of the residues and previous biochemical studies,[10] it seems unlikely that backbone mutations will significantly impact GABA binding events. The structural information available indicates the region does not have a defined secondary structure (Figure 7.1)[1,2] and it is unlikely there are critical backbone interactions at both αM111 and αM113 that are not part of a secondary structure. However, the structural data is of the closed state of the receptor,[2] thus we cannot omit the possibility that this region adopts a β-strand configuration upon channel activation. If this is the case, α-hydroxy acid incorporation will de-stabilize the secondary structure because stabilizing hydrogen bonding interactions (Figure 7.5) have been deleted. Since the secondary structure is only present in the open state, these mutations will selectively de-stabilize the open state resulting in an increase in GABA EC_{50}. Furthermore, for a β-strand configuration we expect similar α-hydroxy acid incorporation at alternating residues to have similar affects, as seen here.

In addition to removing a potential hydrogen bond donating group, incorporation of α-hydroxy acids replaces an amide bond with a more flexible ester bond. We anticipated the added flexibility would either rescue FLZM potentiation at αM113 or impair FLZM potentiation at αM111. The data indicate that the added flexibility can

both impair and repair the potentiation pathway. Although this result is surprising, a straightforward interpretation exists: αM111 and αM113 undergo different changes during FLZM potentiation. The general activation pathways for GABA and BZD are anticipated to be similar, thus it is not surprising that αM111Lahβγ which has a large increase in GABA EC_{50} also has a decrease in FLZM potentiation, while αM113Aahβγ, which has a much smaller increase in GABA EC_{50}, has little affect on FLZM potentiation. Taken together, the α-hydroxy acid data indicate that GABA and FLZM induce similar structural rearrangements of the backbone within the linker region.

7.4 Conclusions

In conclusion, both side chain and backbone mutations between loops A and E of the α subunit affect GABA and FLZM activation pathways of the $GABA_AR$. Side chain mutagenesis, which is potentially more structurally perturbing, has a smaller affect on GABA EC_{50} than the more subtle mutation to a α-hydroxy acid, suggesting structural rearrangements of the entire linker are more critical than a particular side chain interaction. Furthermore, side chain mutations did not give consistent trends between changes in GABA EC_{50} and FLZM potentiation as expected, while backbone mutations both impaired GABA activation and decreased FLZM potentiation. The structural rearrangements within the linker likely initiate from loop E when GABA is applied and from Loop A when BZDs are applied. Thus it is possible that the final state of the backbone is similar for both activation pathways while the nature and sequence of the conformational changes are not. Different conformational changes to arrive in the same final state would allow for different affects on GABA EC_{50} and FLZM potentiation for side chain mutations, while still accounting for the similar affects for the backbone

mutations. Overall the data support a structural rearrangement of the primary sequence between loops A and E of the α subunit during GABA activation and FLZM potentiation.

7.5 Materials and Methods

Mutagenesis and preparation of mRNA: Human α_1 and β_{2S} $GABA_AR$ genes in pGEMHE were obtained from S.C.R. Lummis (Department of Biochemistry, University of Cambridge, Cambridge, United Kingdom). Quickchange PCR was used to make α_1 mutant DNA and mutation was confirmed by sequencing (Laragen Sequencing). The cDNA was linearized using Nhe1 (Roche) for the α_1 subunit and either Spe1 (Roche) or Sph1 (Roche) for the β_{2S} subunit. The mMessage mMachine kit (Ambion) was used to generate capped mRNA for oocyte injection.

7.5.1 Oocyte Injection

$\alpha\beta$ $GABA_AR$: For wild type and conventional mutations $\alpha_1\beta_{2S}$ mRNA was mixed in a 1:1 ratio and diluted to a final concentration of 100 ng/μl unless otherwise noted. Each oocyte was injected with 50 nl (5 ng) of mRNA mix. For suppression experiments, a 5:1 mix of the mRNA of the mutated α_1 gene and β_{2S} at a final concentration of 1 μg/μl was used.

$\alpha\beta\gamma$ $GABA_AR$: For wild type and conventional mutations, the β_{2S} gene was linearized with Spe1 and a 2:2:1 ratio of α:β:γ diluted to a final concentration of 10 ng/μl (unless otherwise noted) was used for mRNA mix as this yielded a pure population of αβγ receptors (see Appendix for additional details) with I_{max}values between 1 and 10 μA. For suppression experiments, the β_{2S} gene was linearized with Sph1 and a 5:1:5 ratio of α:β:γ at a final concentration of 1 μg/μl was used for the mRNA mix.

Suppression experiments: The mRNA mix was mixed 1:1 (by volume) with the deprotected aa-tRNA or ah-tRNA ($tRNA_{CUA}$ charged with either a naturally occurring amino acid or a α-hydroxy acid). Each oocyte was injected with a total volume of 50 nl of RNA mix; 25 ng mRNA and 15-50 ng of aa-tRNA (or ah-tRNA). The aa-tRNA was stored with the amino group protected by an NVOC group. Prior to mixing the aa-tRNA with the mRNA mix, the aa-tRNA was deprotected by photolysis. α-Hydroxy acids are not stored with a protecting group.

Met-, Aah- and Lah-tRNA were prepared as described previously.[17-19] Briefly, Met was protected using a nitroveratryloxycarbonyl group. The carboxylic acid of Met-NVOC, Aah and Lah were activated as the cyanomethyl esters and the activated compound was coupled to the dinucleotide dCA, which was then enzymatically ligated to 74-mer THG73 $tRNA_{CUA}$.

7.5.2 Characterization of Mutant Receptors

After injection, oocytes were incubated for 24-48 hours at 18°C prior to electrophysiology recordings. For a control, cRNA alone and cRNA mixed with dCA-THG (no unnatural amino acid attached) were injected into oocytes.

Determination of GABA EC_{50}: Peak GABA-induced currents were recorded at 19-22°C from individual oocytes using the OpusXpress system (Axon Instruments, Molecular Devices). A stock solution of 10 mM GABA (Sigma, St. Louis, MO) in ND96 buffer (in mM: 96 NaCl, 2 KCl, 1 MgCl2, 1.8 CaCl2, 5 HEPES, pH 7.5) was made fresh for each recording session. Drug solutions were made from the stock by dilution in ND96 buffer. Drug was delivered to cells via the automated perfusion system of the OpusXpress. Glass microelectrodes were backfilled with 3 M KCl and had a resistance

of 0.5-3.0 MΩ. The holding potential was -60 mV. To determine EC_{50} values, GABA concentration-response data were fitted to the Hill equation (Equation 7.2), where I_{max} is the maximal peak current and n is the Hill coefficient.

$$I = \frac{I_{\max}}{1 + EC_{50}/[A]^n} \qquad \textbf{Equation 7.2}$$

Flurazepam Potentiation: Potentiation was determined using $EC_{5\text{-}10}$ of GABA. A high dose of GABA (>EC_{50}) was applied for 30 seconds then washed out (315 seconds between drug applications) and followed by $EC_{5\text{-}10}$ GABA applied three times (315 seconds between doses). A final drug application of 1 μM FLZM and $EC_{5\text{-}10}$ GABA was then applied. The average I_{max} of the three GABA applications was calculated and is represented by I_{GABA} in Equation 7.2. The peak of the potentiated current (I_{FLZM}) is the peak current due to application of both FLZM and GABA. Potentiation (P) was calculated according to Equation 7.1. Only oocytes with a standard error < 10% of I_{GABA} were considered to have stable currents. Only oocytes with stable GABA currents were used to determine potentiation.

Determination of Flurazepam EC_{50} ($EC_{50,P}$): For these experiments, the total concentration of mRNA used for oocyte injection was increased to 100 ng/μl to increase current size. The EC_{50} of potentiation, $EC_{50,P}$, was determined with a background GABA concentration of $EC_{5\text{-}10}$. FLZM was added in increasing concentrations (stating with 0 μM) until maximal potentiation was achieved. The data were fit to the Hill equation (Equation 7.1) to obtain the $EC_{50,P}$ and Hill coefficients. For each dose, oocytes were washed with ND96 for 30 seconds, followed by ND96+GABA ($EC_{5\text{-}10}$) for 30 seconds, then 1 mL of FLZM+GABA was applied over 30 seconds, followed by a 285 second

wash with ND96. The peak current was calculated by measuring the peak of the FLZM+GABA current and subtracting out the GABA only current immediately prior to application of FLZM+GABA.

7.6 References

(1) Brejc, K.; van Dijk, W. J.; Klaassen, R. V.; Schuurmans, M.; van Der Oost, J.; Smit, A. B.; Sixma, T. K. *Nature* **2001**, *411*, 269-76.
(2) Unwin, N. *J Mol Biol* **2005**, *346*, 967-89.
(3) Berezhnoy, D.; Nyfeler, Y.; Gonthier, A.; Schwob, H.; Goeldner, M.; Sigel, E. *J Biol Chem* **2004**, *279*, 3160-8.
(4) Buhr, A.; Baur, R.; Malherbe, P.; Sigel, E. *Mol Pharmacol* **1996**, *49*, 1080-4.
(5) Kucken, A. M.; Teissere, J. A.; Seffinga-Clark, J.; Wagner, D. A.; Czajkowski, C. *Mol Pharmacol* **2003**, *63*, 289-96.
(6) Oakley, N. R.; Jones, B. J. *Neuropharmacology* **1982**, *21*, 587-9.
(7) Macdonald, R. L.; Twyman, R. E.; Ryan-Jastrow, T.; Angelotti, T. P. *Epilepsy Res Suppl* **1992**, *9*, 265-77.
(8) Macdonald, R.; Barker, J. L. *Nature* **1978**, *271*, 563-4.
(9) Braestrup, C.; Schmiechen, R.; Neef, G.; Nielsen, M.; Petersen, E. N. *Science* **1982**, *216*, 1241-3.
(10) Kloda, J. H.; Czajkowski, C. *Mol Pharmacol* **2007**, *71*, 483-93.
(11) Fasman, G. D. *Prediction of protein structure and the principles of protein conformation*; Springer, **1989**.
(12) Jabs, A.; Weiss, M. S.; Hilgenfeld, R. *J Mol Biol* **1999**, *286*, 291-304.
(13) Lee, W. Y.; Sine, S. M. *Nature* **2005**, *438*, 243-7.
(14) Sharkey, L. M.; Czajkowski, C. *Mol Pharmacol* **2008**, *74*, 203-12.
(15) Changeux, J. P.; Edelstein, S. J. *Neuron* **1998**, *21*, 959-80.
(16) Olsen, R. W. *Annu Rev Pharmacol Toxicol* **1982**, *22*, 245-77.
(17) Nowak, M. W.; Gallivan, J. P.; Silverman, S. K.; Labarca, C. G.; Dougherty, D. A.; Lester, H. A. *Methods Enzymol* **1998**, *293*, 504-29.
(18) Nowak, M. W.; Kearney, P. C.; Sampson, J. R.; Saks, M. E.; Labarca, C. G.; Silverman, S. K.; Zhong, W.; Thorson, J. S.; Abelson, J. N.; Davidson, N.; Schultz, P. G.; Dougherty, D. A.; Lester, H. A. *Science* **1995**, *268*, 439-442.
(19) England, P. M.; Lester, H. A.; Davidson, N.; Dougherty, D. A. *Proc Natl Acad Sci U S A* **1997**, *94*, 11025-30.

Appendix 1

Guidelines for future $GABA_AR$ Researchers

Intent: This Appendix is intended to be of aid to members of the Dougherty lab that wish to work on the $GABA_AR$ in the future. The observations collected here are based on my experiences and discussion with others working on the $GABA_AR$ from different labs. The conjectures are not necessarily rigorously tested and therefore are not included elsewhere in this thesis. However, there is no need for someone else to hit the same bumps in the road. All data herein are limited to those collected using the α_1, β_{2S}, and γ_{2L} human $GABA_AR$ genes subcloned into the pGEMHE vector and obtained from Sarah Lummis (Department of Biochemistry, University of Cambridge, United Kingdom).

A1.1 $\alpha_1\beta_2$ versus $\alpha_1\beta_2\gamma_2$ $GABA_AR$

The $\alpha_1\beta_2\gamma_2$ is the most abundant $GABA_AR$ in the mammalian brain. As such, it is the subject to much research. It is well-established, however, that when trying to express these receptors in a heterologous expression, such as *Xenopus laevis* oocytes, that you can also express $\alpha_1\beta_2$ $GABA_AR$. I found this finding to be true. Literature reports indicate the $\alpha_1\beta_2\gamma_2$ and the $\alpha_1\beta_2$ $GABA_AR$ differ in several ways including single-channel conductance, desensitization kinetics, deactivation kinetics, voltage dependence, and Zn^{2+} inhibition.[1]

I found that for wild type and conventional mutations, the overall mRNA mix for $\alpha_1\beta_2$ $GABA_AR$ needed to be 10 times more concentrated than for $\alpha_1\beta_2\gamma_2$ to achieve similarly sized macroscopic currents. This difference is likely due in part to the lower single-channel conductance of the $\alpha_1\beta_2$ $GABA_AR$ and partially due to lower surface

expression. Like $\alpha_1\beta_2\gamma_2$ $GABA_AR$, the $\alpha_1\beta_2$ $GABA_AR$ has two α and two β subunits, but the identity of the 5th subunit is still unknown. Concatamer studies from different groups have offered compelling electrophyiological evidence that the 5th subunit is both α_2 and β.[3] Given the ambiguity in these results, it was necessary to reassure myself that varying the mRNA ratios did not alter the EC_{50} or Hill coefficient of the $\alpha_1\beta_{2S}$ $GABA_AR$ (Figure A1.1, Table A1.1). Unlike the αβ $GABA_AR$, the αβγ $GABA_AR$ is highly sensitive to the mRNA ratios used, as discussed in the following sections.

Table A1.1 EC_{50} values for αβ only receptors

ratio	EC_{50} (μM)	n_H	I_{max}
1:1 αβ	1.5 ± 0.1	1.17 ± 0.08	-21 ± 4
1:6 αβ	1.6 ± 0.1	1.33 ± 0.08	-9 ± 2
6:1 αβ	2.1 ± 0.1	1.24 ± 0.08	-16 ± 4

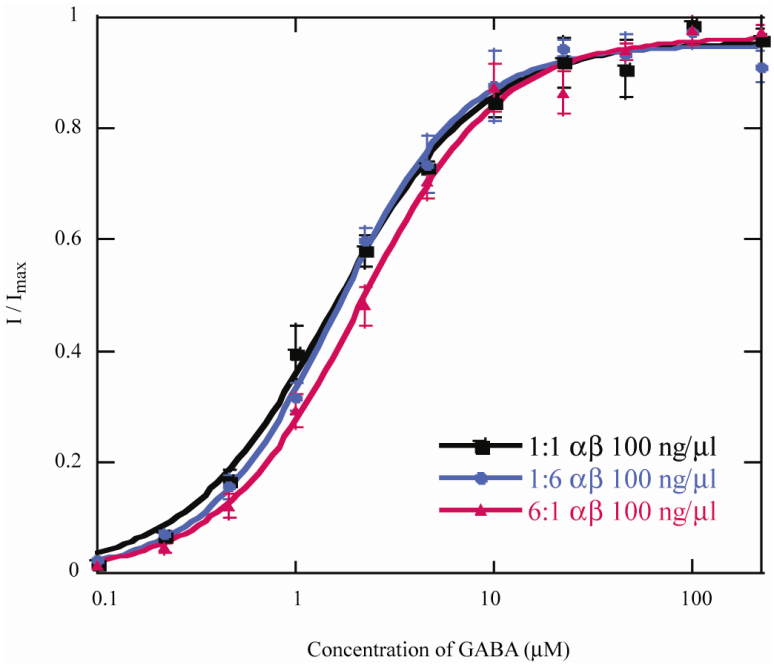

Figure A1.1 The GABA dose response relationship for wild type αβ $GABA_AR$ does not vary when the mRNA ratios are varied.

The αβ $GABA_AR$ is not physiologically relevant, but is often studied in place of the αβγ $GABA_AR$ because it is difficult to ensure the γ subunit is completely incorporated. Zn^{2+} block of the receptors has been reported as a means to determine the purity of the receptor population. The αβ $GABA_AR$ is reported to be sensitive to blockade by Zn^{2+} while the αβγ $GABA_AR$ is not. In principle then, application of Zn^{2+} with no corresponding decrease in macroscopic current would indicate a pure population of αβγ receptors. In my experience, pure populations of αβ $GABA_ARs$ could be blocked up to 70-90% with 10 mM Zn^{2+} however pure populations of αβγ $GABA_ARs$ showed variable blockade by the cation, sometimes up to 50%. Additionally, mixed populations of receptors behaved more similarly to the αβγ $GABA_AR$ than to the expectations based on a mixed population. As such, I concluded that the Zn^{2+} block test was not sufficient to determine a pure population of receptors. At more recent conferences, I have commented on this observation to members of the Czjakowski lab (Department of Physiology, University of Wisconsin, Madison) and they have seen similar behavior, substantiating the claim that this test is not useful experimentally. Indeed, recent papers on the $GABA_AR$ no longer mention Zn^{2+} block to differentiate between receptor subtypes.

A1.2 αβγ $GABA_AR$: mRNA Ratio

A1.2.1 Linearization Sites

When the gene of interest is contained within the pGEMHE vector, Nhe1 is most often used to linearize the DNA prior to *in vivo* transcription. Nhe1 was used to linearize both the α_1 and γ_{2L} genes. The Nhe1 cut site for these two genes was located after both the terminus of the gene and the poly-A tail within the vector. The β_{2S} gene, however,

contains a Nhe1 site within the gene, therefore an alternate restriction enzyme must be chosen. Initially, I chose the enzyme Spe1 which has a cut site after the gene terminus but before the poly-A tail. Capped mRNA made from the linearized DNA yielded functional $GABA_AR$ with the anticipated pharmacology in *Xenopus laevis* oocytes. In the more recent months, however, the entire lab has experienced lower expression levels and considerable effort on my part was put into increase expression of the $GABA_AR$ so I could finish some suppression experiments. In my quest, I found (through conversations with Kiowa Bower and Fraser Moss) that the poly-A tail of the mRNA helps stabilize the mRNA *in vivo*. As such, I tried Sph1, another restriction enzyme, when linearizing the β_{2S} DNA. The Sph1 restriction site is located after both the gene terminus and the poly-A tail. I found that for both the Spe1 derived and Sph1 derived capped mRNA, the ratios of mRNA for αβ receptors was 1:1 for wild type, though macroscopic currents were larger for oocytes injected with the Sph1-derived mRNA.

A1.2.2 βγ $GABA_AR$

A common problem when working with the αβγ $GABA_AR$ is that a mixed population of αβ and αβγ $GABA_AR$ can result. This problem is typically dealt with by using an excess of γ mRNA. When I initially attempted this using the DNA constructs originally provided by Neurion Pharmaceuticals (Pasadena, CA), I found that the more γ mRNA I used, the higher the EC_{50} and the lower the Hill coefficient. This eventually led me to try all combinations of the $GABA_A$ subunits. I found that in addition to expression from α/β mRNA mix, I also saw GABA-induced currents from β/γ mRNA mixes. I had hoped that the pGEMHE DNA constructs from Sarah Lummis would not have this same problem, but I did explicitly test for the problem and found that there was significant

GABA-induced current. More interestingly, I found that lower concentrations of 2:1 βγ mRNA resulted in higher levels of expression (Table A1.2, Figure A1.2). To me, these results suggest something endogenous to the oocyte is able to assemble with these subunits. These studies used β_{2S} linearized with Spe1, however, I did test for 2:1 βγ currents using β_{2S} linearized with Sph1 and found significant GABA-induced currents. In all cases, the βγ $GABA_A$Rs had hill coefficients less than 1, providing a defining characteristic.

Table A1.2 EC_{50} values for oocytes injected with βγ mRNA

ratio	EC_{50} (μM)	n_H	I_{max}	N
2:1 βγ (dil)	380 ± 50	0.69 ± 0.04	-1.2 ± 0.2	4
2:1 βγ (conc)	140 ± 10	0.95 ± 0.05	-0.55 ± 0.05	5

I_{max} is reported in μA. Dilute (dil) mRNA mix had a total mRNA concentration of 0.25 μg/μl while the concentrated (conc) mRNA mix had a total mRNA concentration of 1 μg/μl. The mRNA mix was mixed 1:1 (by volume) with water immediately prior to oocyte injection.

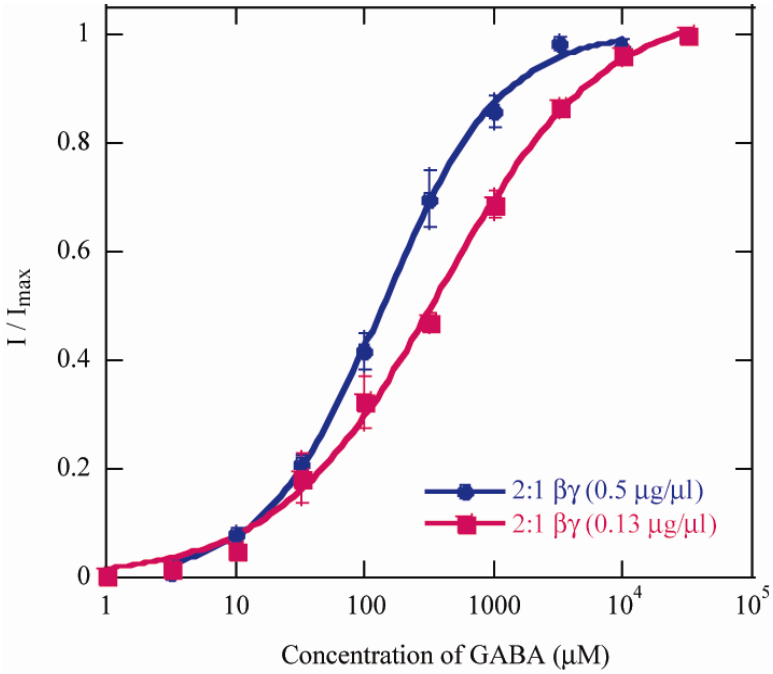

Figure A1.2 Dose response relationship for βγ $GABA_A$R

A1.2.3 αβγ mRNA Ratio

To determine the correct ratio of mRNA needed to produce a pure population of αβγ $GABA_A$Rs, I varied the relative amounts and then determined the GABA EC_{50} and Hill coefficient as well as the flurazepam potentiation, for each ratio. Literature values indicated the αβ $GABA_A$R has a significantly lower EC_{50} than the αβγ $GABA_A$R but similar Hill coefficients. Additionally the αβ $GABA_A$R is insensitive to benzodiazepine potentiation. The complicating factor is that overexpressing the γ subunit to a greater extent could lead to a mixed population of αβγ and βγ receptors. However, the βγ receptors were also determined to be relatively insensitive ($P < 0.7$) to benzodiazepines. Therefore, I reasoned that the ratio giving an EC_{50} greater than that of αβ $GABA_A$Rs (3 μM) and less than that of βγ $GABA_A$Rs (120 μM), with a hill coefficient of at least 1.2 (indicating a pure population), and maximal flurazepam (FLZM) potentiation would indicate the purest population of αβγ $GABA_A$R. The results for both β_{2S} linearized with Spe1 and with Sph1 are summarized in Table A1.3 and Figure A1.3.

Table A1.3 Results of various αβγ mRNA ratios on GABA EC_{50} and FLZM potentiation

αβγ	β_{2S} – Spe1				β_{2S} – Sph1			
Ratio	EC_{50}	n_H	I_{max}	P	EC_{50}	n_H	I_{max}	P
2:2:1	44 ± 1	1.3	-3.2 ± 0.8	2.6 ± 0.3	11.2 ± 0.5	1.4	10 ± 1	1.5 ± 0.3
1:1:1	47 ± 3	1.7	-9 ± 2	2.3 ± 0.1				
1:1:3	110 ± 10	0.96	-3 ± 1	2.0 ± 0.2	19.2 ± 0.5	1.4	8 ± 1	2.0 ± 0.3
1:1:5	110 ± 10	1.1	-3.4 ± 0.9	2.5 ± 0.5	39.3 ± 0.8	1.4	8.6 ± 0.9	1.7 ± 0.3
1:1:8	70 ±10	1.1	-1.5 ± 0.7		53 ± 2	1.1	5.5 ± 0.6	1.4 ± 0.1
1:1:10					49 ± 1	1.2	4.6 ± 0.7	1.6 ± 0.2

EC_{50} is reported in μM, I_{max} in μA. FLZM potentiation experiments were carried out at $EC_{5\text{-}10}$ of GABA (Spe1) and $EC_{15\text{-}10}$ (Sph1) using 1 μM FLZM.

For the β_{2S} linearized with Spe1, a 2:2:1 mRNA ratio was selected. Although the 1:1:1 ratio gave a higher Hill coefficient and I_{max} value, the error bars were also greater,

indicating more variability in the data. The 2:2:1 mRNA ratio gave the greatest potentiation and GABA EC_{50} and Hill coefficients consistent with literature values. FLZM potentiation for the β_{2S} linearized with Sph1 was lower in these experiments than previously seen with Spe1. I attribute this to the higher relative concentration of GABA used. The 1:1:3 mRNA ratio had the highest potentiation value but was not chosen as the standard because of the larger error bars for the GABA dose response relationship. The 1:1:5 ratio had a high hill coefficient and higher potentiation than all but the 1:1:3 ratio. Additionally the values obtained for the 1:1:5 ratio are consistent with the literature. Therefore 2:2:1 was used for wild type and conventional mutants for β_{2S} mRNA made from DNA linearized with Spe1 and 1:1:5 was used for wild type and conventional mutants for β_{2S} mRNA made from DNA linearized with Sph1.

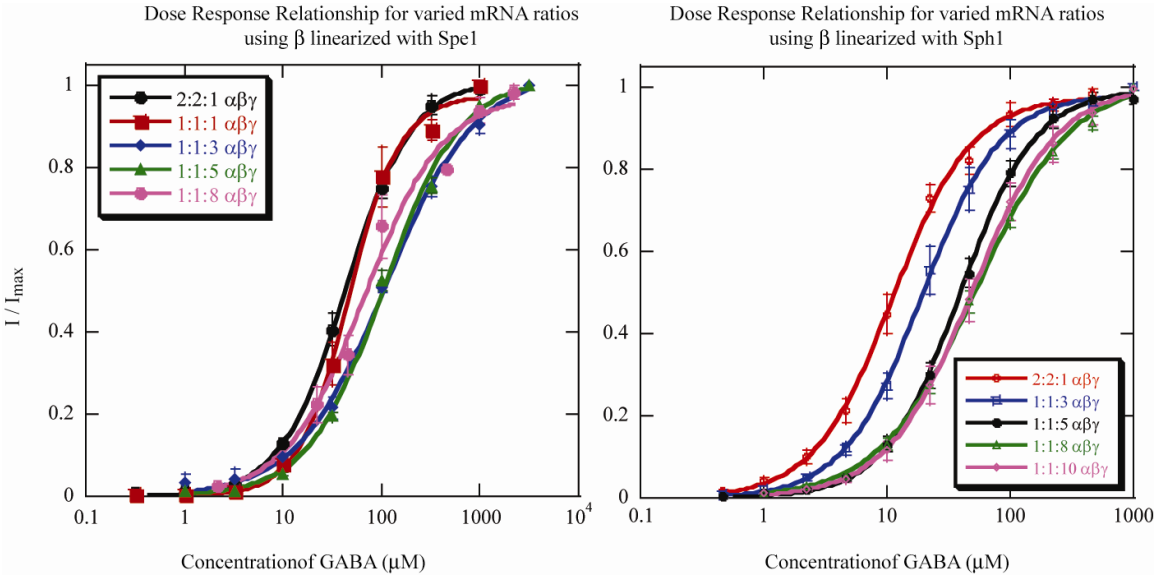

Figure A1.3 GABA dose response relationships for various mRNA ratios of the αβγ $GABA_AR$. *Left*: mRNA made from β_{2S} DNA linearized with Spe1. *Right*: mRNA made from β_{2S} DNA linearized with Sph1

A1.3 Unnatural Amino Acid Incorporation

For suppression experiments, I found the standard 5-fold excess of the subunit containing the TAG mutation to be sufficient for expression. Thus for suppression in the α subunit, I used a 5:1 mRNA mix for the αβ $GABA_AR$ and 10:2:1 (β_{2S}-Spe1) or 5:1:5 (β_{2S}-Sph1) for the αβγ receptor. Since injections of βγ respond to GABA, there are always significant read-through and re-aminoacylation currents when suppressing in the α subunit. These control experiments will yield receptors that are pharmacologically different from wild type and the unnatural amino acid. Alterring the mRNA ratio used for different unnatural amino acids may help with these problems, however I have not investigated this possibility thoroughly.

A1.4 Recommendations

My recommendation to future $GABA_AR$ experimenters is to use only β_{2S} mRNA made from DNA linearized with Sph1. Generally this mRNA led to higher expression and less variability. When mutating in the α and β subunits, it is worthwhile to first figure out the affect of the mutation in the αβ $GABA_AR$. In my experience, the GABA EC_{50} shifts in the same direction for both the αβ $GABA_AR$ and the αβγ $GABA_AR$. Additionally, there are fewer complicating factors with the αβ $GABA_AR$, thus these are useful intitial experiments to give a sense of what to expect in the αβγ $GABA_AR$.

BZD potentiation can be used to determine if the γ subunit is incorporated – but this test is not reliable if the mutation may affect BZD potentiation. I tried using fluorescent antibody labeling and TIRF microscopy to determine whether or not the γ subunit was completely incorporated. However the results were ambiguous. This may

be due to the primary antibodies not binding tightly enough or to nonspecific labeling by the secondary antibody. In either case, I do not recommend this method to detect surface expression.

When doing experiments, I recommend using the 1 ml plastic 96 well plates for everything except the benzodizapines. The BZDs are sticky and can be absorbed into the plastic of the 96 well plates, thereby altering the concentration in the solution. Therefore, it is best to use the glass-coated plates for your drug solutions. It is also necessary to make the BZD solutions in glass bottles or tubes (no flacon tubes). Similarly, the BZDs are hard to wash off the receptors and out of the Opus chambers. Thus, you should do BZDs after you finish the GABA dose response experiments because trace amounts of BZDs left on the Opus will affect your GABA EC_{50} values. After using the BZDs, wash the Opus by running 10% DMSO (in water) through pump B for at least 10 minutes at 1 ml/min, followed by Millipore water for the same amount of time. The glass-coated plates need to be washed with 70% isopropanol and then three times with deionized water at the end of the recording session.

Based on the pentobarbital structure, it seems likely that pentobarbital will be prone to crystallization, therefore the pentobarbital solutions should be kept at room temperature and if possible kept stirring constantly to prevent crystallization. I also found it helpful when trying to compare two things using pentobarbital, it's a good idea to run the experiments in parallel as this will control for any crystallization that has taken place.

GABA solutions should be made immediately prior to recording. Weigh out 30-50 mg of GABA (on the balance in the Chemistry lab) in a 50 ml falcon tube, then

calculate the volume of ND96 necessary to make a 10 mM solution. This is the stock solution. GABA is soluble up to 100 mM, thus higher concentrations are possible. In my experience, mutations where 10 mM GABA was needed have also had quite low Hill coefficients and tend not to truly turn over. Therefore I recommend using higher concentrations of GABA only if there is a high enough (>1.1) Hill coefficient or no response at concentrations < 50 μM.

Despite the complications of working with the $GABA_AR$, I hope the lab will continue to work with them as they have many allosteric modulators including barbiturates, anesthetics, and benzodiazepines. The mechanisms of action of these modulators are not well understood thus there are many experiments to be done. Additionally, there are benefits to working with the $GABA_AR$. For starters, you can record in ND96 with calcium which means the oocytes tend to be healthier. While longer Opus runs mean fewer runs can be performed during a given recording session, it also means other experiments can be performed while the Opus is running, which can be immensely useful.

A1.5 Opus Protocols

Table A1.4 Fluidics profiles for the OpusXpress

Profile	Initial Rate	Initial Duration	Subsequent Rate
1	0.1 ml/min	0 sec	2 ml/min
2	0.1 ml/min	0 sec	2 ml/min
3	4 ml/min	30 sec	3 ml/min

All experiments were carried out at -60 mV. The OpusXpress has at least three profiles for fluidics, defined in Table A1.4. In the subsequent sections, I have given the protocol name and then outlined the Opus protocols and setup for each experiment type.

A1.5.1 GABA EC_{50} Protocol

Table A1.5 GABA EC_{50} Protocol

Time	Application	Source	Fluidics
30 sec	ND96	B	Profile 1
30 sec	GABA	Drug plate	Profile 2
285 sec	ND96	B	Profile 3

Repeat for each dose.

This protocol is named "GABA_30sapp_285swash" and requires only pump B and the drug plates. ND96 with calcium is in pump B and the drug plates contain varying concentrations of GABA. I generally use three concentrations of GABA per order of magnitude (1, 2.2, 4.6, etc.). When determining the dose response relationship, I first apply a "high" concentration of GABA (usually 10 μM for αβ receptors and 100 μM for αβγ receptors), then the concentrations for the dose response relationship from low to high concentration and finally a zero concentration. The high dose at the beginning "wakes up" the receptors according to Sarah Lummis. The data varies less when I adhere to this rule. The zero dose at the end should not give current, thereby ensuring the previous responses were accurate. For wild type αβ $GABA_AR$ I use GABA concentrations from 0.1-100 μM GABA to determine the dose-response relationship. For wild type αβγ $GABA_A$Rs I use 0.46-1000 μM GABA.

A1.5.2 BZD Potentiation Protocol

This protocol is called "GABA_BZD_no prewash" and uses only pump B and the drug plates. For the BZD potentiation experiments, I repeat the EC_{5-10} dose of GABA three times and then average the responses and calculate the percent standard error. If the percent standard error is less than or equal to 10, the current is stable and the oocyte can be used to calculate the potentiation. Note that the last wash step is not saved as a

clampfit file since it is just a wash step. For multiple BZD potentiation runs, start with the experiments using the lowest concentrations of GABA and work up to the ones using the highest concentrations. The ten minute wash between BZD application and the beginning of the next run is sufficient to remove all the BZD. Remember that for BZD experiments you need to use glass (not plastic) for the drug solutions and drug plates and need to clean the opus (10% DMSO) and drug plates (70% isopropanol) specially.

Table A1.6 BZD Potentiation Protocol

Time	Application	Source	Rate
*			
30 sec	ND96	B	Profile 1
30 sec	GABA	Drug Plate	Profile 2
287 sec	ND96	B	Profile 3
*	*Repeat * to * 4 times with a high [GABA] the first time and EC_{5-10} GABA the next 3 times.*		
30 sec	ND96	B	Profile 1
30 sec	EC_{5-10} GABA + BZD	Drug Plate	Profile 2
241 sec	ND96	B	Profile 3
360 sec	ND96	B	Profile 3

A1.5.3 BZD $EC_{50,P}$ Protocol

Table A1.7 BZD $EC_{50,P}$ Protocol

Time	Application	Source	Rate
30 sec	ND96	B	Profile 1
30 sec	High dose of GABA	Drug Plate	Profile 2
285 sec	ND96	B	Profile 3
*			
30 sec	ND96	B	Profile 1
30 sec	EC_{5-10} GABA	A	Profile 1
30 sec	EC_{5-10} GABA + BZD	Drug Plate	Profile 2
279 sec	ND96	B	Profile 3
*	*Repeat * to * for all concentrations of BZD.*		
30 sec	ND96	B	Profile 1
30 sec	ND96	Drug Plate	Profile 2
285 sec	ND96	B	Profile 3

This is a modified version of the GABA EC_{50} protocol and is called "GABA_BZD_EC50." The set-up uses ND96 with calcium on Buffer B, EC_{5-10} GABA in ND96 with calcium as Buffer A and the drug plates contain EC_{5-10} GABA and the BZD unless otherwise specified. The protocol begins by simply applying a high dose of GABA as normally done to "wake-up" the receptors. The second part of the protocol is where the BZD dose-response relationship is determined. I use 0 μM BZD for my lowest dose and then increase the concentration (1, 3.2, 10, 3, etc.). BZD have nM EC_{50} values and only one binding site, so Hill coefficients are between 0.8 and 1.1. I usually start with 1 nM and go as high as 10 μM for FLZM. Diazepam (which we also have in the drug cabinet) is supposed to have a slightly lower EC_{50}.

There are two ways to analyze this data. The first is to take the average of all the EC_{5-10} peak currents and then subtract this value from the peak current for each of the BZD doses. This method works especially well if the GABA response does not drift. The second method is to use the GABA response right before the BZD application as the baseline for the BZD peak current. In general, the data from the BZD $EC_{50,P}$ takes longer to analyze than for a GABA EC_{50} as each oocyte usually needs to be analyzed one at a time. Additionally BZD solutions must be made for each concentration of GABA used. Again, don't forget to use glass-coated drug plates and glass tubes and to wash the Opus and drug plates carefully.

A1.5.4 Pentobarbital EC_{50} Protocol

Use the same protocol as the GABA EC_{50} but use pentobarbital instead of GABA. Pentobarbital has a Hill coefficient between 2 and 3 so the dose response curve is much steeper and therefore a smaller range of concentrations are needed. The PB EC_{50} for the

wild type αβ $GABA_AR$ is around 1.4 mM. I have not used PB with the αβγ $GABA_AR$. Evidence indicates that PB binds to the transmembrane region of the β subunit,[4-6] thus it is possible the PB EC_{50} is similar for both the αβ and αβγ receptors. My data (Chapter 6) suggest PB is a full agonist at the wild type αβ receptor, therefore PB can be used to determine whether GABA has become a partial agonist for a given mutation. The caveat with PB is that in addition to activating the $GABA_AR$, it also blocks the channel, thus the rebound current is used to determine the "peak current" at blocking concentrations of PB.

A1.6 Wild type tTraces

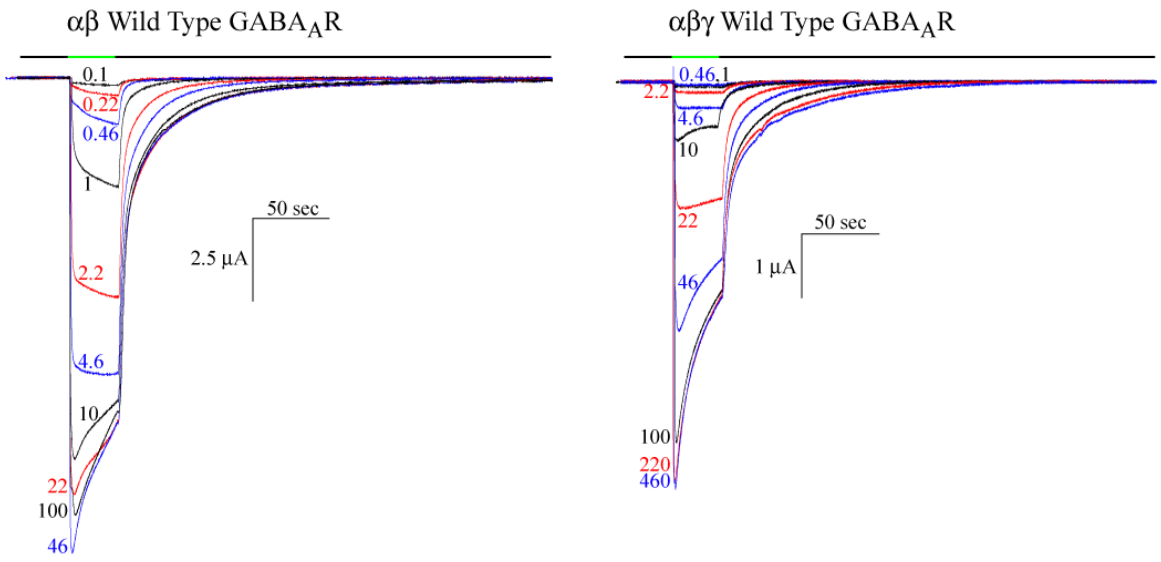

Figure A1.4 GABA traces of the wild type $GABA_AR$. Concentrations are given in µM. The αβγ (*right*) has more desensitization than the αβ (*left*) receptor. *Left*: For the oocyte shown here, the αβ $GABA_AR$ has an EC_{50} of 2.4 µM, a hill coefficient of 1.3, and I_{max}=-12.8 µA. *Right*: For the oocyte shown here, the αβγ $GABA_AR$ has an EC_{50} of 33 µM, a hill coefficient of 1.7, and I_{max}=-7.8 µA. Black bars denote ND96 and green bars denote application of GABA.

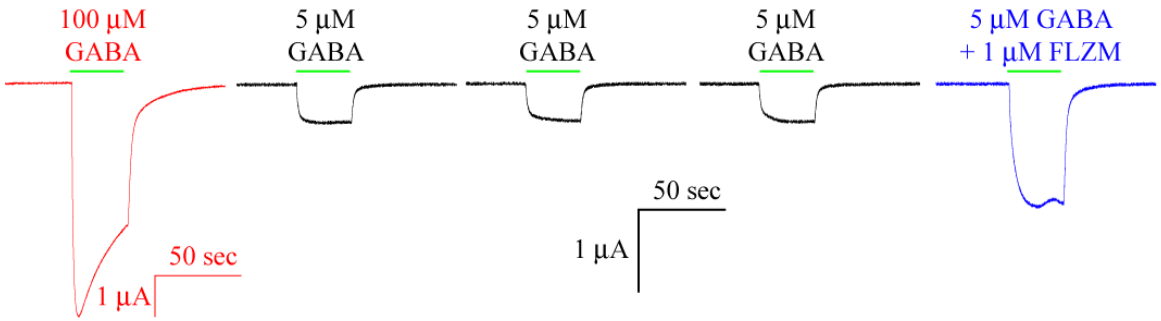

Figure A1.5 Sample traces from a FLZM potentiation experiment. This oocyte contained wild type αβγ $GABA_AR$ and had a FLZM potentiation of 2.18. A high dose of GABA is applied first (red, separate scale bars), then three doses of $EC_{5\text{-}10}$ GABA (black) and finally $EC_{5\text{-}10}$ GABA with 1 µM FLZM (blue). The average and standard error of the black traces is used to determine if the GABA response is stable. Green bars denote drug application. *Note*: Part of the washout has been removed from the trace to fit all traces on one line.

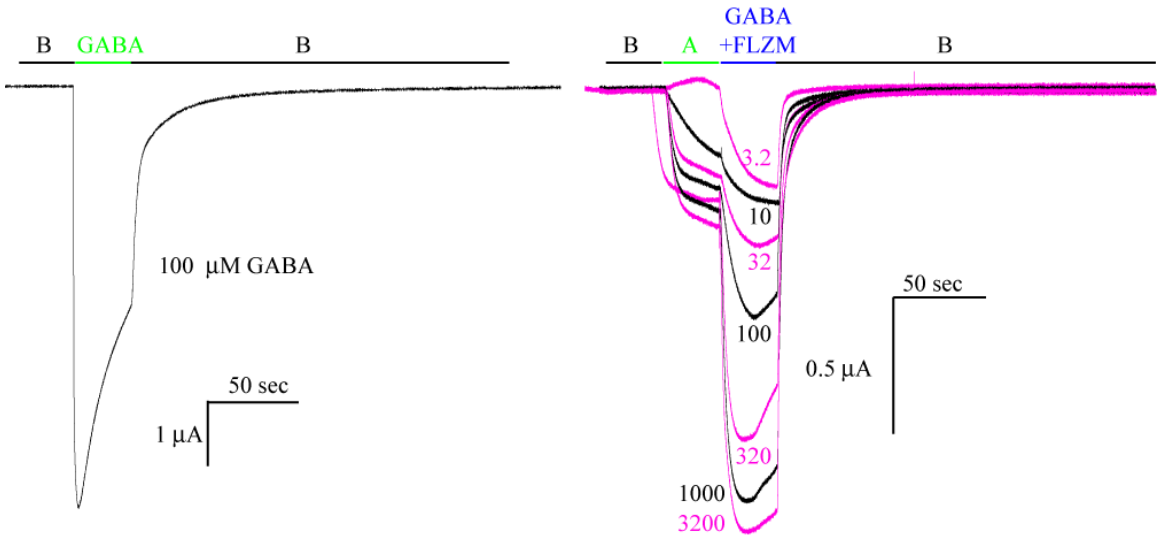

Figure A1.6 Sample traces from a FLZM EC_{50} experiment. *Left*: A high dose of just GABA is applied first to "wake-up" the receptors. Black horizontal bars at the top denote ND96 while the green bars denote GABA application. *Right*: Determination of FLZM dose-response relationship. Initially ND96 is applied (black bar), then $EC_{5\text{-}10}$ of GABA (green) is washed on through pump A, followed by application of $EC_{5\text{-}10}$ GABA and FLZM (blue bar), and finally the drugs are washed off with ND96 (black bar). In this case, the GABA induced current (under the green bar) was not stable. Concnetrations of FLZM are provided in nM. For the wild type αβγ receptors shown here, $EC_{5\text{-}10}$ is 5 µM GABA.

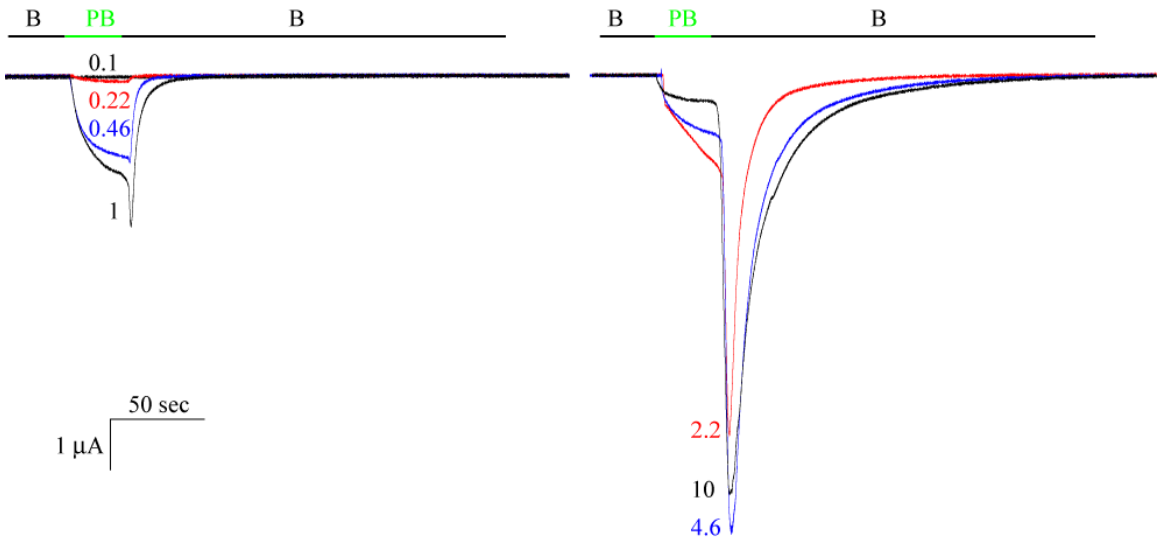

Figure A1.7 Sample pentobarbital traces for wild type αβ $GABA_AR$. Concentrations are given in mM. For [PB] > 0.46 mM, there is significant rebound current which is used as the peak response. Black horizontal bars (B) represent ND96 and green bars represent drug application.

A1.7 References

(1) Boileau, A. J.; Baur, R.; Sharkey, L. M.; Sigel, E.; Czajkowski, C. *Neuropharmacology* **2002**, *43*, 695-700.
(2) Boileau, A. J.; Pearce, R. A.; Czajkowski, C. *J Neurosci* **2005**, *25*, 11219-30.
(3) Baumann, S. W.; Baur, R.; Sigel, E. *J Biol Chem* **2001**, *276*, 36275-80.
(4) Amin, J. *Mol Pharmacol* **1999**, *55*, 411-23.
(5) Amin, J.; Weiss, D. S. *Nature* **1993**, *366*, 565-9.
(6) Serafini, R.; Bracamontes, J.; Steinbach, J. H. *J Physiol* **2000**, *524 Pt 3*, 649-76.